TORONTO METROPOLITAN UNIVERSITY
FACULTY OF ENGINEERING AND APPLIED SCIENCE
DEPARTMENT OF MECHANICAL AND INDUSTRIAL ENGINEERING

Exploration into the Use of Gas Power for Lifting Operations

Souren Pashangpour, 500972936
Gibran Ahmed Rajput, 500899819
Karim Akl, 500899562
Dat Huynh, 500923321

MEC825 - Design Project Report

Submitted in partial fulfilment
of the requirements for the degree of
Bachelor of Engineering (B.Eng)

Faculty Advisor: Professor S. Yu
Date: April 6th, 2023

Acknowledgements

The authors would like to acknowledge Dr Shudong Yu, for his guidance and support throughout the duration of this project.

The authors would also like to acknowledge the contributions of Milijanko Jovkovic, for his skilled support in the design and machining of the model.

Abstract

Personnel lifting operations are essential for various industries, especially in high-altitude scenarios, such as mountainous terrains, high-rise buildings, and natural disasters. Despite the significant amount of research on human VTOL, very few practical solutions have been implemented. Existing research suggests the use of internal combustion engines may be advantageous for such operations due to high energy density of engine fuels allowing for increased payload capacity and operation time. This report presents an investigation into this suggestion through the design, development and assessment of a gas-powered propeller device designed to lift users for high-altitude operations. The approach and methodology for the project includes research into existing solutions, an iterative design process, as well as benchmarking for performance. The device's performance was assessed by conducting a series of functional evaluations, such as payload capacity and flight time calculations. The results were analysed, and the device's viability was compared to the previously established criteria. The author’s conclude that the gas-powered VTOL designed has potential to provide a versatile, low-cost solution that can overcome the challenges of existing VTOL. While results are promising, they are not definitive however, and thus the authors’ recommend significant future work to improve the performance and efficiency of the device.

Table of Contents

List of Figures

List of Tables

Nomenclature

Acronyms

ICE:	Internal Combustion Engine
VTOL:	Vertical Takeoff and Landing
RC:	Radio Control
FOS:	Factor of Safety
EFI:	Electronic Fuel Injection
RPM:	Rotations per Minute
PID:	Proportional, Integral, Derivative
FEA:	Finite Element Analysis

Symbols

C_0:	Basic static load rating
C_{10}:	Basic dynamic load rating
C_L:	Stress-cycle factor for pitting resistance
C_p:	Elastic coefficient
C_R:	Reliability factor for pitting
C_s:	Size factor for pitting resistance
C_{xc}:	Crowning factor for pitting resistance
D, d:	Diameter
D_G, d_p:	Outer pitch diameters of gear and pinion respectively
d_r:	Minor diameter
e:	Abscissa
F:	Force
F_a:	Axial force
F_r:	Radial force
F_e:	Equivalent force
F_N:	Net face width
J:	Geometry factor for bending strength
k_a:	Surface condition modification factor
k_b:	Size modification factor

k_c: load modification factor

k_d: Temperature modification factor

k_e: Reliability factor

k_f: Miscellaneous effects modification factor

K_F: Stress correction and concentration factor

K_f: Fatigue stress concentration factor for bending

K_{fs}: Fatigue stress concentration factor for torsion

K_i: Inertia factor for bending strength

K_L: Stress cycle factor for bending strength

K_m: Load distribution factor

K_o: Overload factor

K_R: Reliability factor for bending strength

K_S: Size factor for bending strength

K_T: Temperature factor

K_v: Dynamic factor

K_x: Lengthwise curvature factor for bending strength

L_{10}: 90% Bearing life rating

M: Moment

M_a: Alternating component of moment

M_m: Midrange component of moment

m: Gear module

N: Number of gear teeth

n: Safety factor

n_t: number of engaged threads

P: Design power through gear pair

p: Pitch

R_{frame}: Radius of frame

s_e: Endurance limit at the critical location

s_e': Rotary-beam test specimen endurance limit

S_F: Bending safety factor

$(s_t)_G$: Calculated bending stress number

$(s_{wt})_G$: Permissible bending stress number

$s_{c:}$: Calculated contact stress number

s_{ut}: Ultimate strength

$(s_{wc})_G$: Permissible contact stress number

T: ` Tension

T_a: Alternating component of torsion

T_m: Midrange component of torsion

V: Rotation factor

W^t: Engine load on gear

θ_x: Wrap angle of pulley x

σ: Normal stress

σ_a': Alternating stress for von Mises

σ_m': Midrange stress for von Mises

σ_b: Root thread bending stress

CHAPTER 1: Initiation

1.1 Introduction

Personnel lifting operations have been a crucial aspect of various different industries. The need for efficient and effective lifting methods has become increasingly important, particularly in high-altitude scenarios such as mountainous terrains, high-rise buildings, and during natural disasters. Whether for rescue or other purposes, specialised equipment and training are required for such operations and the lack of suitable devices has been a persistent challenge.

While there has been a significant amount of research into the development of human VTOL, especially for high altitude rescue operations, virtually no solutions have been implemented for real world use. The only existing solutions in use today are aerial lifting platforms, which have been in use since the mid 20th century and are limited in accessibility and height while simultaneously being expensive. The work done by the ModMans Engineering group aims to address the lack of solutions by developing a gas powered propeller device, designed to lift users for high altitude operations. The use of a gas powered propeller device has potential to overcome many of the challenges faced by other VTOL that are currently being researched or are in use today. These challenges primarily being viability, accessibility and cost.

A gas powered VTOL has the potential to address these challenges by providing a solution that is versatile in a variety of different settings, at a relatively low cost. The utilisation of an internal combustion engine (ICE) provides significant benefits over alternative power sources such as electric motors which are commonly seen in multicopter aircraft such as commercial drones. Aerial devices with ICE engines can carry significantly more payload

with much longer flight times than their electric counterparts as they do not need to devote weight to batteries. Engines are more flexible as they can be refuelled quickly, unlike batteries which take substantial time to charge, minimising downtime. In addition to this, ICE powered devices in general are less expensive than their electric counterparts as they do not require the same level of advanced technology. These specific benefits make ICE a viable choice for rescue, as reliably long flight times are essential.

The scope of this project involves the design and building of a scaled model of a gas powered propeller device, similar to a quadcopter, intended to lift a structure which can raise and lower persons. It is important to note that the project's primary focus is on the designing and building of the gas-powered VTOL, rather than on the structure itself. As such, the device is designed with modularity in mind, with the possibility of lifting different types of structures depending on the situation. The use of a scaled model provides many benefits, such as seeing the practicality and utility of a functional prototype in a cost-effective, risk-reduced setting. This is a necessary preceding step to any full scale implementation of an engineering design problem. It is noted however, that there are significant limitations of a scaled model and as such this project only serves as a preliminary exploration into the concept.

The approach and methodology for this project involves several key steps. First, ample research was conducted on literature relating to the use of ICEs for multi propeller devices, as well as existing devices which implement combustion engines. Next, our design requirements and performance criteria were established based on an analysis of the intended use case and requirements. These requirements were then used in an iterative design process, where multiple different concept solutions were created and evaluated based on the performance goals. A concept based on a nitro RC car platform was decided upon, even so, continuous iterations on the structure

design were made until an adequate design was finalised. Once the design was finalised, a scaled model was then assembled with the use of thermoplastic 3D printing, and custom ordered steel machined parts. Once assembled, a series of functional tests and assessments such as payload capacity and flight time calculations were then conducted on the scaled model. Data from these tests were collected and analysed to assess the performance and identify any key areas of improvement. The performance of the device was compared to the previously established criteria and a discussion analysing the viability of this scaled model was written. In the end of the report, the authors' detail their conclusions regarding the viability of a gas powered lift device for use in high altitude operations along with recommendations for potential future work.

1.2 Literature Review

1.2.1 Review Summary

Examining the literature, there exists significant research into the design and development of high altitude VTOL, however, virtually no research exists into the use of gas powered lift devices for high altitude operations. Much of the research that exists on gas powered multicopters involves the use of hybrid gas-electric systems, with research on sole gas power being limited. As such, to match the scope of the project, the overall research review is focused on multicopter aircraft which implement ICE systems, with sections on engine choice and fuel, engine control, and propeller design and structure. This is to gain insight on the use of gas powered engines and control systems, along with their capabilities for high altitude operations. The results compiled from this review suggest several conclusions that ultimately will influence the methodology and design of this project. Firstly, it is established that the high energy density of fuels used in ICE propulsion systems allow for substantially longer flight times with greater payloads

than an electric battery system. In fact, this difference is so great, when comparing caloric energy density of batteries and liquid fuels, american physicist and former US secretary of energy, Steven Chu, found that the energy density of liquid fuels is greater than lithium ion batteries by two orders of magnitude [1]. This characteristic of ICEs makes them suitable for use in VTOL designed for high altitude operations which require high payloads and reliably long flight times. It is important to mention that the characteristics of ICE are prone to change based on a variety of factors (i.e. Operating temperature, fuel mixture, ambient pressure, etc.) It is also evident that ICE possess slow response times in addition to causing significant vibration and noise. This vibration paired with the slow response times of engines, make stabilisation of a VTOL difficult to manage with a propulsion system solely utilising ICEs. As a result of these characteristics, many studies have developed and investigated the use of engine control systems to ensure flight stability in different environments. Research was also conducted into the design and structure of propellers. Generally, studies have found that larger propeller diameters result in greater thrust but require more power to turn, while higher pitch can increase acceleration but lower efficiency. The number of blades also affects performance, with more blades providing greater lift and stability but also producing more noise and requiring more power. It is apparent that the trade-offs between these factors can vary depending on the design requirements of a specific application.

1.2.2 Engine Choice

ICEs have been widely used as power sources for a variety of applications, including propeller devices such as drones and other aerial vehicles. The most common types of ICEs used in propeller devices are gasoline engines, diesel engines, and turbine engines. Reviewing existing research and existing solutions, one can evaluate the suitability of these main engine types for use in a propeller VTOL.

Gasoline engines have been a popular choice for propeller devices due to their high power-to-weight ratio, high fuel density, and relatively low cost. In existing literature, the majority of multi propeller devices using a combustion propulsion system utilise gasoline engines. A study focused on the design and implementation of a gasoline-electric hybrid propulsion system for a multi-rotor system concluded that the use of gasoline engines results in long flight times and extended range. However, the thrust to weight ratio and thermal efficiency of these engines are poor, meaning they are less efficient at converting the energy in fuel into usable power. This results in higher fuel consumption as well as higher emissions. One potential redeeming factor is that a vast variety of gasoline engines exist, making them a popular choice for hobbyists and small-scale applications. Two stroke engines specifically are popular in scaled applications due to their simplicity, low cost and high power to weight ratio. In fact, researchers at the University of Ovida in Spain, utilised a twin two stroke engine found in RC aircraft for their scaled model [2]. The engine choice was primarily based on the high specific output power of the engine of 11.3hp with a weight of only 2.5kg [3].

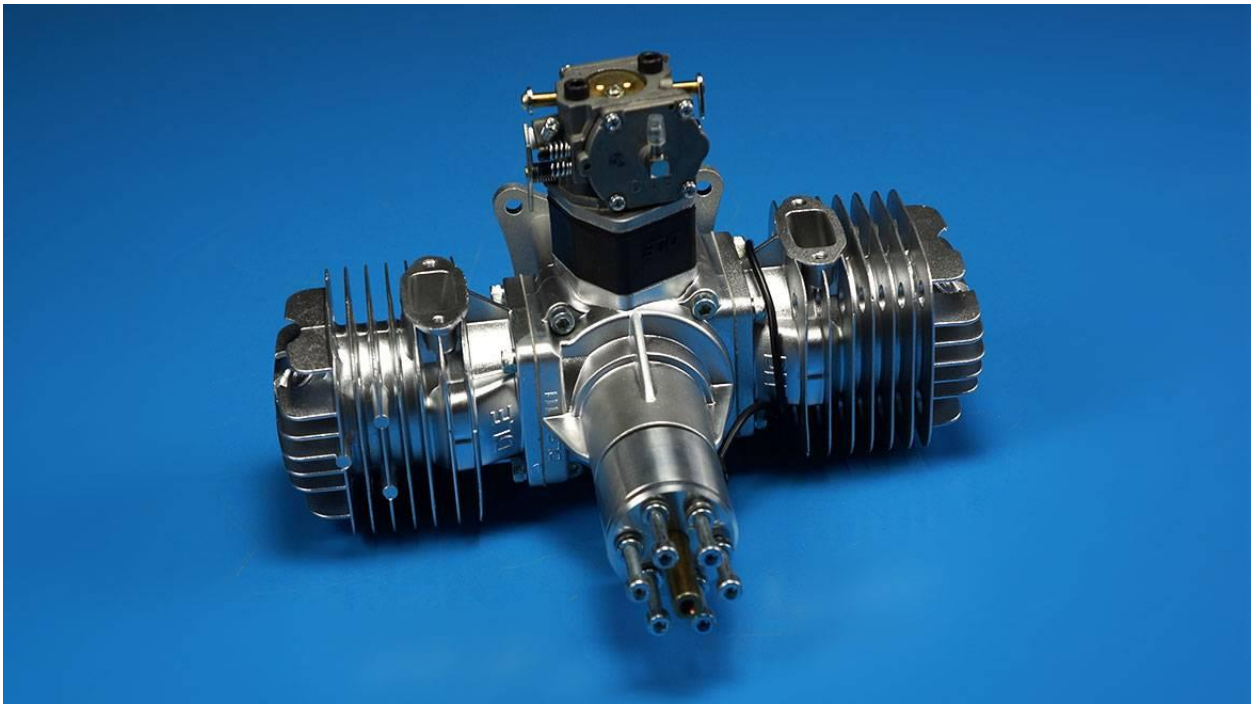

Figure 1.1 DLE111 Twin Two Stroke Gasoline RC Model Engine

Diesel engines are known for their high thermal efficiency, long lifespan, and lower fuel consumption compared to gasoline engines. While common for use in large aircraft, the use of diesel engines, as well as the literature is limited in smaller scale. One study focusing on the benefits of Hybrid Diesel-Electric Propulsion for small scale VTOL aircraft, notes the advantage of diesel to be the high energy density of diesel fuel relative to energy density of batteries [4]. Moreover, diesel engines can run on a large number of different heavy fuels such as biodiesel [5]. Unfortunately, the major downside is the fact that diesel engines are often significantly heavier and more expensive than gasoline engines. The study was partnered with Cosworth, a prominent engine manufacturer, who provided their AG two stroke diesel engine for use due to its notably high output power. The output of the engine was 12bhp, however the total weight was over 20.5 lbs or around 9 kg [6]. This specific output power is considered good with a diesel engine, however when compared to the RC gasoline engine above, the Gasoline engine generates 3.5 times more power per weight. This significantly higher

weight plus larger size attributed with diesel engines makes them generally unfavourable for small-scale operations.

Turbine engines offer high power-to-weight ratios, high reliability, and low maintenance requirements, making them a popular choice for larger, more powerful propeller devices. There also exists micro turbine engines which have been used in actual small scale drone applications. One existing solution developed by a company named FusionFlight is the JetQuad, which is a quad micro Turbine VTOL drone [7]. This drone utilises four micro turbines to lift a large suitcase sized drone to perform delivery operations. These four microturbine engines combine for a total output of 700N, allowing the aircraft to carry a payload of 16kg, on top of its already hefty 44 kg weight. Micro turbine engines are versatile and consume a variety of heavy fuel such as Kerosene, Jet-A and Diesel. One research study focused on micro turbine engines for drone propulsion looked into different types of Micro turbine engines and their use of fuel [8]. The study found that the fuel consumption is higher than piston engines, however when accounting for power to weight ratio, the fuel consumption is acceptable. Turbine engines are unfortunately much more expensive than piston ICEs. In addition to this, one needs to obtain multiple engines to ensure stability driving up the cost substantially. This paired with the lack of fuel efficiency make turbine engines impractical for small-scale prototype models.

1.2.3 Engine Control

There have been numerous studies focusing on the control systems of multicopter devices. These studies often include research or investigation on engine control specifically. Engine control is critical in the design and development of gasoline powered multicopter devices, because it directly impacts the performance, efficiency, and safety of the device. Precise control of the engine's power output and fuel consumption is necessary to ensure the drone can lift heavy loads and operate for an extended period of time while

also minimising the risk of engine failure or malfunction.

Beginning with fuel to air mixture, fuel injection is a key component of engine control, the type of fuel injection system used can have a significant impact on engine control. Electronic fuel injection (EFI) systems, for example, use electronic sensors to measure various engine parameters and an onboard computer to precisely control the amount of fuel injected into the engine. In contrast, carbureted engines rely on mechanical devices, such as a carburetor, to mix fuel and air, which can be less precise and responsive. Many unmanned aerial devices utilising gasoline power rely on carburetors for fuel injection due to its ease of use. However, this often results in less intricate control systems that struggle to keep up with changing demands. An example of this is reflected in the work of Researchers at the University of Ovida who have implemented a basic throttle control system for a multirotor aircraft utilising a servo motor and carburetor [2]. While throttle performance is accurate, with no slack between the servo and the carburetor lever, it is the author's intention to replace this system with a fuel injection system for increased control in a later design.

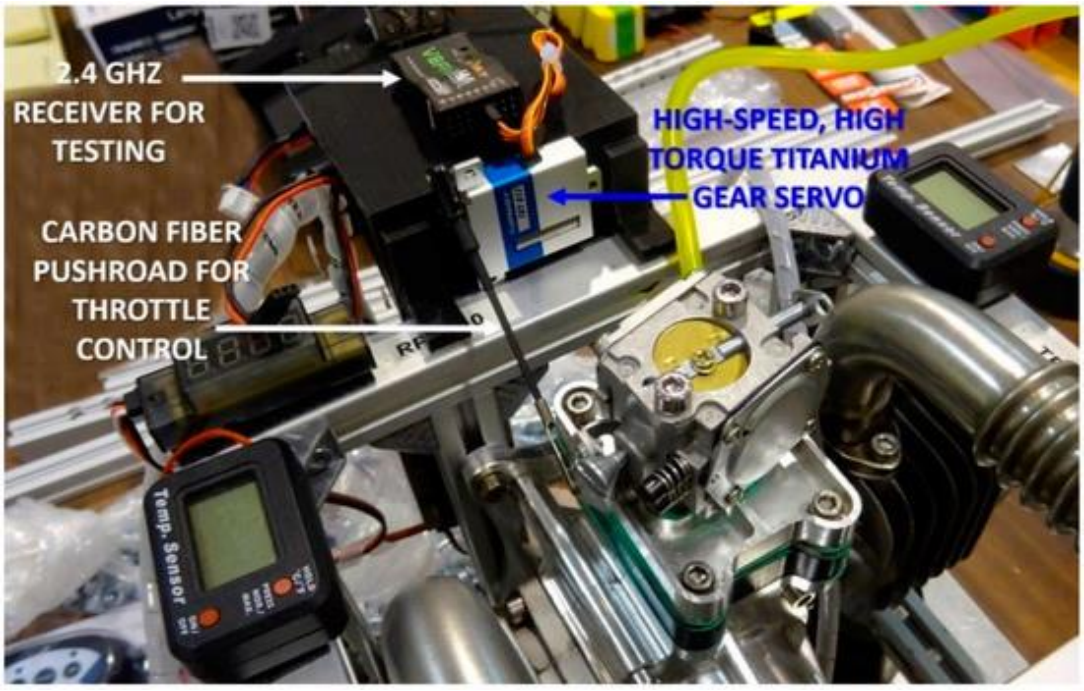

Figure 1.2 Throttle control system used by researchers from the University of Ovida

Researchers from Cheng Kung University in Taiwan developed an engine controller designed for a hybrid gasoline-electric powered multirotor device. In this project, the researchers assessed the use of gas power for multicopters and determined that including a gasoline engine will substantially improve the lifting power of a VTOL system [9]. However, gasoline engines have characteristics that are naturally unfavourable towards the control of multi-rotor systems, namely their inadequate response time. In addition, the characteristics of a gas engine vary with fuel mixture adjustment, ambient pressure and temperature, as well as the engine's own temperature. Thus, electric motors are preferred to control the pitch of the device due to the response time needed for small adjustments.

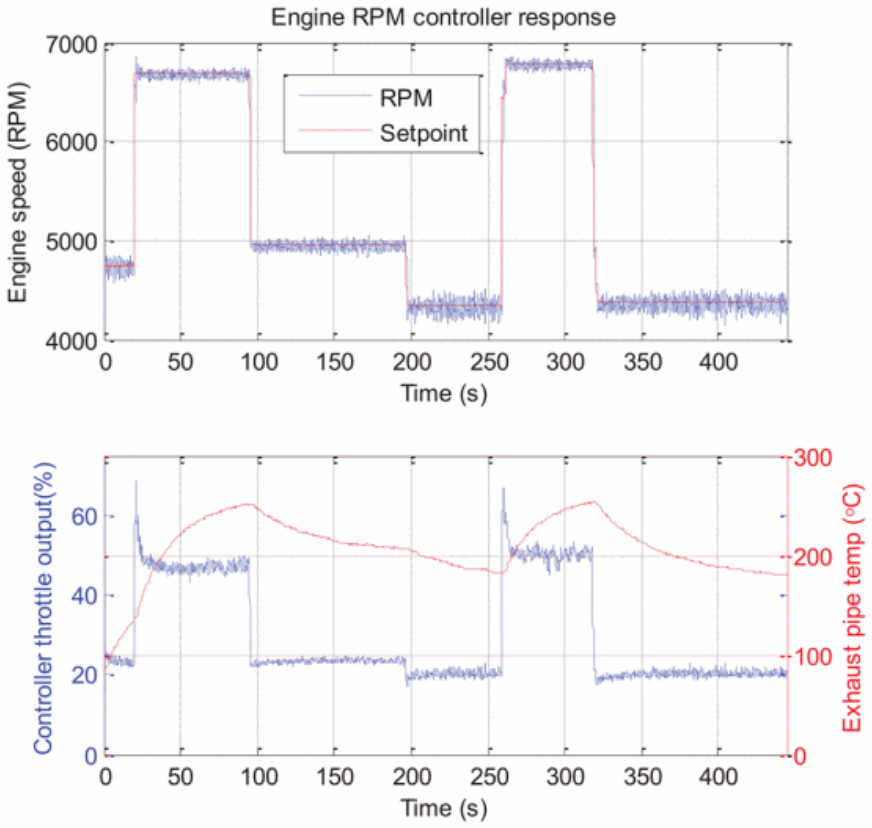

Figure 1.3 Engine RPM controller response graph and controller throttle

output and exhaust temperature from Cheng Kung University [9]

With regards to engine control, researchers were able to implement an incremental PID controller to account for different factors such as operating temperature, to ensure engine output was consistently matched to throttle inputs. Prior to implementation, the controller linearization was set by mapping the throttle input directly to engine rpm output. The implementation of this system resulted in multiple successful test flights of the multi rotor system, which were repeated in various different operating temperatures.

In a follow up paper two years later, the researchers further improved the performance of the engine controller by adding three different modes of the engine [10]. These modes are: start up, in flight, and shut down respectively. In addition, one thing to also consider with regards to engine control is the communication between the flight controller and engine controller. This communication may be impaired from factors such as engine vibration. Engine vibration is also an important factor which will significantly affect the stability of a system while elevated.

1.2.4 Propeller design and structure

Research on the design of propellers for gasoline-powered engines has been ongoing for many years, with numerous studies focusing on various aspects of propeller design, such as the number, size, and pitch of the blades, as well as their spacing and location. Research into propellers suggests that pitch and diameter may have the largest effect on a propeller's performance, with the pitch affecting the total acceleration of air and the diameter having a greater effect on the total thrust achieved [11]. It is noted however, that greater pitch results in lower efficiency, and propellers with larger diameters require more power to turn [12]. Another major factor of design is the number of blades and spacing. The number of blades influences the device's lift

capacity, stability, and noise level, with more blades generally providing greater lift and stability but also producing more noise and requiring more power. One study focused on designing a VTOL aircraft to carry a payload found that a hexacopter design has an endurance potentially 60% higher when compared to a quadcopter of the same width [13].

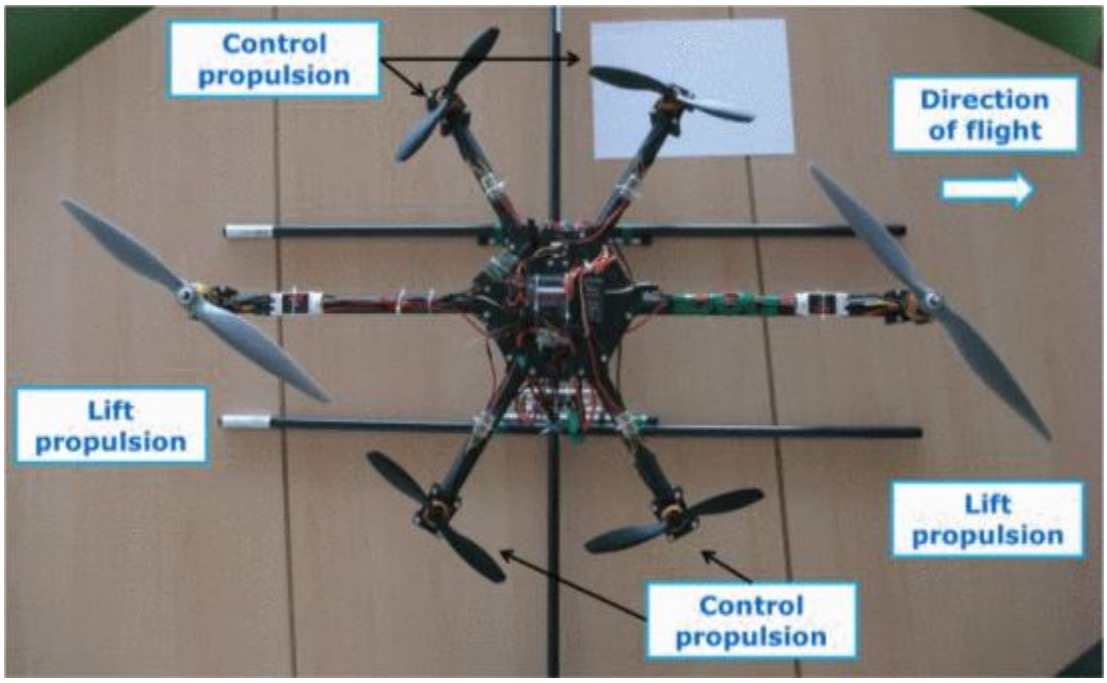

Figure 1.4 Top view of a demonstrator with a hexacopter configuration from KU Leuven, Belgium

Another One study from the 2016 International Conference on Unmanned Aircraft Systems discussed the effects of propeller configuration on the propulsion system efficiency of a multi-rotor system. It was found that three bladed propellers are less efficient compared to two blade propellers, however they result in a lower RPM for the same thrust, making them potentially viable for reducing noise [14]. Pusher vs puller configurations were also examined and it was found that pusher configurations result in a small increase in efficiency however, the configuration will ultimately result in more weight.

1.3 Structural Considerations

In the design of an intervention for high-altitude rescue operations, many considerations must be made to the structural stability of the intervention. As it stands, existing variations can be categorised structurally into two groups: free-standing, as is the case with aerial ladders and aerial platforms; and structurally mounted, as is the case with controlled descent devices and spiral slides. Both of these groups present their own individual challenges which must be addressed for the successful implementation of an intervention for high-altitude rescue operations.

For any free-standing structure, it is crucial to pay attention to the external forces that the structure will be subject to. The most important forces pertaining to an intervention for high-altitude rescue operations are forces due to dead loads, live loads, and wind loads. Other considerations include snow load and hydrodynamic loads. The National Building Codes of Canada, Section 4 demands that all of these loads be considered in the construction of a high-rise building [10], so it is only logical to consider these loads in the design of a device meant to rescue people from high-rises. These loads can create many modes of failure for the intervention, such as toppling, twisting, or buckling, so specific considerations must be made to prevent these modes of failure.

One of the most common methods for improving the structural stability of a freestanding structure is through the usage of guy wires. These are often seen on tall, thin structures such as radio towers and telephone poles, and can greatly extend the height of freestanding structures with relatively small

bases. Guy wires exert a tensile force on the structure to counterbalance any lateral forces being exerted by crosswinds, which may otherwise cause the structure to sway or topple [15]. Multiple guy wires can be implemented to counterbalance forces exerted in multiple directions to address any twisting forces caused by the crosswinds as well. The principles of guy wires can be incorporated into the design of the intervention to address these modes of failure.

Conversely, a mounted device is more resistant to external forces as it can rely on the building upon which it is mounted to provide structural stability to the device. However this has the consequence of reducing the device's versatility as compared to a free-standing device, as a mounted device requires an existing mounting point to interface with. Versatility is an especially moot point when one realises that most existing interventions which are mounted, are designed to be permanently mounted from when the building was initially constructed.

One possible solution is to combine the best of both worlds, by designing a freestanding intervention, with the option to be mounted if viable. For instance, many high rises include mounting points on their roofs for window cleaning platforms. In instances where a freestanding intervention could extend a device to attach to these mounting points, the motion of the intervention could be further constrained, leading to an even greater reduction of degrees of freedom and thus a more structurally sound intervention.

CHAPTER 2: Design Process

2.1 Statement of the Problem

The need for a reliable and cost-effective high altitude VTOL has become increasingly important in recent years. The current options available, such as aerial lifting platforms and helicopters are often expensive and not easily accessible. As a result, there is a growing interest in the development of multi propeller lift devices, such as quadcopters, which can be used for a wide range of applications such as high altitude lifting or rescue operations. Most of these existing devices rely on electric motors due to their quick response time and feasibility for multi propeller platforms. While electric motor and battery systems have been successful in many applications, they possess poor power density, which limits the endurance and payload capacity of these devices. This limits their practicality for high altitude lifting operations, which often require longer flight times and greater thrust. The use of an Internal Combustion Engine (ICE) may be a potential solution to this issue, as it can provide longer flight times and greater thrust than current electric motor systems. Therefore, the purpose of this project is to investigate the viability of using an ICE in a gas-powered VTOL for high altitude lifting operations, and to explore the potential benefits and limitations of this approach.

2.2 Requirements Analysis

To initiate the design process and establish criteria to measure the performance of the device, the following characteristics, functional requirements, constraints and performance metrics were developed. These four criteria specify the desired design requirements, and provide a guideline of goals to be achieved. The criteria specified in this section is kept in mind throughout the entire design, development and construction of the final device. Reviewing the criteria listed in the table below, a high payload capacity is necessary to ensure that the device can lift heavy loads to high altitudes. Additionally, a long flight time is important to enable the device to reach and maintain its desired altitude for extended periods. To ensure that the device is practical for use in various settings, it is important to also consider its size and weight. A compact design is ideal as it allows for ease of transport and manoeuvrability. Low vibrations and noise are important features to minimise any disturbances during operation. Furthermore, the stability of the lifting structure is crucial in preventing the device from flipping or rotating, especially at high altitudes where the effects of wind and turbulence can be significant.

Table 2.1 Definition of problem

Characteristics	Functional Requirements	Constraints	Performance Metrics
Robust	VTOL device does not deform under operation	Deflection in the metal chassis must be <5°	$\frac{L}{2} \times tan(\theta)$ (Deflection at each end of the VTOL device wing)
Payload capacity	VTOL device must produce enough thrust for carrying a payload	Net thrust>20N	$T_{Net-Thrust} > 20N$
Enduring	System components must operate within temperature ranges they are designed for as well as run for a substantial amount of time	Clutch assembly between 200°C-250°C Engine must between 82°C-115°C Gearbox 30°C-40°C Must maintain operation for at least 30 minutes	$200°C < T_{clutch-op} < 250°C$ $82°C < T_{engine-op} < 115°C$ $30° < T_{gearbox-op} < 40°C$ $Operation\ Time\ > 30\ min$
Compact	Must not take up too much volume and be lightweight	Maximum Volume: 120cm x 120 cm x 40cm Mass: 50% of thrust capacity	□□□□ □□□□□□ $< \frac{576000cm^2}{4 \times 50\% \times T_{Rated\ Thrust\ of\ Prop}}$
Safety	Vibrations should not loosen any Fasteners Process of shutting down should be simple	Torque: Allowable deviation of 5% from before operation Distance: Safe distance from Propellers >5m	$\left\lvert \frac{Toque_{after}}{Torque_{before}} - 1 \right\rvert \times 100 \leq 5\%$

2.3 Preliminary Concept Designs

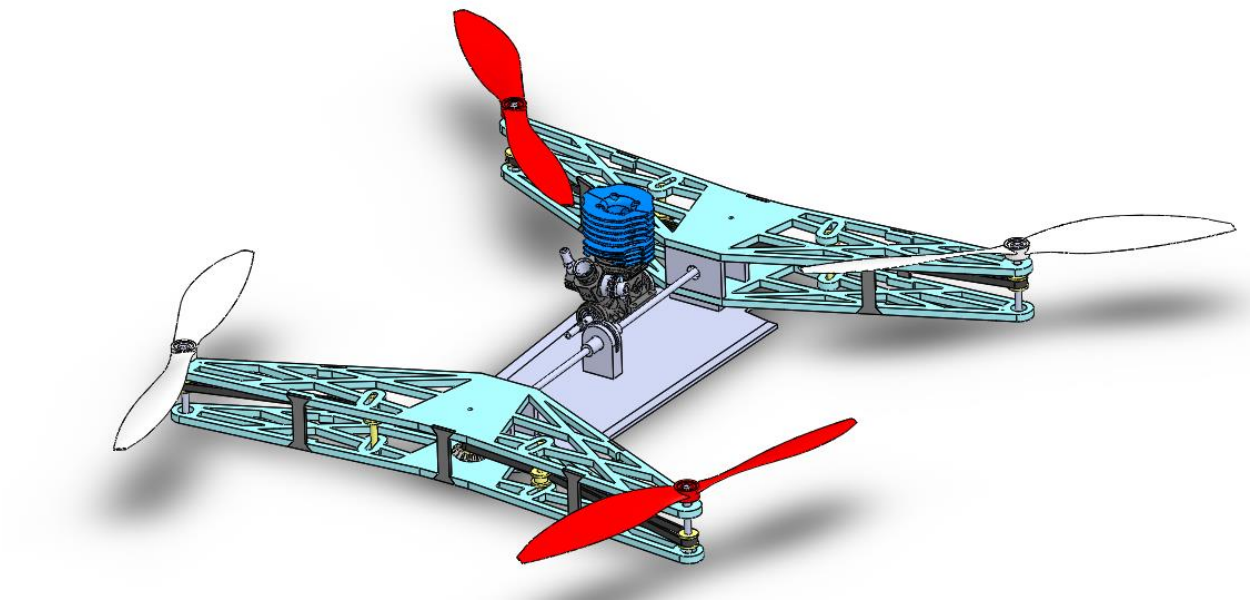

Figure 2.1 Preliminary VTOL Design

This design was made with the concept of modularization in mind. The scaled down model of VTOL device will have all the same characteristics as the actual model. However, to achieve the desired net lift for any application in the real model, multiple VTOL devices will be used together to support its payload. Each VTOL device will be aero cooled engine, capable of generating a net positive thrust.

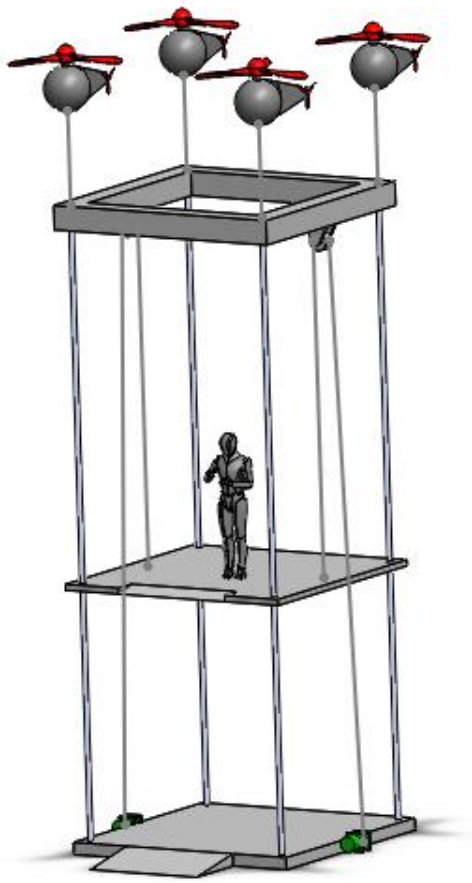

Figure 2.2 Preliminary concept design

Starting from the ground the base platform is there to anchor the system. From the base platform there are 4 sets of steel cables which are attached to the suspended platform. The goal here is to make sure there is enough tension between the platforms to ensure stability and rigidity. There is a pulley attached to the suspended platform and a cable running from the pulley, attached to the transport carriage, and connected to a winch on the anchor. The winch-pulley system is there to actuate the carriage platform which is on top of the anchor and connected to the frame. The suspended platform will then be supported and pulled upwards by a system of VTOL devices, each carrying a portion of the weight of the system.

2.3.1 Mind Mapping

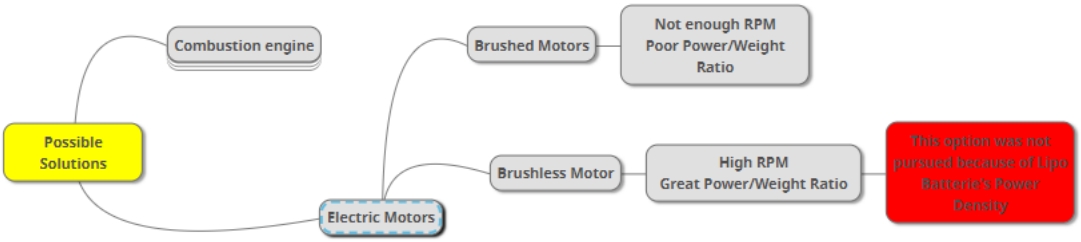

Figure 2.3: Mind Map Part 1

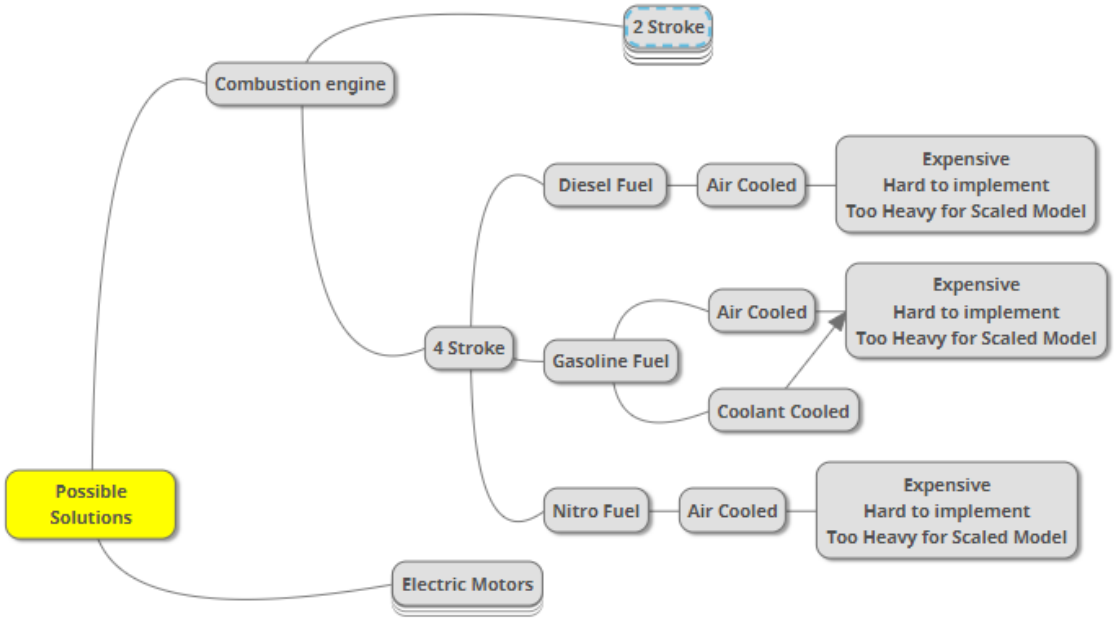

Figure 2.4: Mind Map Part 2

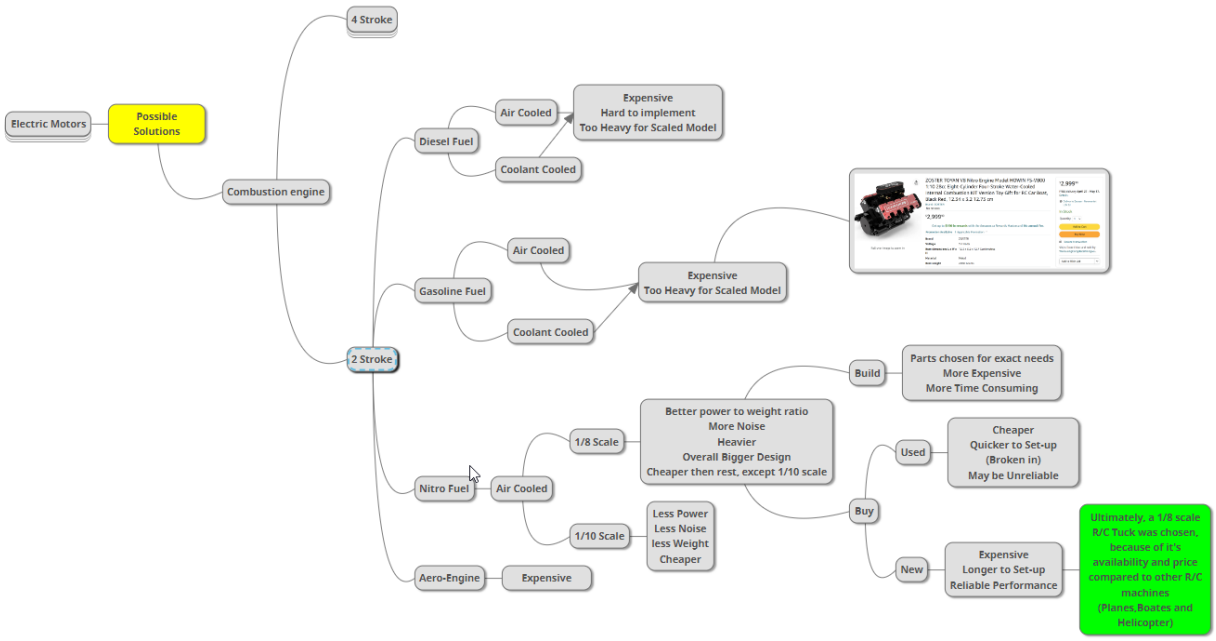

Figure 2.5: Mind Map Part 3

2.3.2 Black Box Method

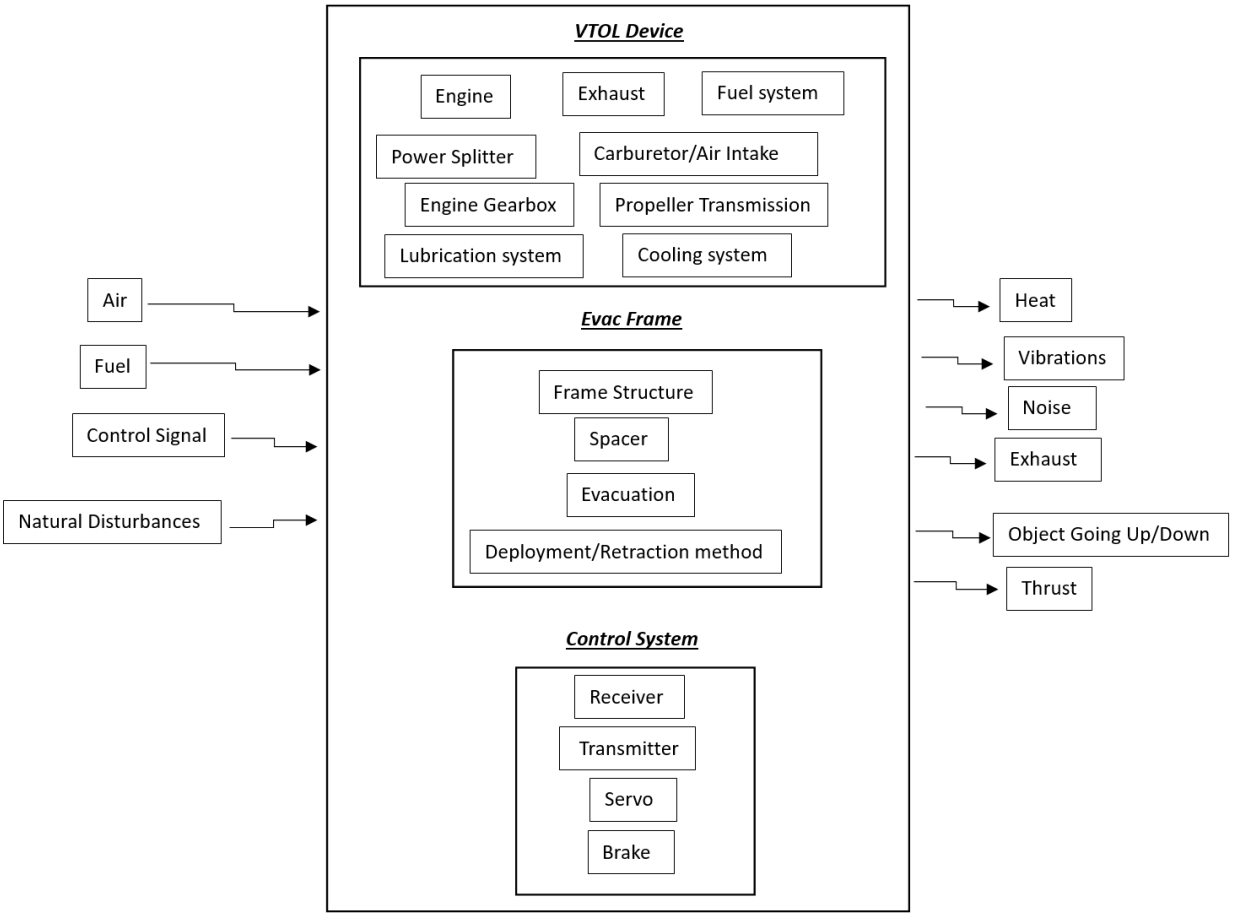

Figure 2.6 Black box Diagram

2.3.3 System and Subsystems

Based on the project scope, research and the requirements analysis, a two stroke engine for the powertrain was pursued. Researching potential options, the 28SH nitro engine was identified due to its reliability, accessibility and good power to weight ratio.

Figure 2.7 28SH Engine used in the design[16]

The team then purchased an RC car powered by this engine, as it readily had components such as the fuel tank, exhaust, gearbox, and chassis to use as a base to build a quadrotor device from. The figures shown below, outline the components and features of the platform.

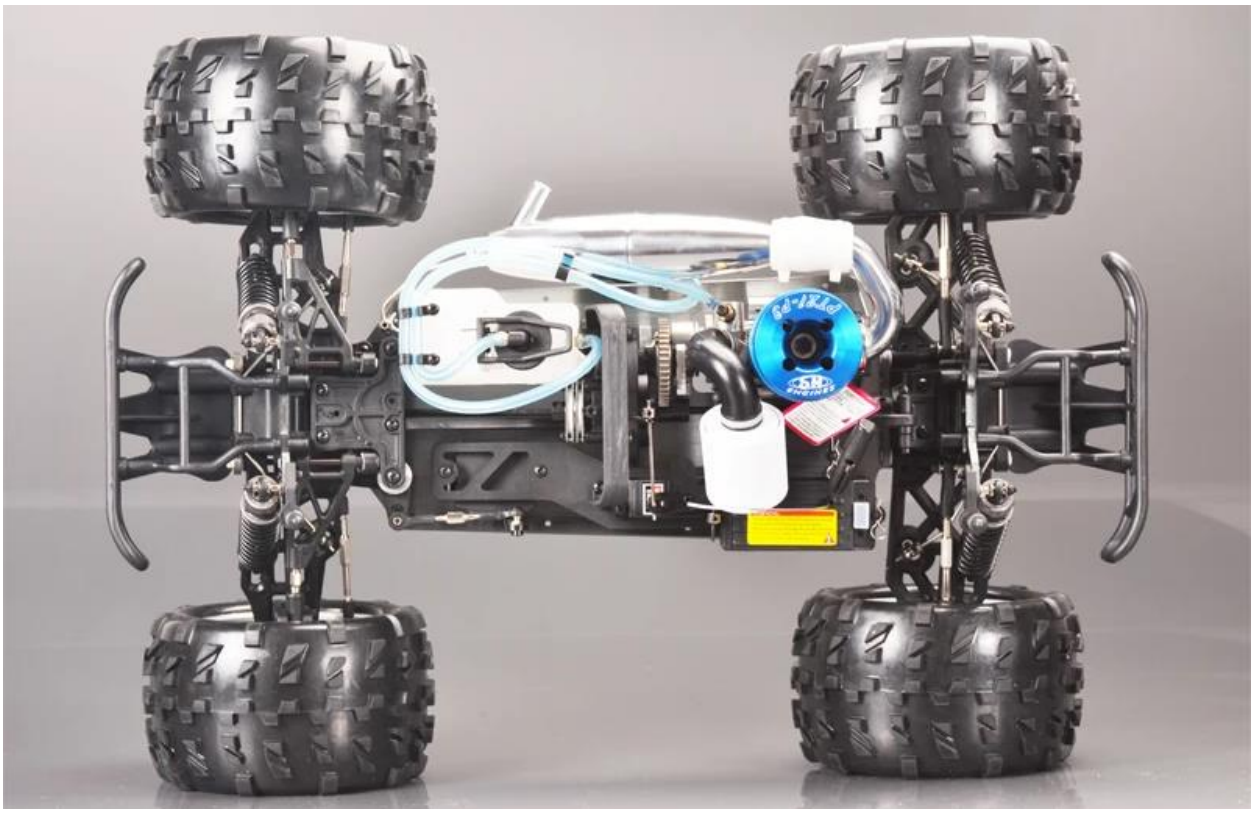

Figure 2.9 The components of the RC truck [17]

Control System

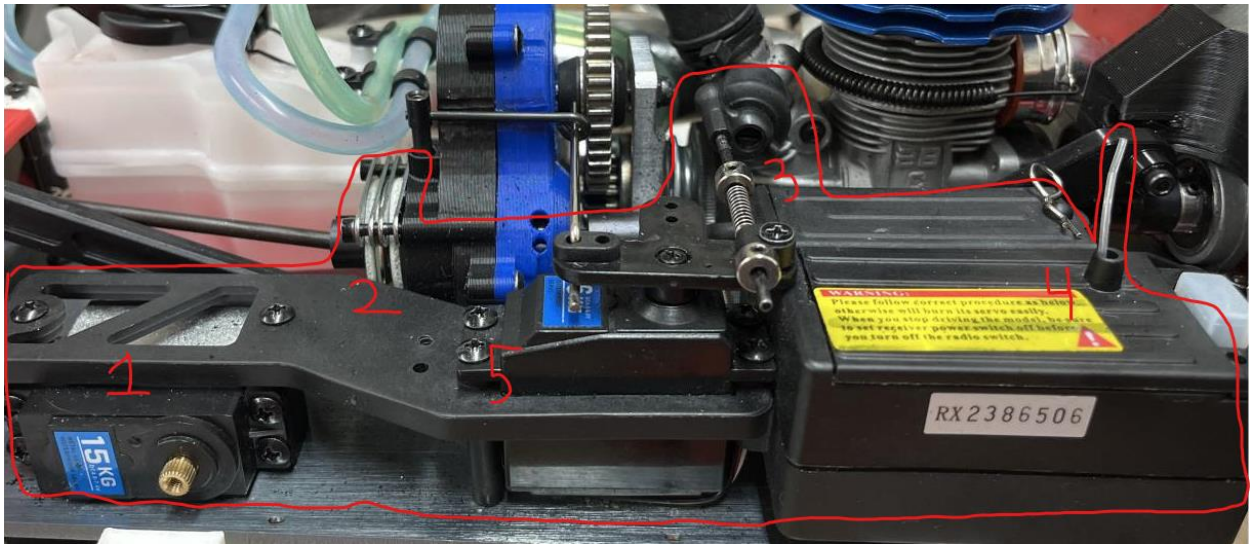

Figure 2.10 Diagram of the engine throttle control

1) Steering servo (unused-disconnected)
2) Brakes, used for slowing down the output shafts of the transmission
3) Carburetor opening- used to adjust the mount of air fuel mixture that is led into the the engine (control RPM)
4) Batteries/Receiver - receives the control signal from the Transmitter (RC)
5) Servo motor used to control carburetor opening

Power Transmission

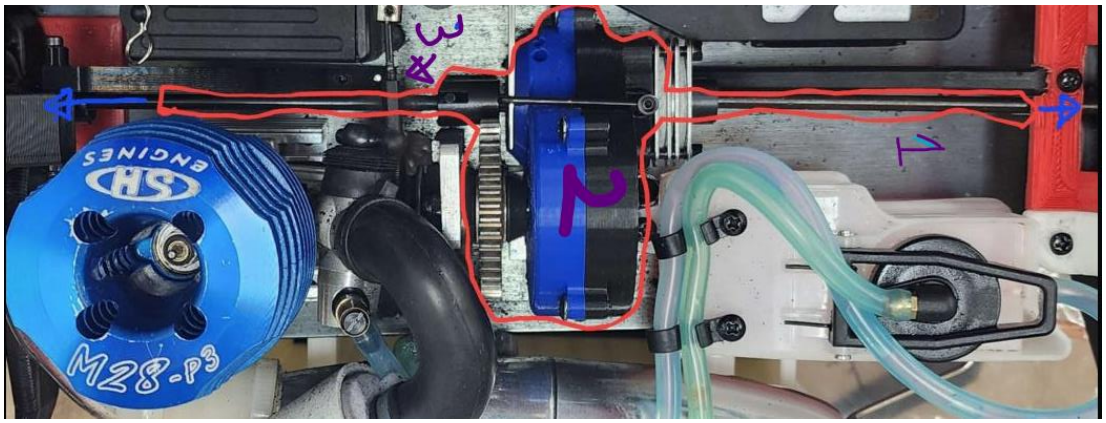

Figure 2.11 Diagram of the power transmission system.

1) Forward output shaft
2) Gearbox which takes the power of the engine and splits it into two output shafts
3) Rear output shaft

Power Generation

Figure 2.12 A closeup of the 1/8th scale nitro engine

Lift Generation

Figure 2.13 The APC 13x6.5 inch Electric motor propeller was chosen [18]

2.3.4 Embodiments and Morphological Chart

Table 2.2 The Morphological Chart for the VTOL device

VTOL Device	
Propeller Transmission	Lubrication
Bevel gears 	Motor Oil 
Belts and pulleys 	Grease 

2.3.5 Evaluation of Concept Designs

For the VTOL device, the preliminary design was used as a basis for the development of all the iterations of the concept designs. The preliminary design served to demonstrate all the key features that were desired in the final design of the VTOL device, as well as their relative locations. These key features included: four propellers arranged in a square pattern, cutouts in the frame components for weight reduction and to allow the lift generated from the propellers to pass through the frame. It was also desired that the propellers be powered by the OEM universal shaft from the RC car.

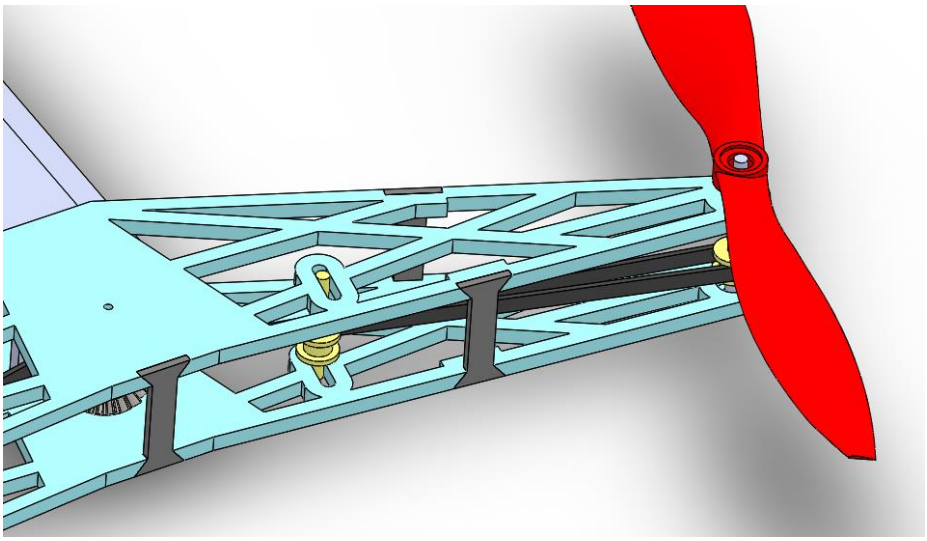

Figure 2.14 Cutouts in the frame components

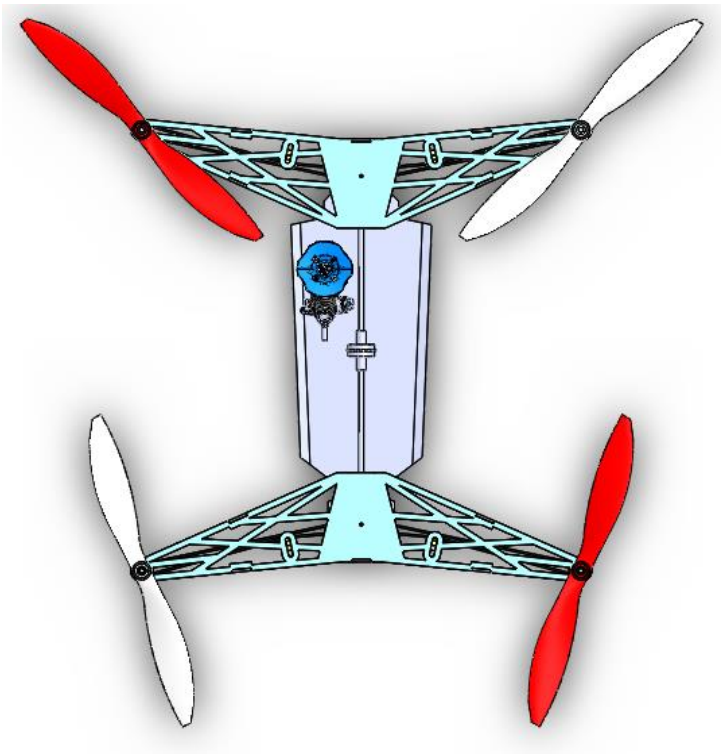

Figure 2.15 The arrangement of the propellers

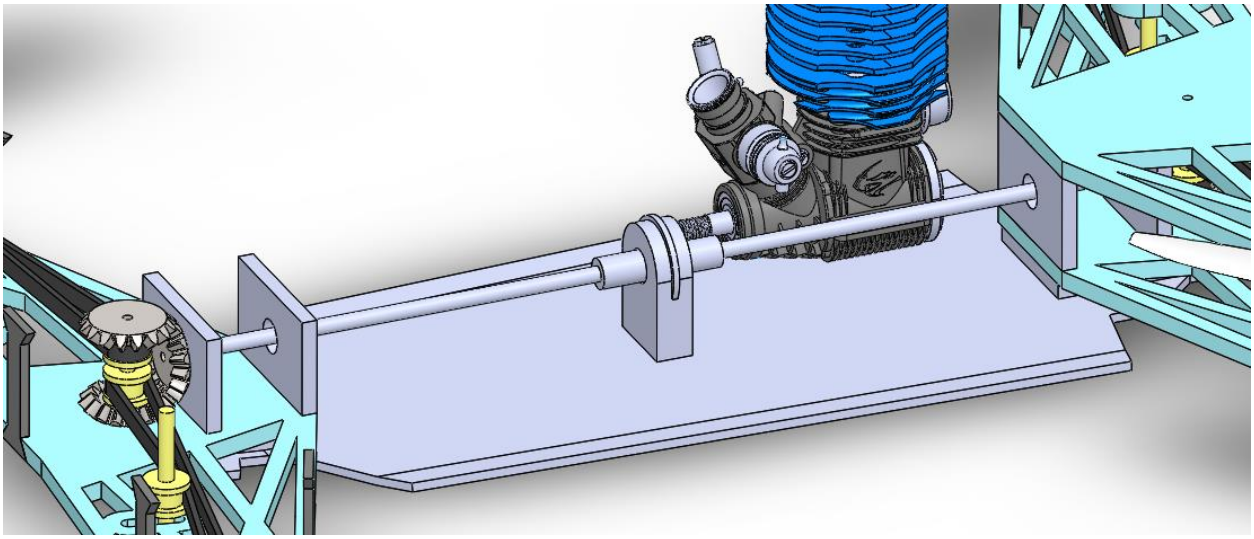

Figure 2.16 The approximate relative position of the OEM universal shaft

For the preliminary design, belts and pulleys were considered due to their ease of implementation when compared to other power transmission mechanisms such as shafts, gears, or chains and sprockets. Despite this, it

was still necessary to employ a set of bevel gears, as the plane of rotation of the OEM universal shaft was perpendicular to the plane of rotation of the propellers. Within the preliminary design, the belts and pulleys were attached to the bevel gears in an over-under configuration such that the belts would cause the propellers to counter-rotate against each other. The implementation of an idler pulley in a slot was considered to act as a tensioner for the belt.

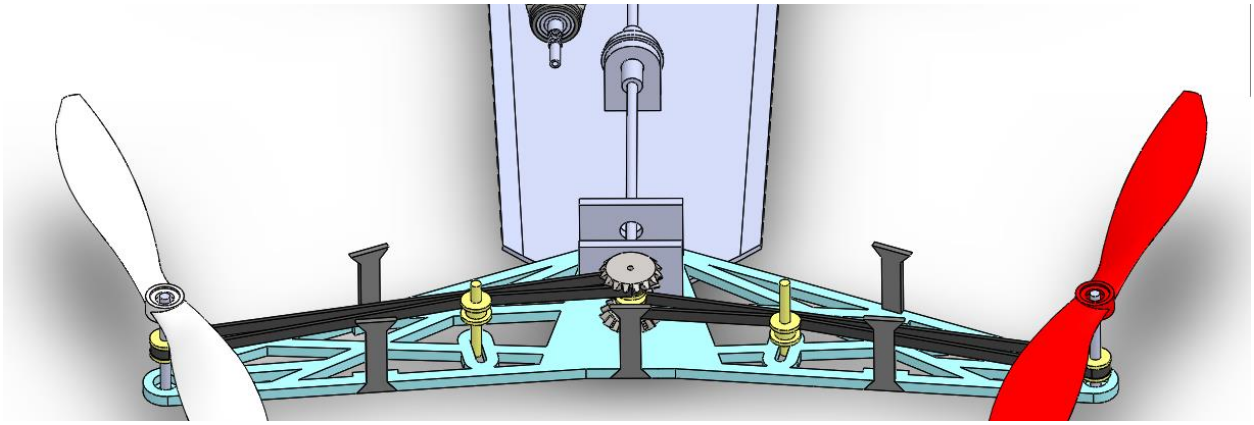

Figure 2.17 A top view of the pulley position and linkage

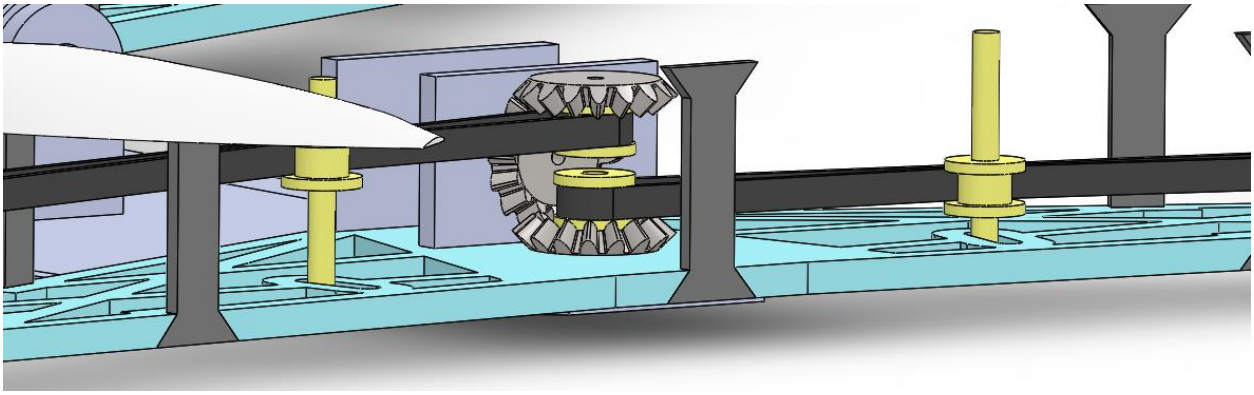

Figure 2.18 The over-under pulley configuration

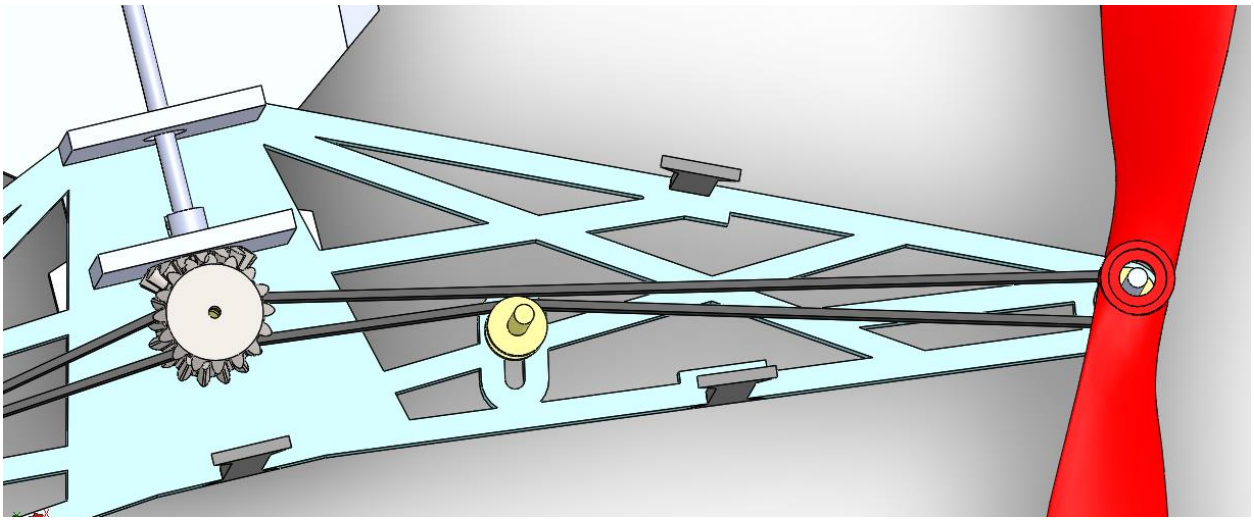

Figure 2.19 The tensioner idler pulley

The next iteration of the VTOL device involved realising the preliminary design using real-world components. Structural and dynamic analysis calculations were used to determine the size and specifications of the components required to construct the VTOL device. Considerations were made specifically to the diameter and lengths of any shafts used, as well as the diameter and force-transferring capabilities of the pulleys used.

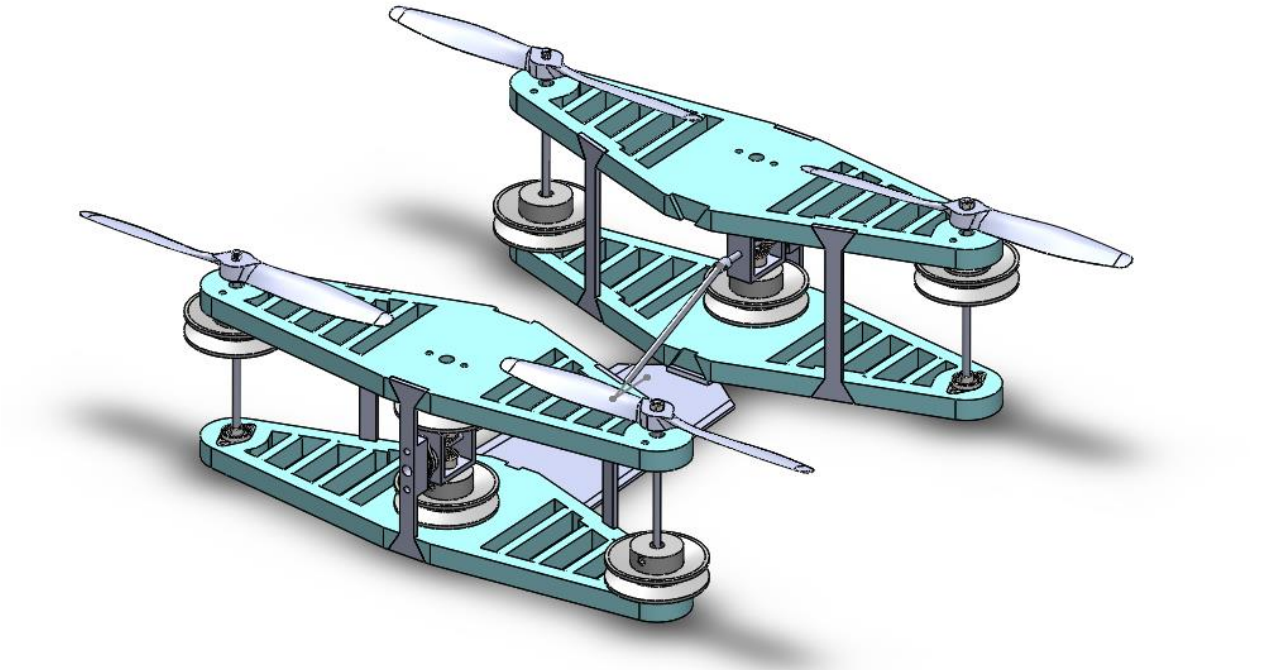

Figure 2.20 Overview of second iteration

For the central bevel gears, a bevel gearbox with a casing made from machined aluminium was considered. The machined aluminium casing was favourable due to how it fully straddles the bevel gears, which helps with the positioning and alignment of the bevel gears.

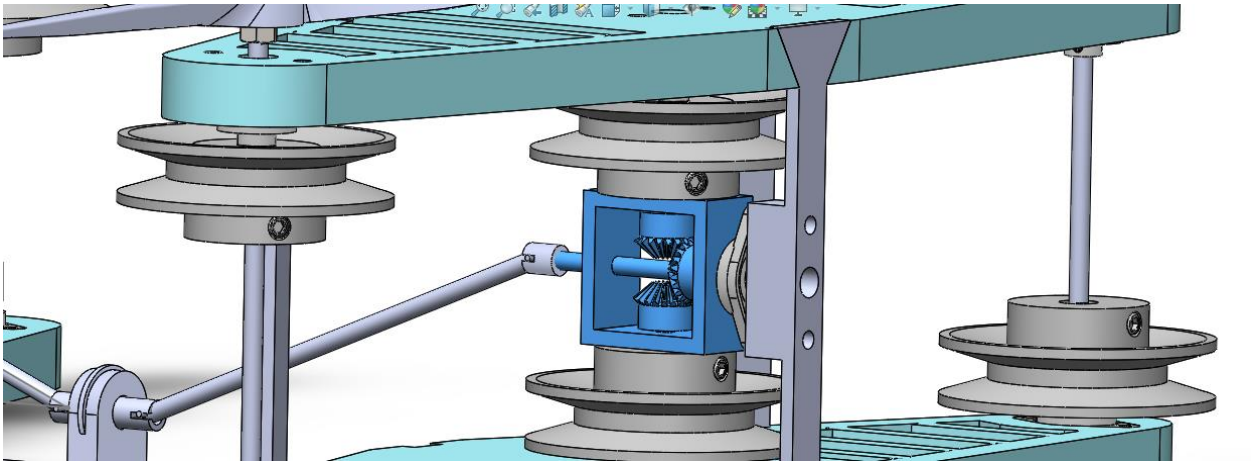

Figure 2.21 The aluminium gearbox

It is of note that during the creation of the preliminary design, the size of the pulley needed to transfer the forces required was severely underestimated. When redesigned to incorporate the pulleys specified by the calculations conducted, it was determined that the design had two major flaws stemming from the size of the pulleys increasing the height of the device to beyond 20cm tall. The height of the pulleys caused the shafts used to mount the propellers to become too long to be safe relative to their diameter; and the excessive height caused the angle of the universal shaft to be raised to an unacceptable value.

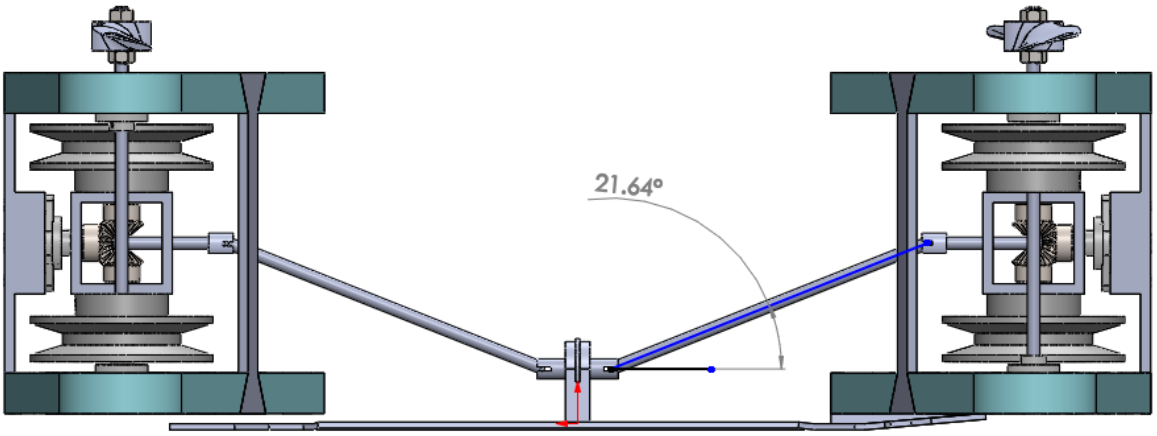

Figure 2.21 The angle of the universal shaft

For the next iteration of the VTOL device, the belt and pulley power transmission system was discarded in favour of another shaft and bevel gear linkage. The main goal of this iteration was to address the height issue of the previous iteration. The aluminium bevel gearbox was preserved in this iteration however its orientation was rotated. This iteration reduced the height of the VTOL device by roughly 10cm from the previous iteration, and was used in the construction of the prototype of the VTOL device.

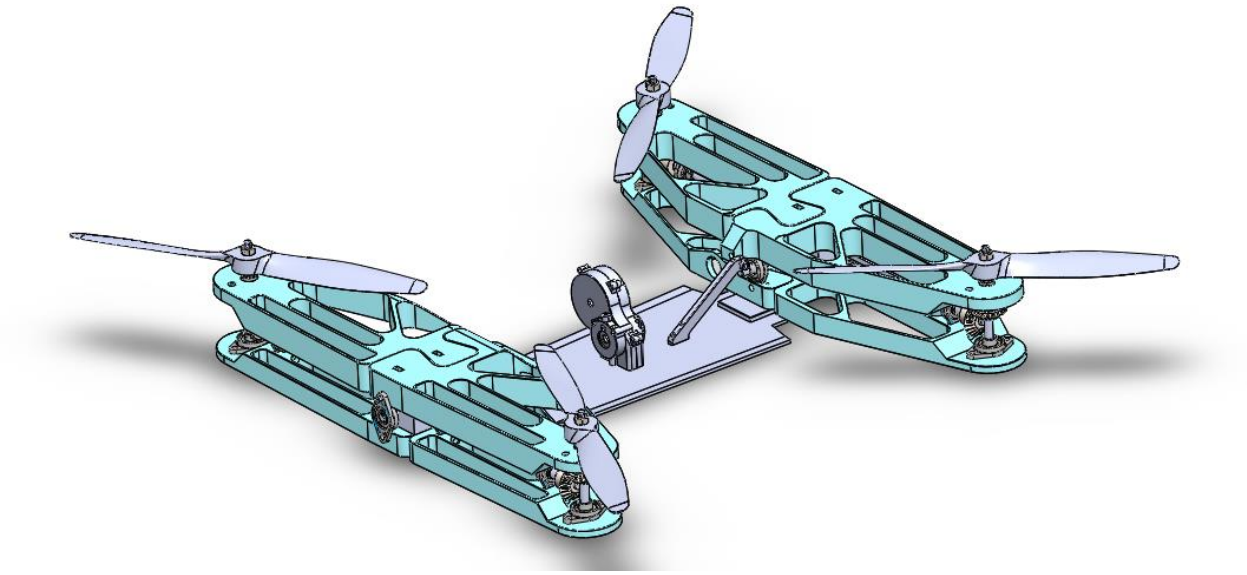

Figure 2.22 An overview of the final concept design

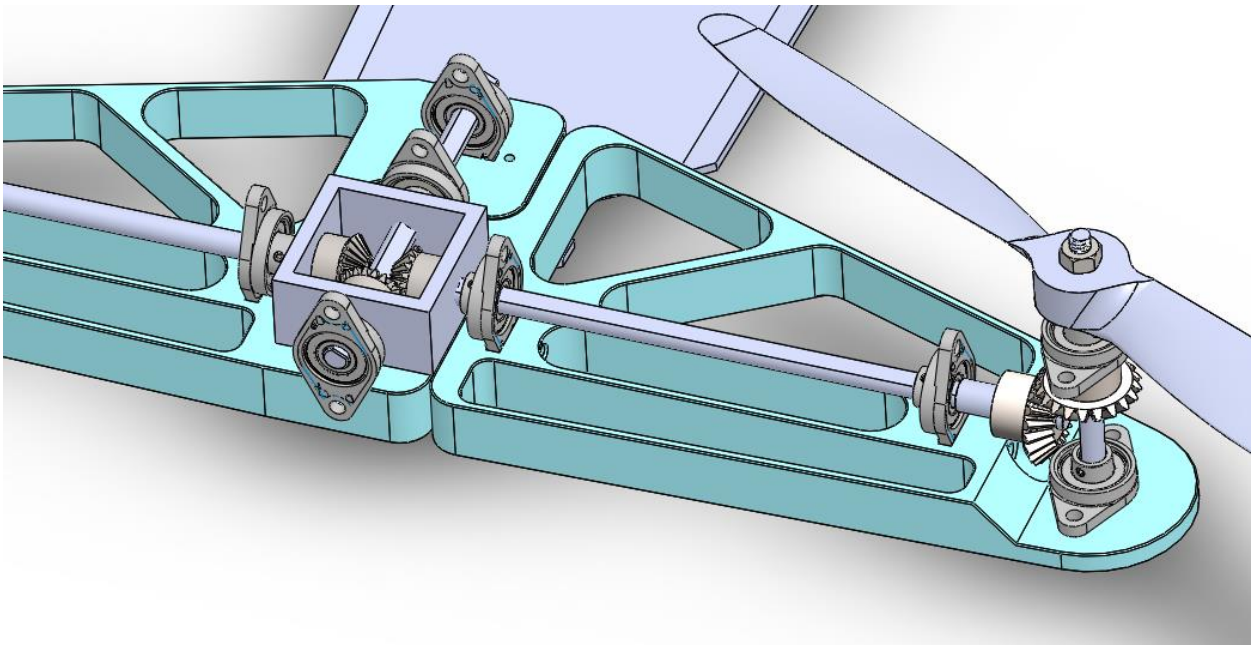

Figure 2.23 The bevel gear shaft linkage

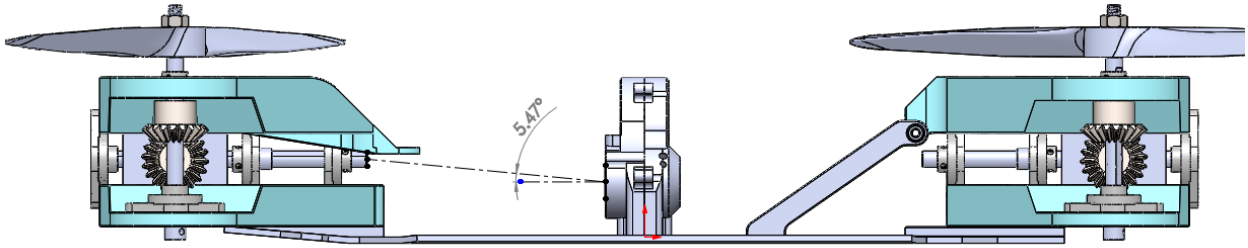

Figure 2.4 The reduced angle of the universal shaft

CHAPTER 3: Design, Development and Construction

3.1 Design Considerations

Design considerations for many different components were conducted. This includes investigations into multiple different solutions for one subsystem. Each component investigated and designed had multiple iterations which progressed independently of other components. It was found that some components were infeasible solutions for the required subsystem as such some approaches were abandoned and not implemented in the final design. This occurred for various reasons, notably, improper scale of application and lack of accessibility. Nevertheless, design and development work for all components investigated are found within this chapter, as well as in Appendix A.2.

3.1.1 Powertrain - Shaft design

The objective of this process is to design a power delivery system which transfers the output of the engine transmission and splits it evenly into two output shafts to which the propellers will be attached to.

The design criteria for the shafts are to be structurally stable, minimise potential vibrations and to provide reliable power transmission while remaining compact

Over the span of the project, the powertrain design of the system progressed through three iterations, beginning with the use of a pulley belt system and finalising on a system solely using shafts. Over these iterations, significant improvements were made on the design, with increased support for reduced bending and increased factor of safety (FOS). The design choice to use shafts

over a pulley was made for numerous practical reasons, however, high cost and low accessibility of high quality components made the choice unsensible for the scale of this project. Details of each design are showcased below in Table 3.1.

Calculations for the shafts were necessary as these shafts are to undergo substantial loading from the powertrain. As such, design calculations to ensure ideal performance and sufficient FOS were conducted. Firstly, the reaction forces and moments to be experienced by the shaft were calculated using Eq 3.1 and 3.2 and a free body diagram was created. It was determined that the shafts will experience radial forces and a torque located at the pulleys, and axial forces caused by the thrust generated. An initial estimate was made for the shaft diameter, 1035 CD steel was chosen for the material and a rough sketch of the shaft design was made with appropriate dimensions.

Using the parameters mentioned above, the deflection of the shaft was calculated, to ensure that during operation there is not a major wobble in the shaft. Secondly, stresses were calculated using Von Mises stresses given by Eq 3.3 and 3.4, in which the critical location on the shaft was determined to be the pulley based on the shear and moment diagram. After calculating the FOS, it was observed that the stresses were too great for the chosen shaft diameter and so a design decision must be made. FOS estimates were calculated using the Goodman failure criterion seen in Eq 3.5.

$$\Sigma F = 0 \ (For\ a\ rigid\ body\ in\ static\ equilibrium) \tag{3.1}$$

$$\Sigma M = 0 \ (For\ a\ rigid\ body\ in\ static\ equilibrium \tag{3.2}$$

$$\sigma_a{}' = [\ (\frac{32K_f M_a}{\pi d^3})^2 + 3\ (\frac{16K_{fs}T_a}{\pi d^3})^2]^{1/2}\ (Midrange) \tag{3.3}$$

$$\sigma_m{}' = [\ (\frac{32K_f M_m}{\pi d^3})^2 + 3\ (\frac{16K_{fs}T_m}{\pi d^3})^2]^{1/2}\ (Alternating) \tag{3.4}$$

$$\frac{1}{n} = \frac{\sigma_a'}{s_e} + \frac{\sigma_m'}{s_{ut}} \ (Goodman\ failure\ criteria) \tag{3.5}$$

$$S_e = k_a k_b k_c k_d k_e S_e' \ (Endurance\ limit) \tag{3.6}$$

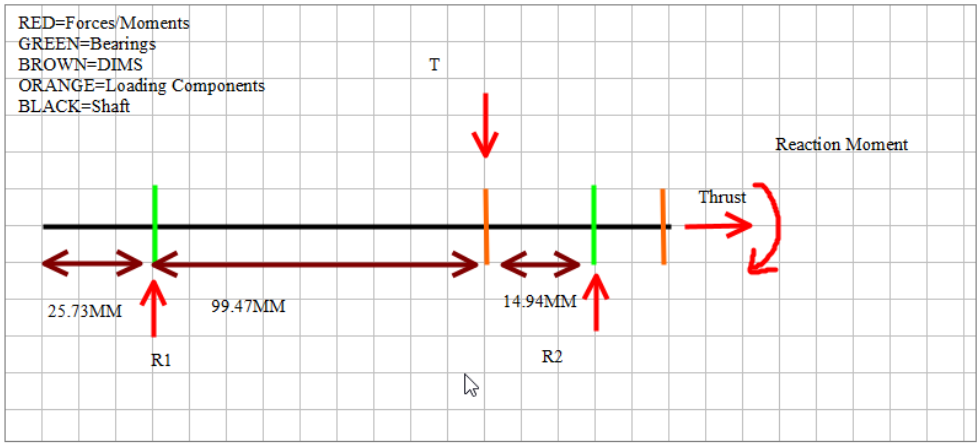

Figure 3.1 Drive Shaft Free body diagram[1]

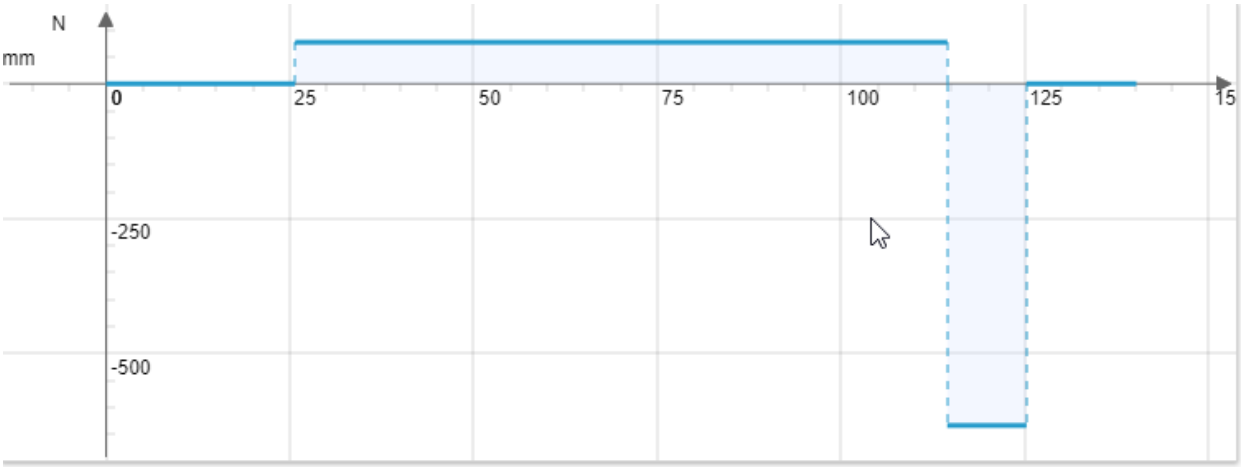

Figure 3.2 Shear Graph[1]

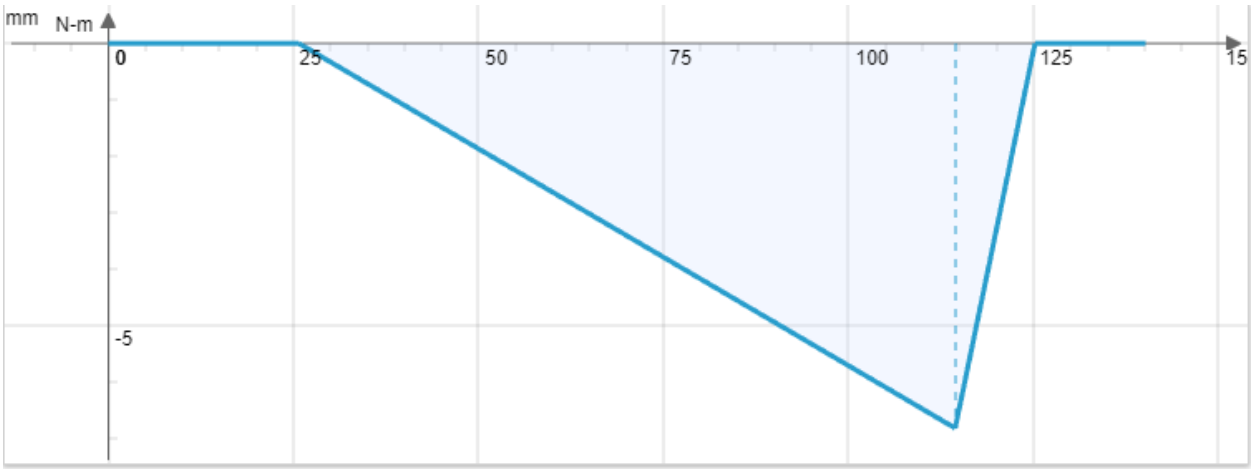

Figure 3.3 Bending moment graph[1]

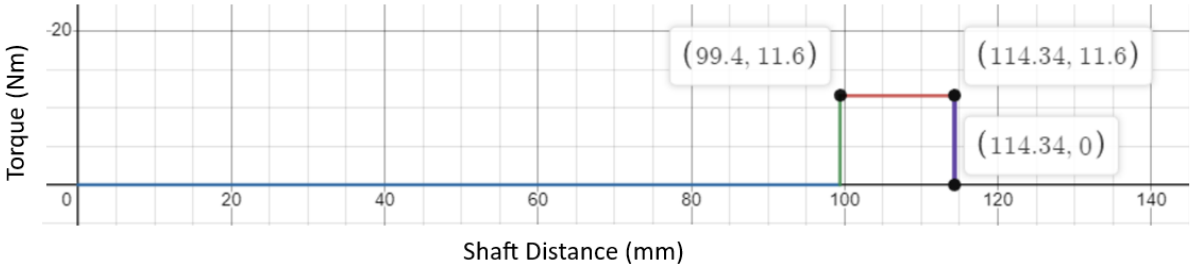

Figure 3.4 The location and magnitude of the torque

In iteration 3 specifically, there existed three support bearings in line with each other, leading to a statically indeterminate problem. To circumvent this, the bearing located in the middle of the other two was discarded. This choice leads to a more conservative calculated FOS compared to the actual FOS.

1 Graphs not to scale

Figure 3.5 The three support bearings. Bearing number 2 was discarded in the final assembly

As a shoulder was added to the shafts in iteration 3, notch FOS calculations were also conducted.

Table 3.1 Design iterations of Power train shaft design

Iteration	Design Features	Improvements over previous iteration	Problems
1	Pulleys attached to driveshafts with belts transmitting power to propellers. Relatively high L/D ratios with only two bearings supporting axial and bending loads.	NA	Maximum bending moment of shaft is too high, requiring at least a 15mm shaft for yield and fatigue safety factors.
2	Smaller length shafts with pulleys located on the sides outside of the bearings, reducing bending moments and ensuring a straight axis.	Decreased L/D ratio. Use of three bearings over two results in much greater FOS with negligible bending moments	Symmetry of structure disrupted with pulley on the bottom half, requiring extra supports and leading to instabilities.
3	Shaft system used instead of pulleys and belts, with each shaft supported at three locations and no radial tension forces.	Replacement of pulleys with shafts removes slack.	NA

3.1.2 Powertrain - Transmission Gearbox

The objective of this gear design process originates from a problem caused by the RC car platform used. The transfer case which came with the RC car was a two stage automatic transmission operated by a centrifugal clutch to step up or step down depending on the rotational speed of the system. In addition, the step down of the transmission system was too great, resulting in a severely decreased maximum output RPM which was too low for the application powering the desired propellers. For the design of this device, complete control over the engine RPM is necessary as the thrust created by the propellers is proportional to the speed at which they rotate.

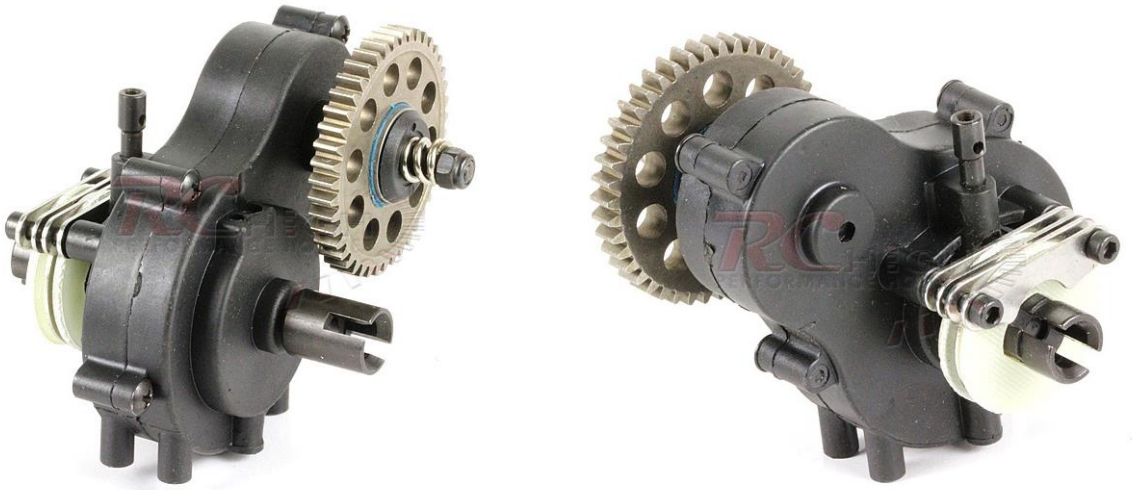

Figure 3.6 The OEM gearbox of the RC car platform [19]

To solve this problem, it was decided to reverse engineer the gearbox used in the RC car platform, and implement an overdrive gear ratio to increase the output RPM of the system. 3D printed PLA+ was deemed suitable to use to construct the replacement, as the OEM gearbox already relied on plastic parts. The internal geometry of the gearbox was modified to accommodate for the removal of the extra gears along with the centrifugal clutch. The brake functionality of the OEM part was also implemented in the redesigned gearbox. It was important that the centre-to-centre distance of the two shafts within the gearbox was maintained, such that the new gearbox would be a drop-in replacement. To this end, the specifications (module, pitch diameter, and number of teeth) of the OEM gears were used, however the gears were arranged in overdrive as opposed to the underdrive arrangement of the OEM gearbox. Shown below are the gear equations utilised to determine the module of the gears to be replicated.

$$Centre\ to\ Centre\ Distance\ = \frac{D_1}{2} + \frac{D_2}{2} \tag{3.7}$$

$$Centre\ to\ Centre\ Distance\ = \frac{N_1 \times m}{2} + \frac{N_2 \times m}{2} \tag{3.8}$$

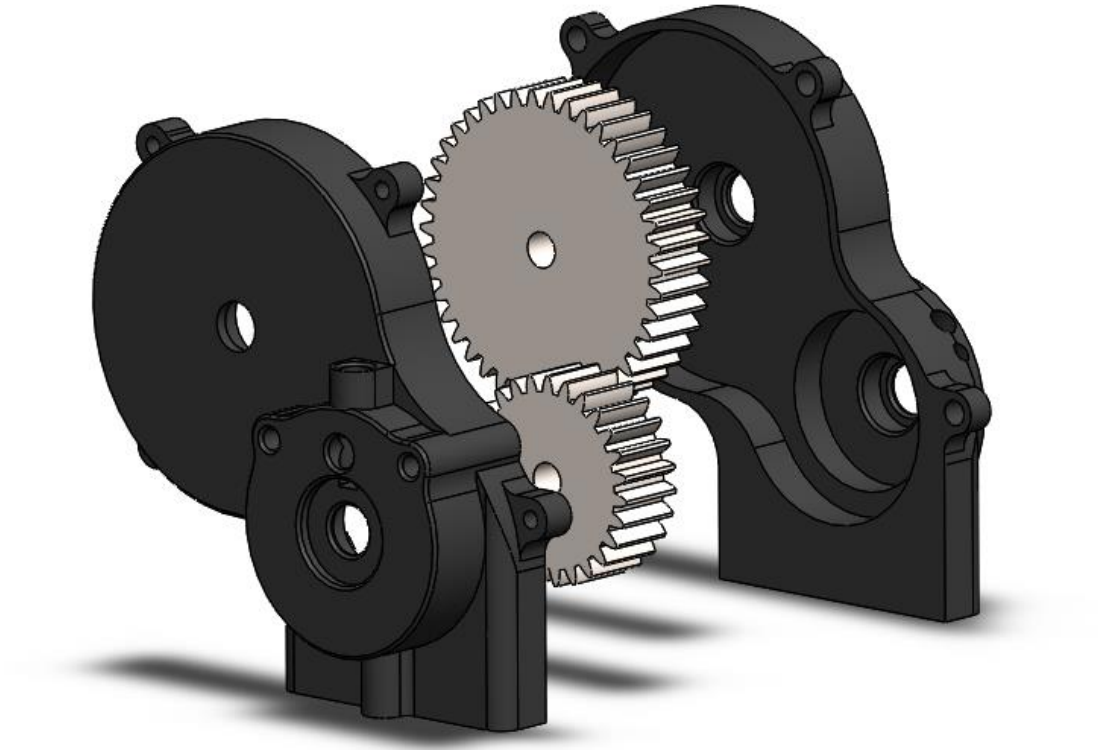

Figure 3.7 The CAD model of the replacement gearbox

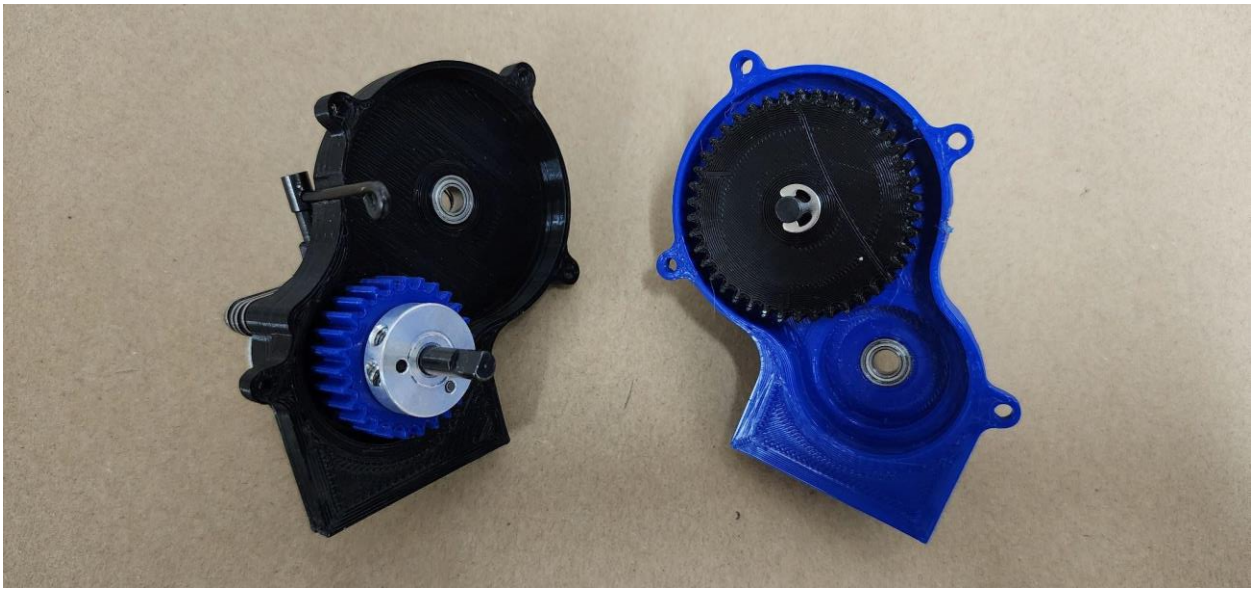

Figure 3.8 The inside view of the partially assembled replacement gearbox

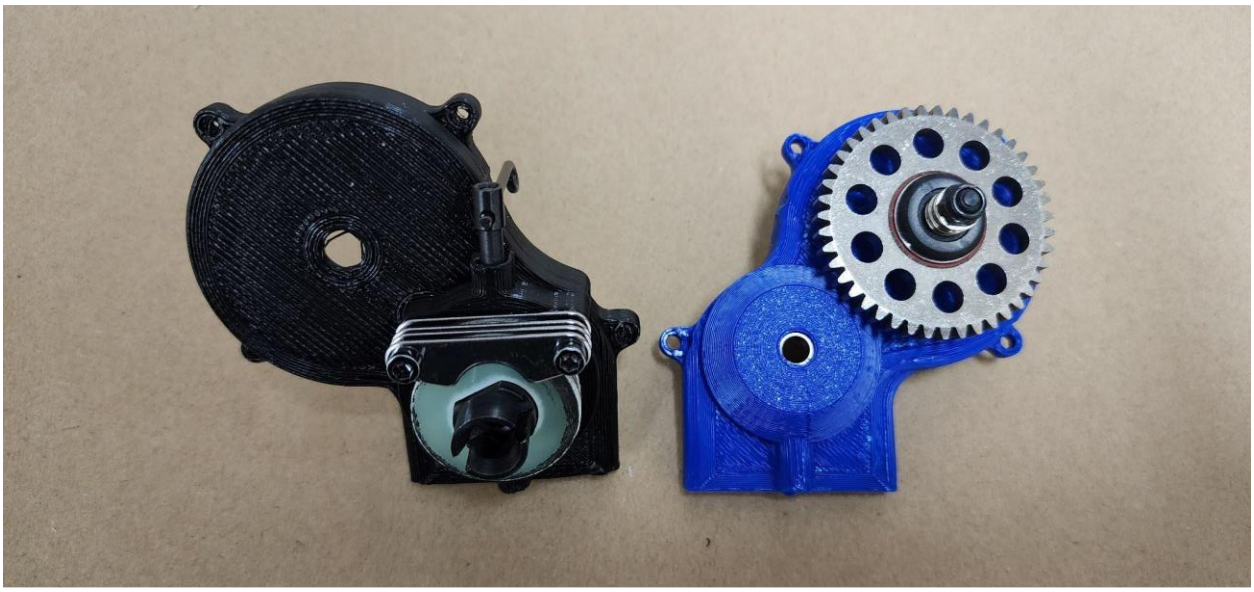

Figure 3.9 The outside view of the partially assembled replacement gearbox

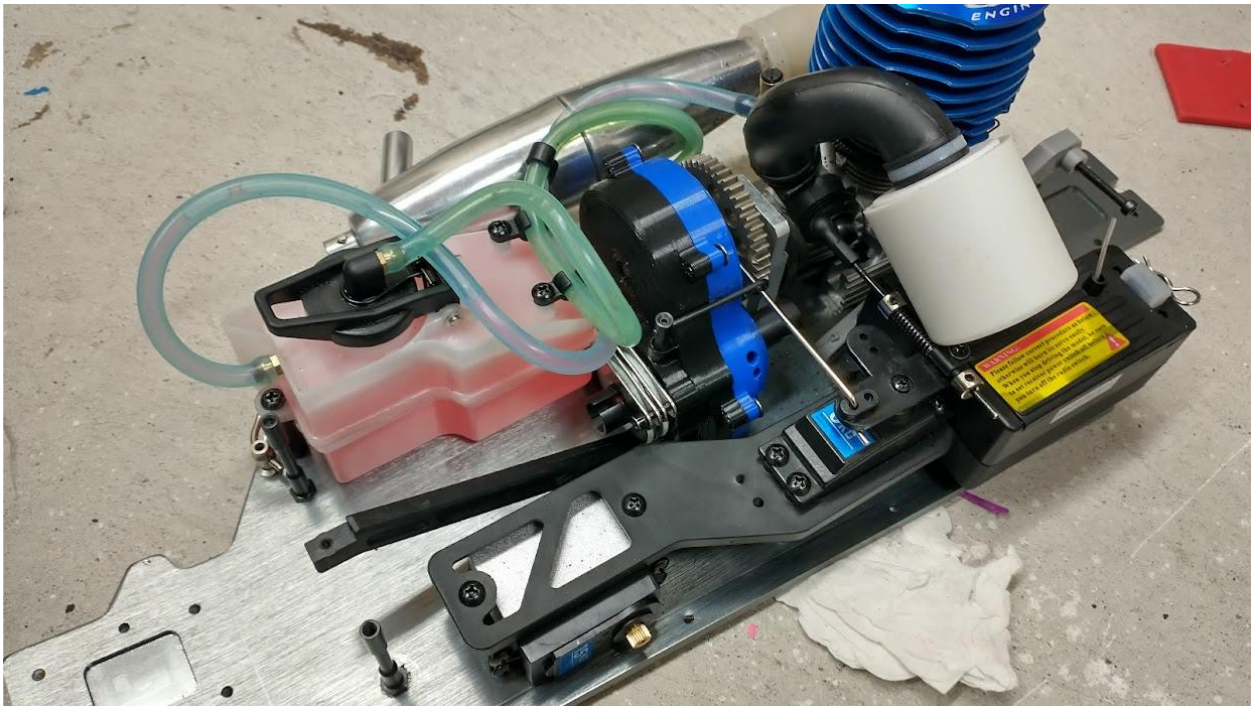

Figure 3.10 The replacement gearbox installed

3.1.3 Powertrain - Bevel Gearbox

The stock drivetrain of the RC car platform utilises a differential to transmit

engine power to the wheels. This drivetrain had implications regarding the stability of the device, as if one propeller encounters more resistance than the other one connected to it, the differential will divert power to the propeller with less resistance. This effect has the potential to start a negative feedback loop, which would indefinitely continue, progressively amplifying the instability. Therefore, the objective of the gearbox is to divert the power from the transmission gearbox and transmit it equally to two drive shafts, no matter the circumstance.

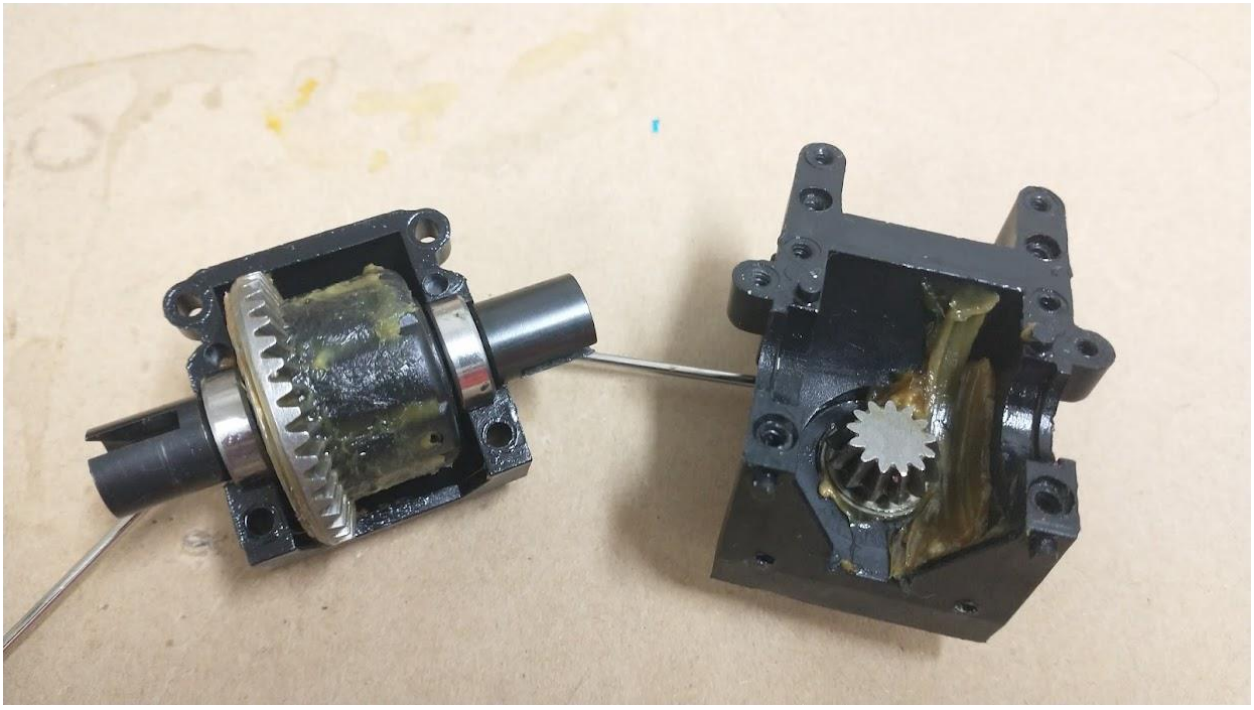

Figure 3.11 The OEM differential gearbox

To accomplish this task, design calculations were first completed analysing the bending strength and contact strength required for the task. Using Eq 3.9 to 3.12, the safety factor of the gear bending strength and contact wear can be found. With these calculations completed, it was decided to pursue a readily available, aluminium bevel gearbox designed for an 8mm shaft[18]. The gearbox is compact and has a 1:1 ratio, while also meeting the requirements established in the calculations. Furthermore, the bevel gears

are straddled by a machined aluminium case, which helps with the positioning and alignment of the bevel gears. While the gearbox is not suitable for high torque applications, it is more than adequate for use in a scaled model.

$$(s_t)_G = \frac{W^t}{F} P_d K_o K_v \frac{K_s K_m}{K_x J} \ (Gear\ Bending\ Stress) \quad (3.9)$$

$$(s_{wt})_G = (\frac{S_{at} K_L}{S_F K_T K_R})_G \ (Gear\ Bending\ Strength) \quad (3.10)$$

$$s_c = C_p (\frac{W^t}{F_N d_p I} K_o K_v \ K_m C_s C_{xc})^{1/2} \ (Load\ induced\ Contact\ Stress) \quad (3.11)$$

$$(s_{wc})_G = (\frac{S_{ac} C_L C_H}{S_H K_T C_R})_G \ (Contact\ Strength) \quad (3.12)$$

Figure 3.12 PGFUN 1:1 Right Angle Bevel Gearbox [20]

3.1.4 Pulleys

The use of pulleys was heavily investigated throughout the duration of the project. The objective of this investigation was to select a belt and pulley system to transmit power from the gearbox to the propeller shafts. The main design criteria is based on availability and integration, an ideal solution should also absorb vibration noise as well.

The design of the pulley system progressed through four iterations, each utilising different pulley systems, flat belts, V-belts, LT timing belts, and GT2 8mm width tooth profiles respectively. One of the recurring issues experienced in this design process was the accessibility and cost, as many of these systems were either very expensive or difficult to procure with long lead times. Moreover, the initial designs were bulky in size and excessive for the use case of this project. As iterations progressed, the size of the pulleys and cost decreased, however it was found that as the pulley systems became more reasonable, the stresses on the system increased. Ultimately, it was decided to not pursue a belt pulley system, due to the increased and unwanted stresses in the shafts experienced in the final iteration. One can see generic images of each system in Figures A, B, C and D below along with specific details for each iteration in Table 3.2.

Table 3.1 Design iterations of Belt Pulley system

Iteration	Design features	Improvements over previous iteration	Problems
1	Flat belts 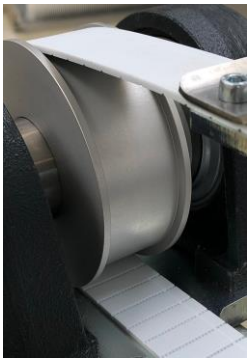 A	NA	The chances of slippage are too high to risk. Would require a lot more tension to make work effectively.
2	V-belts	Reduced chance of slippage Reduced tension required to operate the system effectively	Too rugged and bulky for the application. Resulting in higher frictional losses, reducing power output Costly to implement

	 B		
3	LT style timing belts  C	More procurable design and less bulky than V-belts	Difficult/expensive to find; still too bulky Larger heavier pulleys required increased load on the engine. Excessive for application
4	GT2 8mm width tooth profiles  D	More compact design and widely available tooth profile.	Still expensive; stresses on the system were still too high. Would require major redesign of propeller layout

To determine the wrap angle for an open belt configuration, Eq 3.13 was used:

$$\theta_A = \pi + 2\,(sin^{-1}\,\frac{R_A - R_B}{C}) \qquad (3.13a)$$

$$\theta_B = \pi - 2\,(sin^{-1}\,\frac{R_A - R_B}{C}) \qquad (3.13b)$$

Where θ_A is the wrap angle of pulley A and θ_B is the wrap angle of pulley B.

From the calculations conducted using the general equations shown above, the following parameters were calculated for the belt and pulley system.

Parameters:

$$transmitting\ power = 3.6Hp$$

$$applied\ torque = 11.65nm$$

$$\theta = 173\ deg$$

$$Ratio\ of\ Tension\ side\ to\ Slack\ side\ = 15.224$$

$$Slack\ side\ tension = 39$$

$$Tension\ side\ tension = 594$$

3.1.5 VTOL body

The objective of this design process is to design the body of the device, such that it is capable of supporting the thrust load of the propellers and the stresses induced by the payload. Furthermore, the design of the body should be lightweight and prevent all the interference between the propellers and other components. Accordingly, the design of the VTOL device body takes into consideration the spacing of the propellers and the protection of all vulnerable components, including the powertrain components which will experience load during operation.

The body went through four different iterations throughout the design process. All iterations consisted of eight wing pieces, two shims that level the bottom wings and two support brackets that connect to the top wing. The first iteration had solid, bulky wings, with minimal holes and was found to be far too heavy. Moreover, the clearance between the top and bottom pieces were too great, as shown in Figure 2.20. This clearance required the universal joints to sit at a steep angle, which was undesirable due to increased shaft wobble and inefficiencies. The abandonment of the pulley system allowed for significant weight reduction in the following wing piece iterations, resulting in smaller wings with larger cutouts. Threaded rods that run

through the length and height of the wings, securing the structure along with the bearing components, were also added. This substantially increased the bending strength of the wing material.

In the final design iteration, each shaft going into the propeller gearbox is supported by three pillow block bearings and one bearing on the entry into the bevel gearbox. The central axis of these bearings must align perfectly with one another in order for the shaft to spin freely. However due to a manufacturing defect in the wings, as discussed in section 3.1.6, one of the pillow block bearings is misaligned from the rest. So, the decision to remove the bearing closest to the gearbox was made in order to ensure a free spinning shaft.

The exclusion of this bearing, will result in a reduction of bending support, however, after the abandonment of the pulley belt system, the radial forces acting on the shaft have been severely reduced. Thus the bending moments induced on the shaft are considered negligible.

Table 3.2 Design iterations of device body

Iteration	Design Features	Improvements over Previous Iteration	Disadvantages
1	Eight solid and tall wing pieces. Clearance between wings is high	N/A	Universal joint angle too high, making design weaker. Wings bulky and heavy
2	Smaller wings which now cover gearbox and other components. Added threaded rods	Reduced bending stresses, gearbox covered and lubricated, reduced imbalances	Not enough cutouts for thrust efficiency and weight reduction. Not enough protection for bevel gear transmission
3	Bigger cutouts, for thrust efficiency. Heightincreased to improve bending strength. Bevel gears now enclosed	Increased efficiency, gearbox protection and lubrication. Better safety due to increased height	N/A

4	Similar design to iteration three, however removal of pillow block bearing due to manufacturing defect.	Better alignment and tolerance, reduced friction.	One bearing had to be removed due to manufacturing defects, potentially weaker bending strength of the shaft.

3.1.6 Materials

In the construction of the gas powered multirotor device, the material selection for every custom-manufactured component was carefully considered. Candidates for each component were identified, and the pros and cons were weighed for each material to determine the best choice to satisfy the budget, scope and schedule of the project. Material selection for purchased components such as the pulleys and gears were based solely on availability.

Table 3.3 Manufactured components and candidates for their materials

VTOL Body	Shafts	Fasteners
Wood	Mild steel	Zinc plated steel
Metal	Hardened steel	Black metal oxide
Plastic (3D Printing)	Aluminium	Stainless steel

For the VTOL body, the main concerns for the materials were availability, cost, strength-to-weight ratio, and manufacturability. To this end, the attributes of wood, metal, and 3D printed plastic were considered relative to each other. Of the three materials, wood is the most inexpensive, with a middling strength-to-weight ratio and can easily be used for manufacturing with simple hand tools or power tools. Metal has the highest strength to weight ratio, however this comes at both a greater monetary cost compared to the other two materials, and requires more specialised machinery to be

used to manufacture the VTOL body. Finally, 3D printed plastic was considered because barring more exotic materials, 3D printing plastic is also relatively cheap, and the manufacturing of parts can be entirely automated through a 3D printer which can quickly produce complex shapes that traditional machining and manufacturing cannot.

3D printed plastic was chosen as the material for the VTOL body because its cost, availability, and ease of manufacturing set it above the other two materials. For 3D printed plastics, the most common plastics used are PLA, PETG, and ABS. A publicly available analysis of these three materials was referenced to better understand their three characteristics [19]. Figures from this analysis comparing these three materials are shown below. Of the three materials ABS offers the highest impact resistance, and thermal resistance, however it is the most difficult to 3D print with due to its high thermal warpage and its emission of toxic fumes. PETG is often considered due to its relatively high thermal resistance, and because its ductility is useful in applications where it is desirable for parts to yield when they fail. However, it has the lowest tensile and bending strength of the three materials. PLA is the easiest to 3D print with due to its relatively high thermal stability. It offers the highest bending and tensile strengths, but is brittle, is the least impact resistant, and has very low thermal resistance.

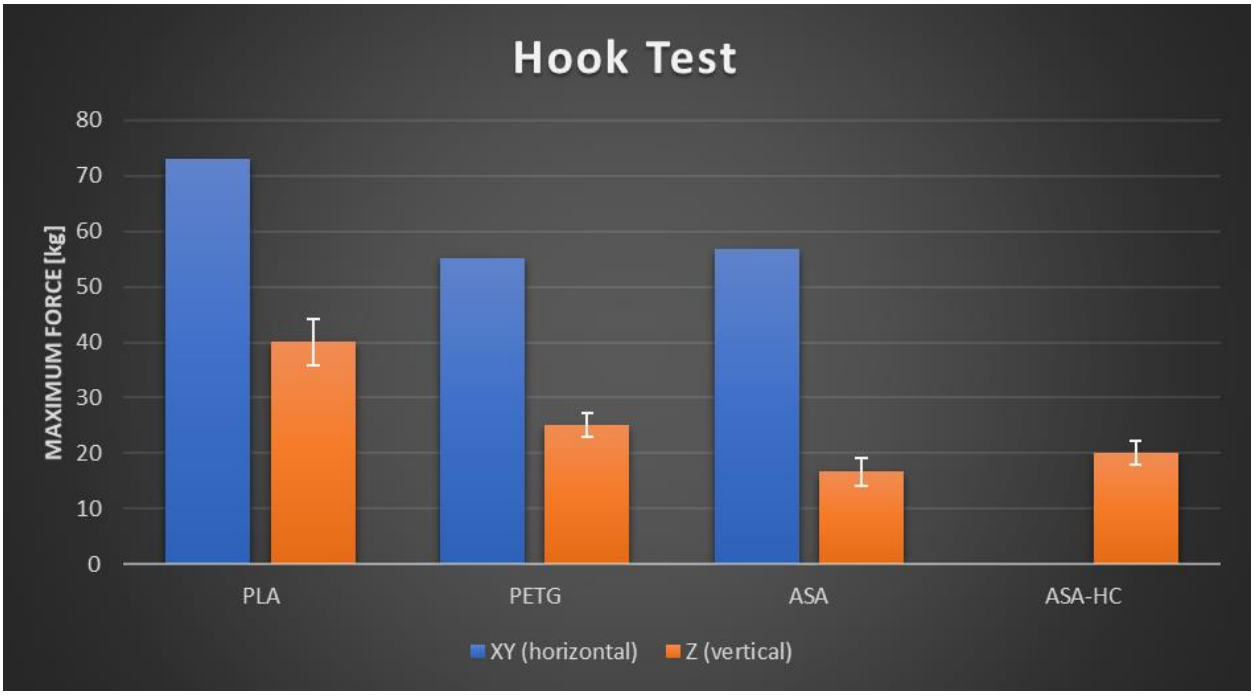

Figure 3.12 The results of the hook test. The XY testing direction represents tensile strength while the Z testing direction represents interlayer adhesion

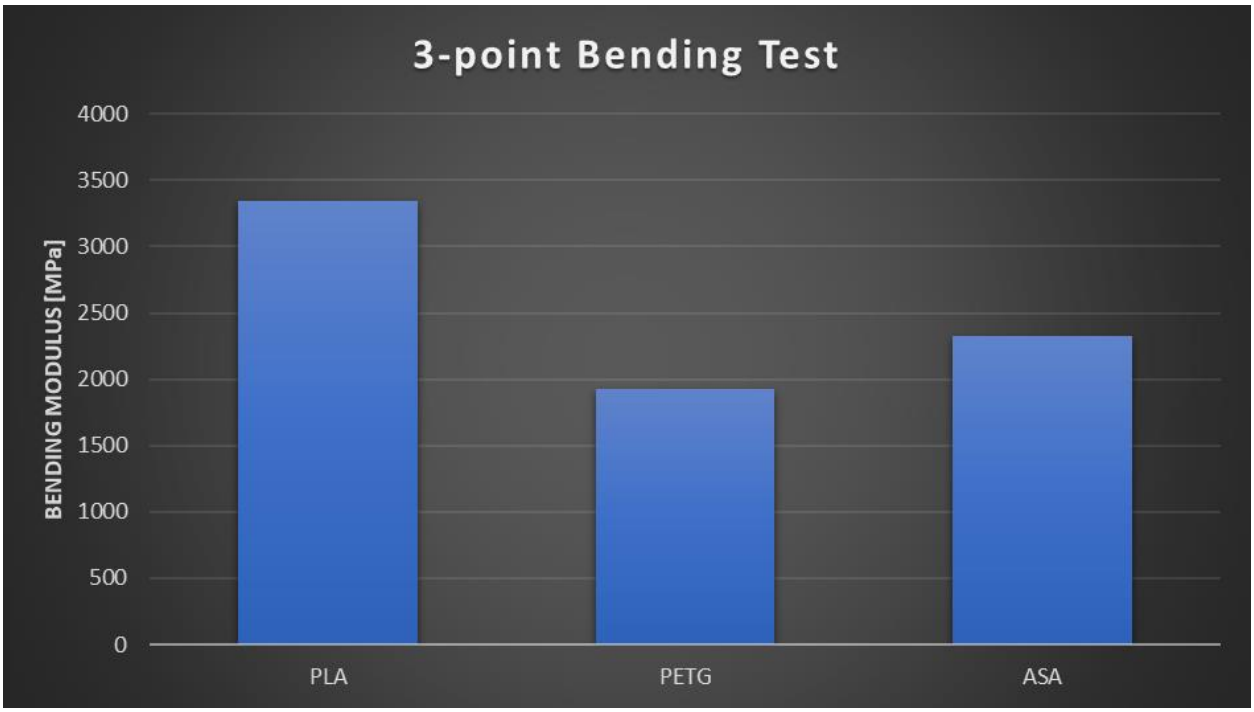

Figure 3.13 The results of the 3-point bending test

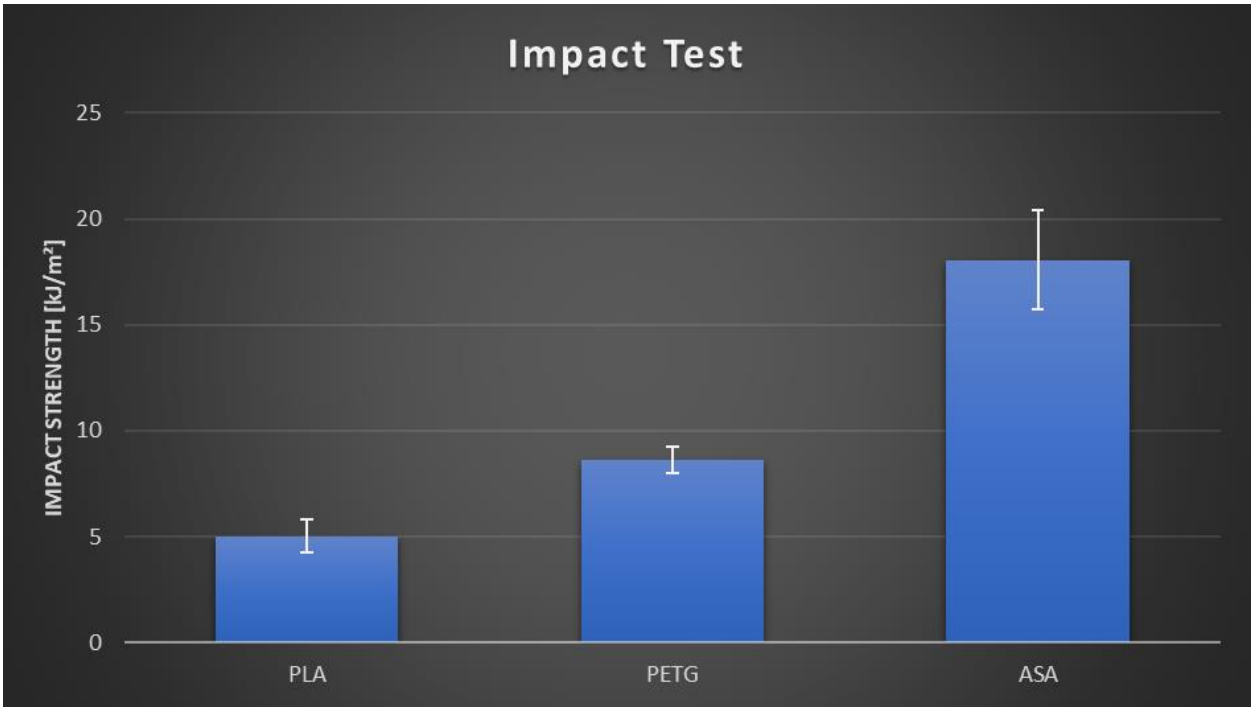

Figure 3.14 The results of the impact test

Contemporary innovations in material science have introduced PLA+, which offers the bending and tensile strength of PLA, with the ductility and thermal resistance of PETG, and the impact resistance of ABS, as confirmed by another publicly available analysis [22]. The comparison of the strength of PLA to PLA+ from this study is shown in Figure 3.15 below. PLA+ was chosen because its properties were best suited for the application of manufacturing the VTOL body. When designing for 3D printing, calculations were made to determine the minimum required thickness such that each part can withstand the forces acting upon it. These calculations are shown in Section 3.2.

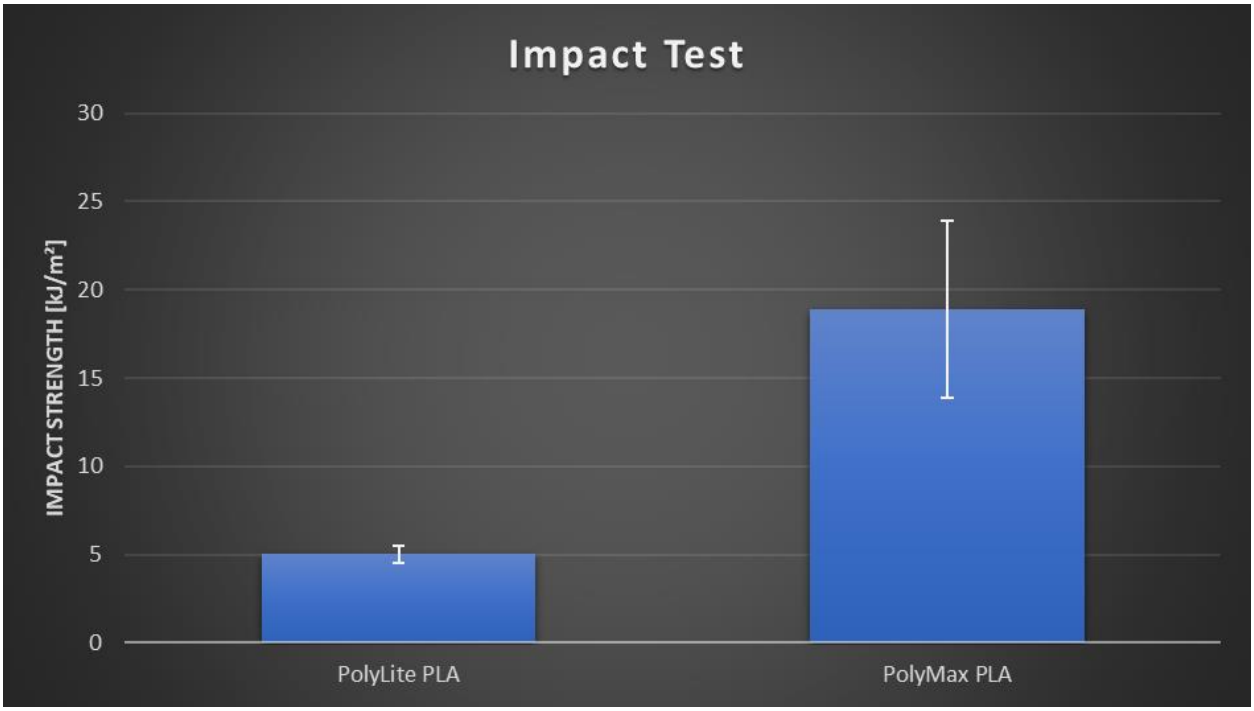

Figure 3.15 The impact strength of PLA compared to PLA+

For the machined shafts, various high strength metals were considered on the basis of cost, availability, and ease of machining. Aluminium was considered due to its low cost, easy machinability, and very impressive strength-to-weight ratio. However, aluminium was ultimately decided against because while its strength-to-weight ratio was impressive, its ultimate strength was far less than that of the other two candidates for shaft material [21]. Because of its properties, hardened steel was considered to be ideal for the application of producing shafts, however the difficulty involved in machining hardened steel made its usage unfeasible with the given schedule of the project. Thus, mild steel was chosen for the shafts to be produced from.

In terms of fasteners, the three most common materials available are all variants of steel: zinc plated steel, black metal oxide steel, and stainless steel. For the fastener material selection, the criteria was based on strength, cost, availability, and durability. Black metal oxide fasteners are made of steel

which has been treated with a black metal oxide coating for corrosion resistance and decorative purposes. Of the three materials, it is both the weakest and least durable. Zinc plated fasteners are the most commonly available ones, with the zinc coating offering some corrosion resistance. They are typically equal in price to black metal oxide fasteners. Stainless steel fasteners offer the best strength and durability, but are typically equal to, or more than zinc plated steel in cost.

3.1.7 Bearing

The objective of this bearing design process is to select bearings to support the shafts undergoing thrust and axial loads. The bearings are also crucial to minimise the wobbling experienced by the shaft while rotating at high speeds. Thus, the selection criteria for these bearings are such that they should be robust enough to support both the axial and radial load demands with a sufficiently long life span. The bearings should also be of high quality to minimise frictional losses as much as possible. To select bearings, a bore diameter which matches the finalised shaft diameter of 8mm had to be selected. The standard catalogue of bearings found within the 11th edition of Shigley's Mechanical Engineering Design [23] only contain ratings for bore sizes of 10 mm or greater. As such, shoulder and laid ratings had to be extrapolated in order to provide an estimate of which shoulder diameter to use for deep groove self aligning ball bearings. The magnitude of the axial thrust and radial load were combined into an equivalent force using Eq 3.9a and 3.9b. This force was used to then calculate the L_{10} value of the bearing, using Eq 3.10, which is the bearing life associated with a 90% reliability. As the bearing bore sizes were interpolated, to ensure a conservative FOS, the radial loading and axial loading were set equal to each other, emphasising the total loading on the bearings.

$$\frac{F_e}{V F_r} = 1, \; Where \; \frac{F_a}{V F_r} \leq e \tag{3.14a}$$

$$\frac{F_e}{V\,F_r} = X + Y\frac{F_a}{VF_r} \quad Where\ \frac{F_a}{VF_r} \leq e \qquad (3.14b)^2$$

$$L_{10} = \frac{10^6}{60 \cdot RPM} \cdot \left(\frac{C_{10}}{F_e}\right)^3 \qquad (3.15)$$

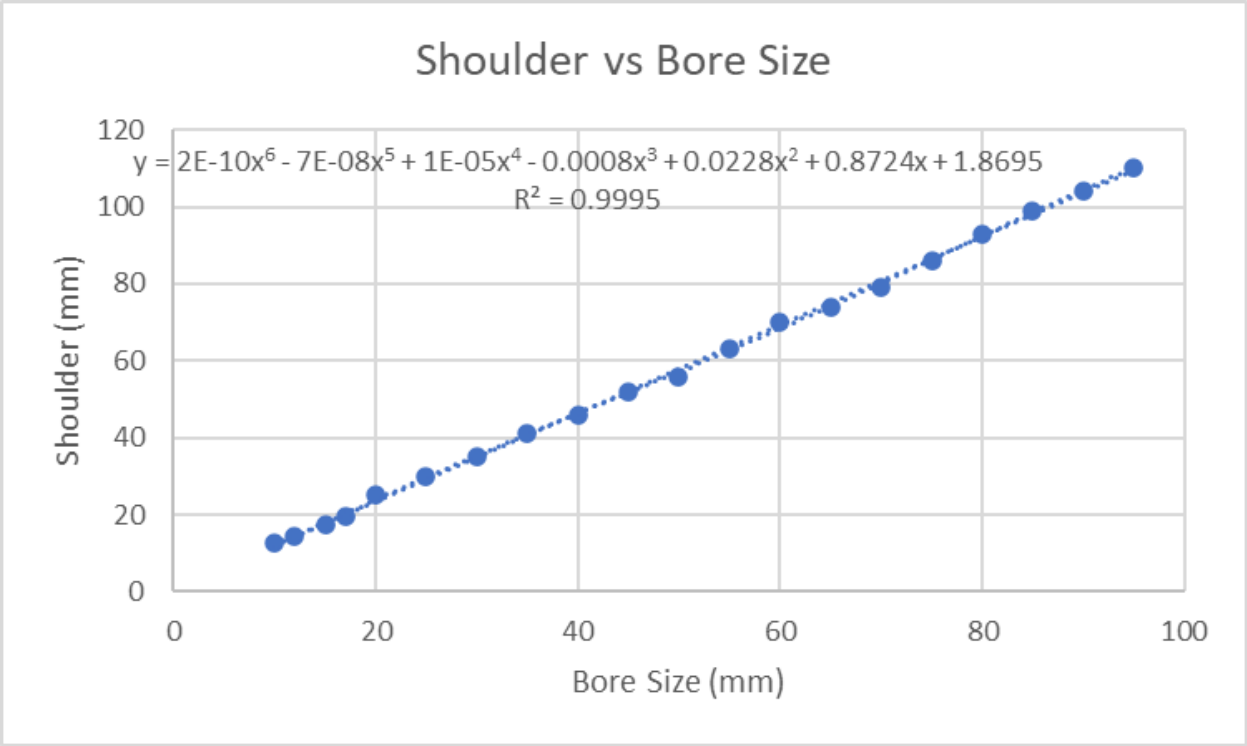

Figure 3.16 Shoulder diameter for bearings of different bore diameters

2 Full equation and Tables are found in Appendix A.2

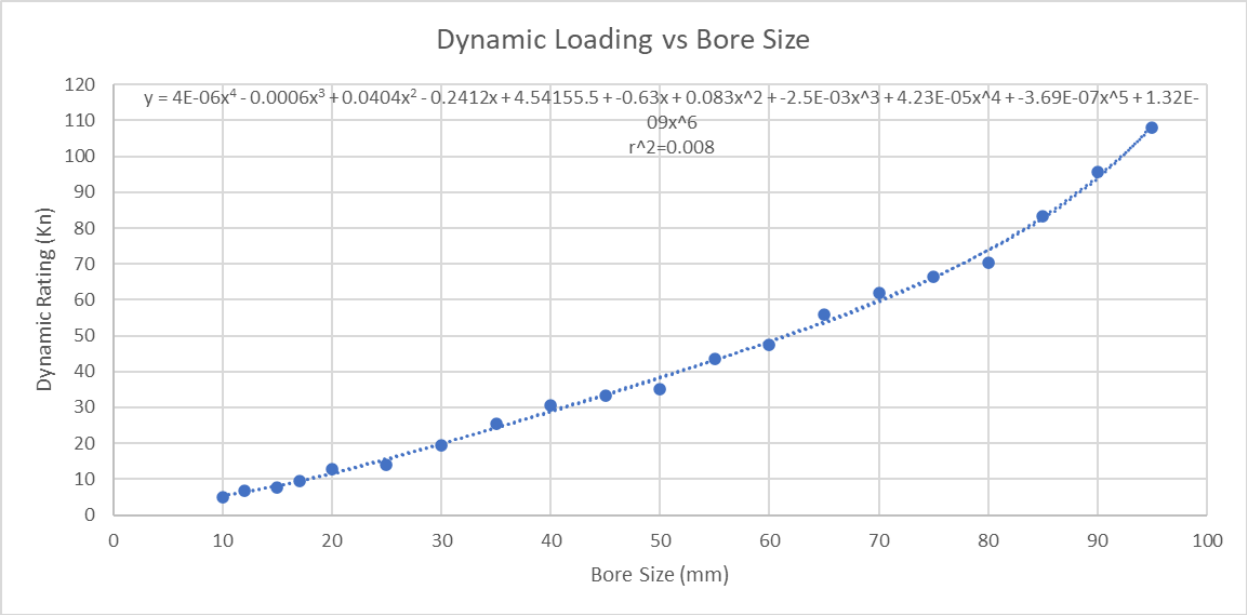

Figure 3.17 Dynamic loading vs bore size

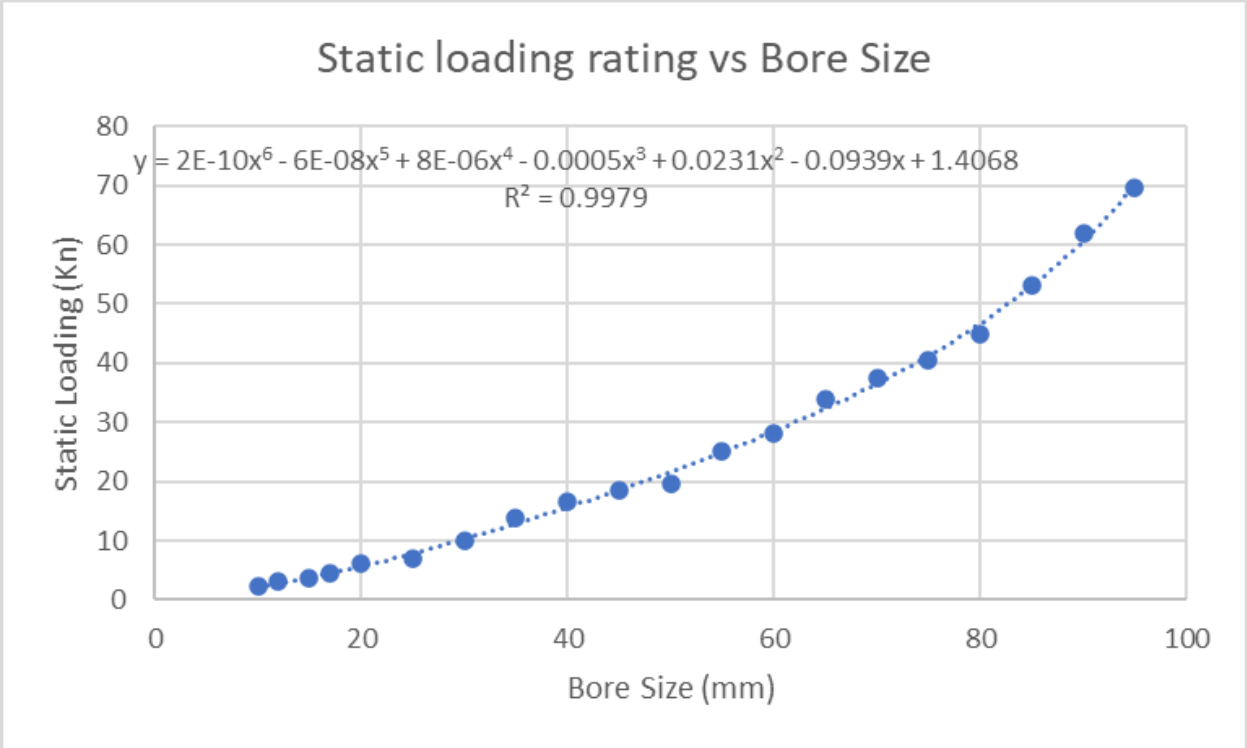

Figure 3.18 Static loading rating vs bore size

Initially, thrust bearings were chosen to support the axial load of the propellers as calculations indicated their capability of supporting the loads. However, they did not prove to be a good design choice because they lacked the functionality to properly secure the shafts to the structure.

Figure 3.19 Initial thrust bearing concept (left) and Pillow Block bearing actually implemented (right) [24] [25]

Because of this, a design change was made to 90 deg Pillow block bearings with flanges. These bearings possess mounting holes that allow for the secure fastenment of the bearings to the structure. The flanges of the bearing also had set screws, which could be utilised on the shaft allowing for better coupling and power transfer.

To accommodate for these bearings, a d-slot was implemented on the shaft to be used with the set screws. A shoulder was also added onto one location to prevent the shaft from sliding through the bearing.

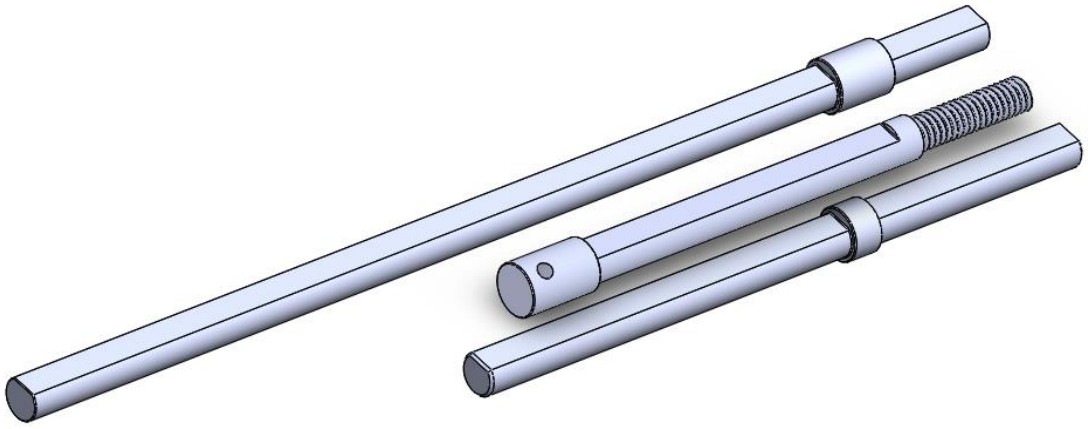

Figure 3.20 D-slot and shoulder added for accommodation.

The following are the values for the relevant parameters of the bearings, as calculated from the general equations shown above:

$$d_s = 10mm$$

$$C_{10} = 4.65kN$$

$$C_0 = 1.91kN$$

$$F_a = 26.67N$$

$$F_r = 26.67N$$

$$e = 0.19$$

$$F_e = 76.33N$$

$$L_{10} = 3.02 \cdot 10^{13}\ Hours$$

3.1.9 Lube

The objective of this design process is to select a lubricant for use with the bevel gears located in the gearboxes as well as the bevel gears attached to

the propellers. This lubricant is essential to protect the gears from wear damage, prevent excessive heat and improve efficiency of operation.

To choose a specific lubricant for this use case, calculations centred around the EHL thickness based on Hertzian contact theory and Sommerfield theories were initially pursued. Multiple approaches to calculations were attempted, however, the authors' were unable to calculate the lubricant requirements for use in bevel gears due to a multitude of factors. These factors primarily were lack of access to reference resources for bevel gear lubricants, excessive time required to verify other calculations, and theoretical work required to arrive at a solution made this task out of scope . As such, a general approach of following gear manufactured recommendations was opted for instead and Mobil DTE 24 light circulating oil was chosen based on gear manufacture recommendations. Unfortunately, the procurement lead time for this lubricant was too long and a multi use synthetic oil was used in place of it.

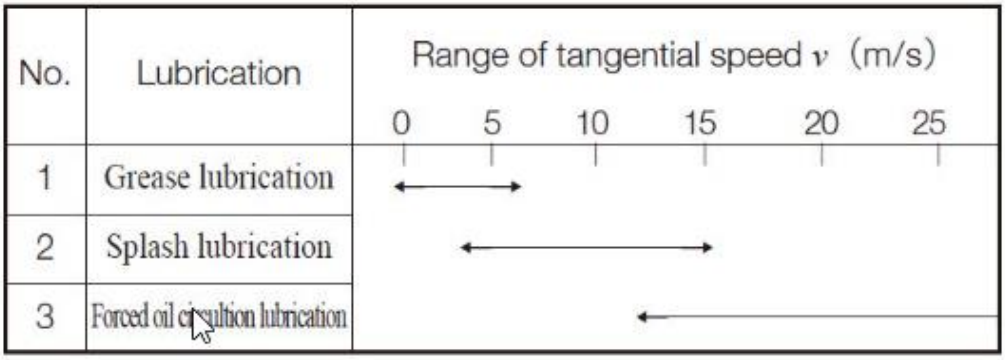

Figure 3.21 Ranges of tangential speed (m-s) for spur gears and bevel gears via KHK gears. [24]

Rotation of Pinion (rpm)	Horsepower (PS)	Reduction Ratio below 10		Reduction Ratio over 10	
		cSt (40℃)	ISO Viscosity Grade	cSt (40℃)	ISO Viscosity Grade
Below 300	Less than 30	5 - 234	150, 220	180 - 279	220
	30 - 100	180 - 279	220	216 - 360	220,320
	More than 100	279 - 378	320	360 - 522	460
300 ' 1,000	Less than 20	81 - 153	100,150	117 - 198	150
	20 - 75	117 - 198	150	180 - 279	220
	More than 75	180 - 279	220	279 - 378	320
1,000 ' 2,000	Less than 10	54 - 117	68,100	59 - 153	68,100,150
	10 - 50	59 - 153	68,100,150	135 - 198	150
	More than 50	135 - 198	150	189 - 342	220,320
2,000 ' 5,000	Less than 5	27 - 36	32	41 - 63	46
	5 - 20	41 - 63	46	59 - 144	68,100
	More than 20	59 - 144	68,100	95 - 153	100,150
More than 5000	Less than1	9 - 31	10,15,22	18 - 32	22,32
	1 - 10	18 - 32	22,32	29 - 63	32,46
	Less than10	29 - 63	32,46	41 - 63	46

Figure 3.22 Recommended oil viscosity for use of closed gears [26]

Copies of calculations regarding lubricants can be found in Appendix A.2

3.1.10 Personnel Frame

The objective of this design process is to develop a system that will attach to the lift device for users to be transported up or down. The design criteria for the development of this device are as follows: Firstly, the structure must, at the minimum, be able to support the maximum payload of the VTOL device. The structure must be stable enough to be used safely during operations, and not add any significant drag forces during operation in order to maintain stability of the system. Moreover, the structure should be collapsable and easily portable such that it does not need to be assembled or disassembled entirely in the process of deployment or retraction between uses.

There were three different sections of the frame which saw design revisions.

The top piece, the payload frame, as well as the bottom piece each saw multiple iterations each which were somewhat independent of each other. However, design choices of one component would ultimately affect the other. The initial concept employed a lifting platform powered by an external motor. This idea was abandoned as the focus of the project shifted towards a focus on the development of the propulsion system for the VTOL, rather than the lifting system as a whole. As such, the frame was simplified to just be an external support frame, with a centred rope, built for modularity. The entire frame is tapered out, with a half angle of 4 degrees.

The twist angle of the frame was calculated utilising the geometrical relationship seen in Figure 3.x. Once this is calculated, the tension horizontal tension components required to cancel out the moments caused about the top of the frame due to environmental forces was determined using Eq 3.16.

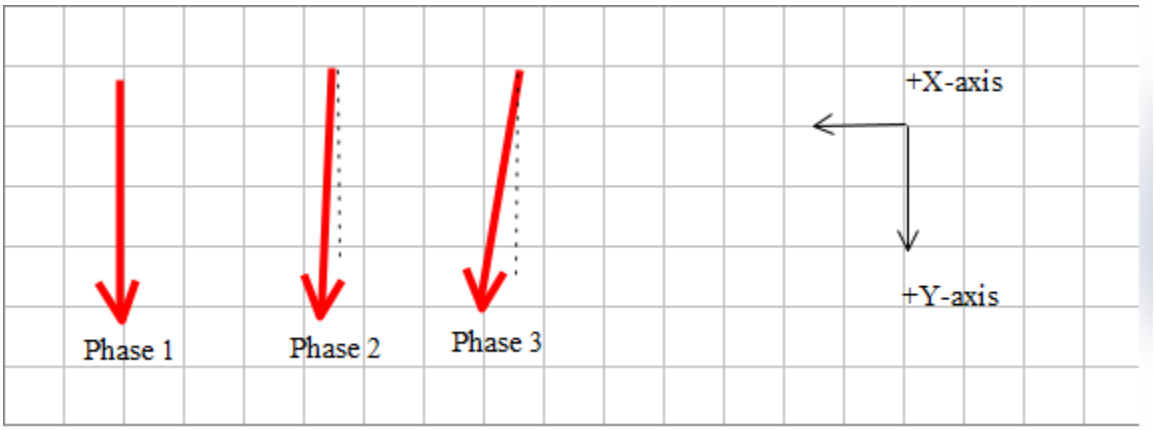

Figure 3.23 Visualisation of tension components resisting torsion

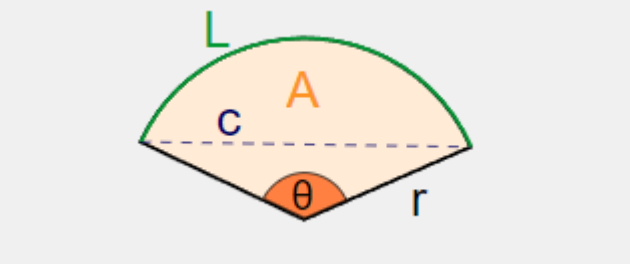

Figure 3.24 Diagram showing relation of twist angle and arc length

$$M_{resist} = T_{tension\ per\ wire} \cdot R_{frame} \tag{3.16}$$

Table 3.4 Design iterations of Top Frame

Iterations	Design Features	Improvements over Previous Iteration	Problems
1	Hollow square shape with 8 mounting holes	-	Amplifies torsional deflections, very unstable geometry. 8 mounting holes results in greater chance of slack Missing modularity
2	Star shape with 3 mounting holes	No longer has mounting location for pulleys (use case changed)	Not strong enough to support tension forces Missing modularity
3	Circular shape with 3 mounting holes and carabiner hook style with clamps for easy attachment	Added modularity, reduced stress build-ups with fillets	The component should be made as one piece to reduce stress concentrations where the hooks meet the frame

Table 3.5 Design iterations of Payload Frame

Iterations	Design Features	Improvements over Previous Iteration	Problems
1	8 nylon wires (4 on the outside, 4 guiding wires) Each capable of withstanding 170 N of tension. Spacers placed in between wires with the goal of adding structural rigidity. Prevent wires from becoming tangled	-	Overly complicated and not needed
2	Reduced to 3 nylon wires running along the outside of the frame Spacers are still implemented between each wire.	Simplified design and improved rigidity.	-

Table 3.6 Design iterations of the bottom frame

Iterations	Design Features	Improvements over Previous Iteration	Problems
1	Square platform with reels on each corner and slot for 2 winch motors used to raise and lower lifting platform.	-	Bulky and not space efficient Design time needed to ensure each reel works individually was excessive
2	Triangular design with central spool powered by a motor which will assist in raising and lowering the platform.	More compact and easier deployment/retraction	Ultimately reel system for lifting platform was abandoned
3	Upside down cone shape for increased structural soundness	Improved structural soundness	Increased size over previous generation

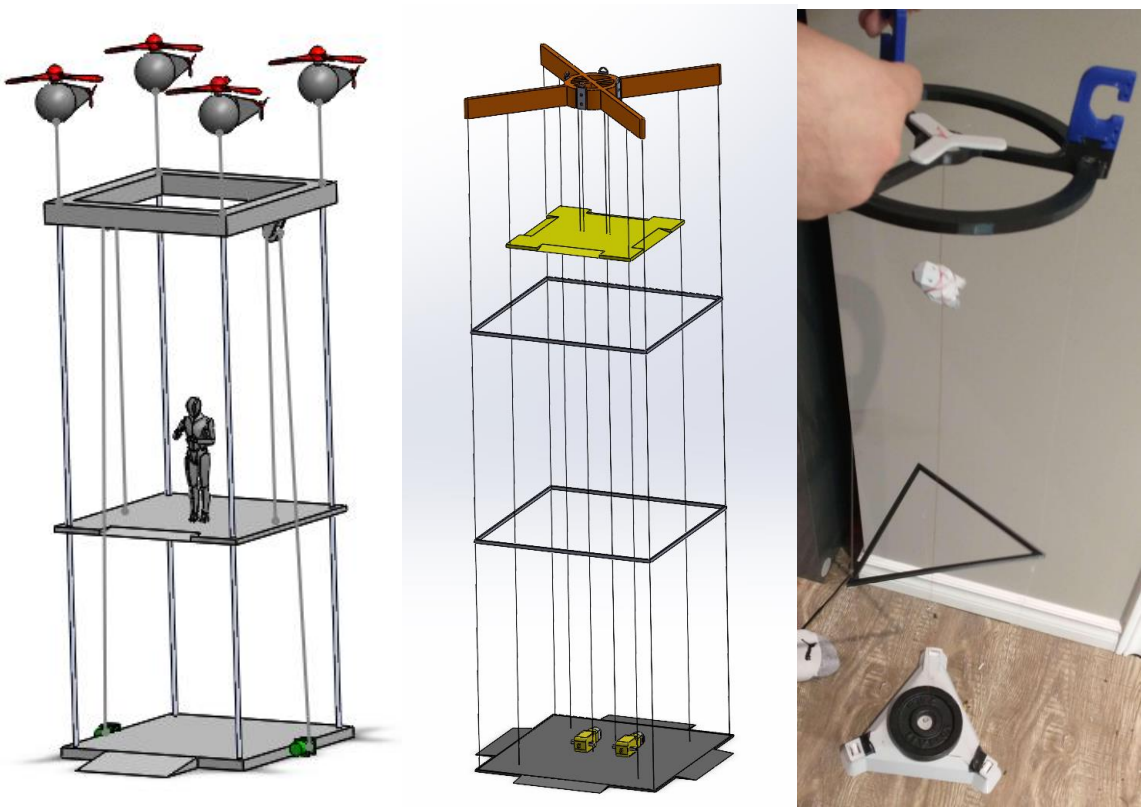

Figure 3.23 Iteration progression of lifting structure from left to right: iteration one, iteration two and iteration three

3.1.11 Propellers and Thrust Curves

In order to assess the chosen set of propellers for the lift device, the potential thrust generated by the propellers must be compared with the thrust required to lift the device. The thrust generated by propellers is proportionally related to their rotational speed. Thus, the theoretical thrust of each propeller along with the horsepower required to drive the propeller can be calculated. These propeller loading numbers have been accurately simulated and provided by the manufacturer within the propeller specifications [25].

Both the load and thrust can then be plotted against propeller RPM, as seen in Figure 3.24 and Figure 3.25 below.

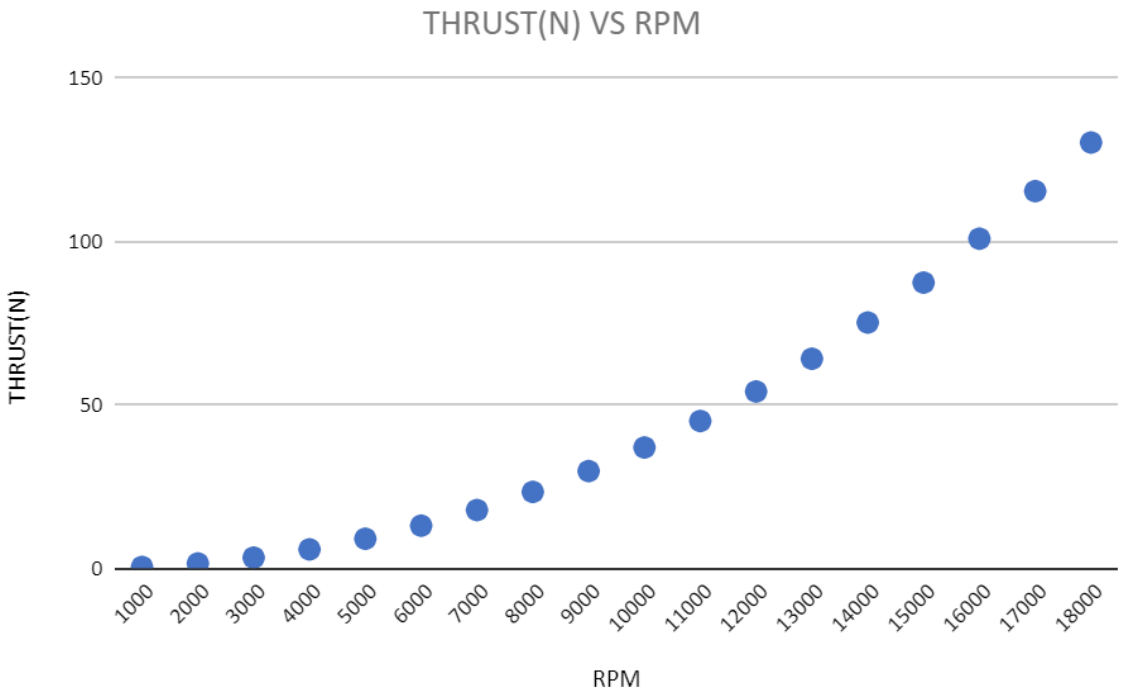

Figure 3.24 Plot of Thrust versus propeller RPM

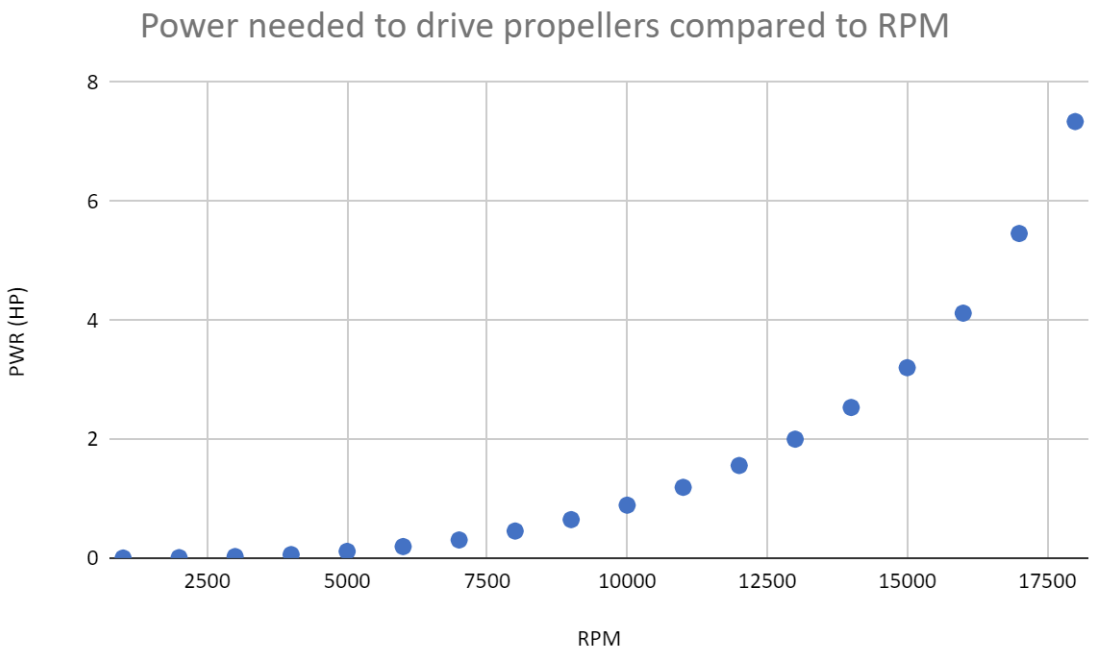

Figure 3.25 Plot of Propeller load versus propeller RPM

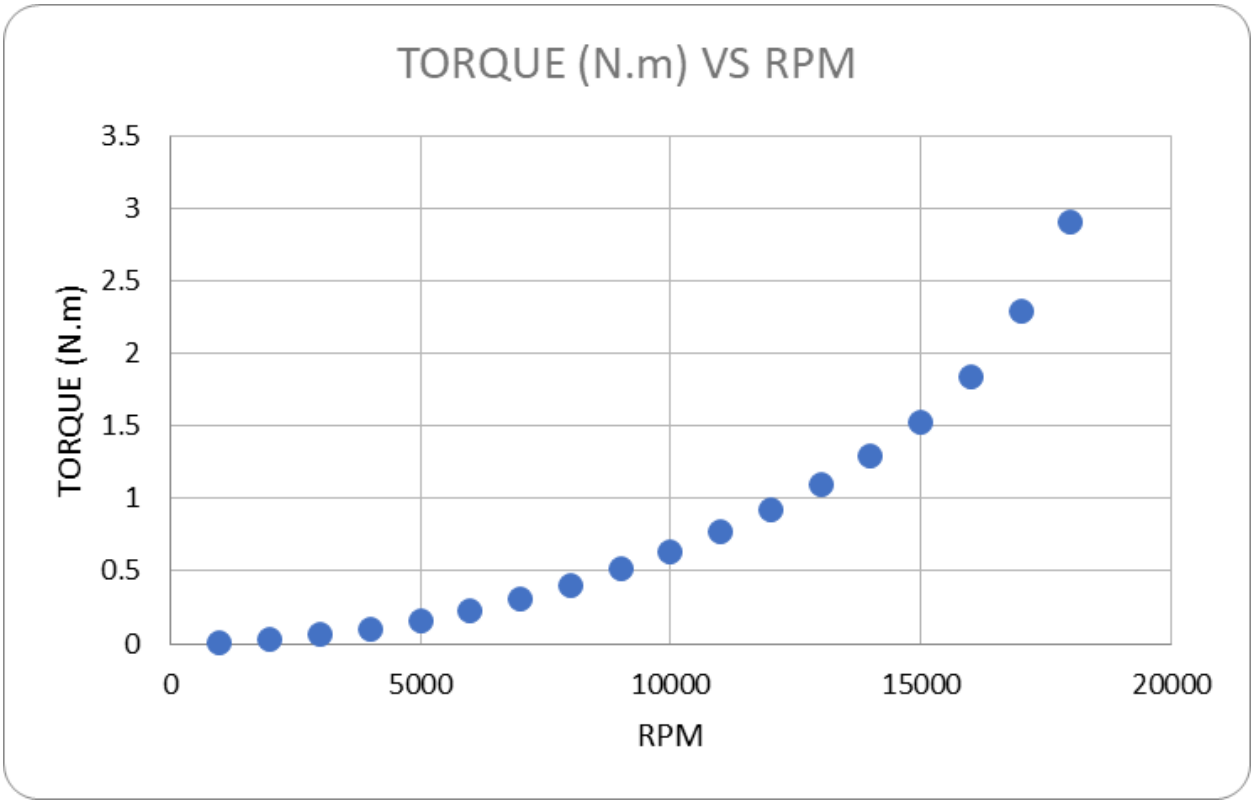

Figure 3.26 Plot of Propeller torque versus RPM

According to specifications of the final concept model, the mass of the platform is estimated to be 5.3kg which equates to a weight of approximately 52N. Thus the thrust generated by all four propellers must equate to 52N to start generating lift. Using this estimate, the required engine power and output RPM to generate lift can be calculated.

It should be noted that the chosen engine is able to produce 3.6Hp at its peak, however, a loss of 1hp is assumed to account for losses as well as the unknown engine load curve. Thus, the max load the engine will be able to support is assumed to be 2.6hp.

Assuming there are four propellers to generate 52N of thrust, each individual propeller would need to generate 13N. According to load curves provided by the propeller manufacturer, an RPM of just over 6000 is needed to generate 13N of thrust. This amount of thrust would require an engine load of 0.472hp,

well within limits. Utilising 2.6hp as the maximum load which the engine can handle, the maximum output RPM achievable by the system is estimated to be approximately 10000 RPM.

Therefore, based on these values from the load graph, the ideal operating range of the device will be **6000 RPM to 10000 RPM.**

3.1.12 Propeller Gearbox

The objective of this component is to transmit the power coming out of the bevel gearbox and transmit it to the propeller shafts. The design criteria are to ensure a system which transmits this power reliably with low friction and component stress.

A bevel gear approach was chosen in replace of the belt pulley system mentioned in section 3.1.4. Once the previous approach was abandoned, bevel gear drive was explored and implemented due to the significantly better efficiency using drive by gear in comparison to pulley and belt drive [28].

The biggest challenge with this design approach is ensuring the gears are secure and supported, such that they mesh accurately during operation. Many factors including the weight of the shafts and the loads exerted on them, along with vibration need to be accounted for in the design. To solve this problem, set screws were implemented to the gears to secure their location on the shaft. In addition, shoulders were added to the shafts at strategic locations being bearings to limit the amount of play the shaft experiences through the bore. Lubrication, as mentioned in section 3.1.9, was also added to reduce the friction between the gears as much as possible. A gearbox cover was made to prevent debris from entering and jamming the gear meshing while also ensuring lubricant does not fly out.

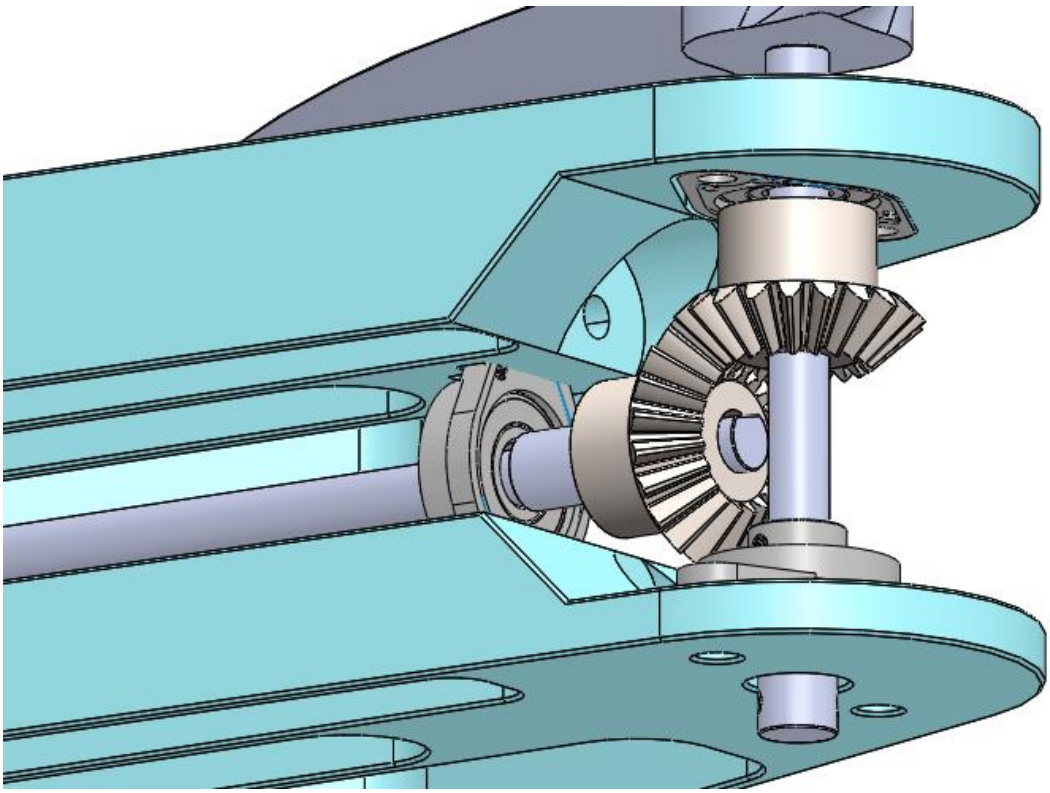

Figure 3.27 Propeller gearbox design without cover

3.1.11 Fasteners

The objective of this design process is to ensure the secure fastening of all structural components of the device. An analysis of the forces on the device was completed and it was determined that with regards to fasteners, the forces acting on the threads holding the propeller are greater than at any other location, while also being most prone to vibrations. With the final design layout, the forces experienced by all other fasteners on the device were determined to be negligible. Due to this, the focus of fastener design and selection was with regards to propeller fasteners as this area was determined to be a critical location of the shaft. The design criteria for this selection process is to ensure the propellers are properly secured during operation, by taking into account the potential thrust and vibrations experienced by the fastener.

To begin the design process, it was first determined that the propellers shall be spinning in a cross pattern, turning towards each other as seen in Figure 3.28. Based on this, two of the propellers will require reverse threading. To determine the thread, a bolt dimension table with tensile strength values was consulted. A thread choice of 1⁄4 -20 UNC was chosen due to its wide availability and sufficient strength. Shear and root thread bending stresses along with FOS calculations were completed utilising the Von Mises stress criterion along with Eq 3.x.

$$\sigma_b = \frac{6F}{\pi d_r n_t p} \ (Root\ thread\ bending\ stress) \tag{3.17}$$

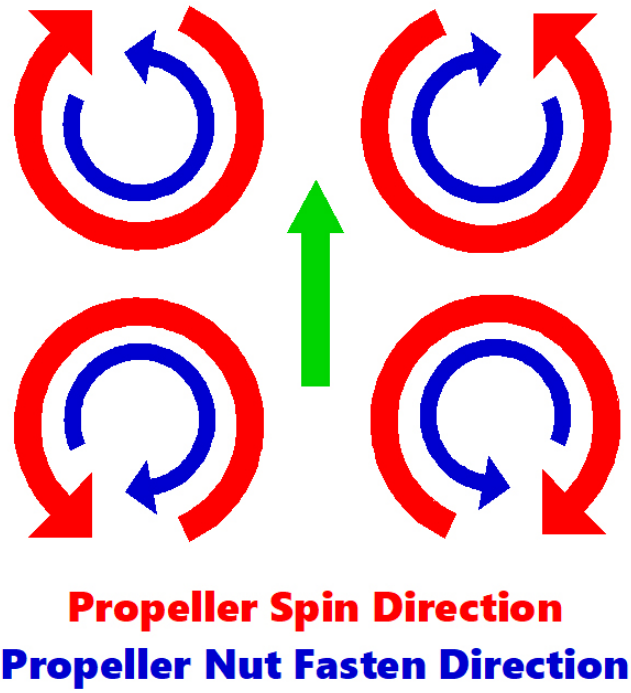

Figure 3.28 Nut fastening direction vs propeller spin direction [27]

A bushing was added between the propeller shaft and the propeller to prevent wear and absorb any friction, thus dampening the propeller. A washer was also added on top of the propeller to ensure the force is evenly distributed onto the propeller itself.

From the calculations conducted using the general equations shown above, the following Von Mises stress and factor of safety was calculated for the fasteners:

$$\sigma' = 62.93\ Pa$$

$$FOS = 7.3 \cdot 10^6$$

3.2 Finite Element Analysis

Throughout the design process of the VTOL device and Evac frame, both structural and dynamic analysis calculations were performed for individual components to ensure that an appropriate factor of safety was achieved by each component for its respective application. In addition to these calculations, rudimentary FEA analyses were conducted as a supplementary tool to confirm the findings of the calculations. It is important to note that the results of the FEA analysis were not in any way relied upon to determine the FOS of the components, and instead were used simply to ensure that the results produced by the calculations were in line or close to the FEA results.

FEA analysis was conducted primarily on the 3D printed components due to their relatively weaker strength to weight ratio when compared to the metal components used in the construction of the VTOL device. The figures below showcase the FEA results for each component, with a loading gradient to highlight the most critical locations. Red arrows mark the component's centre of gravity, while the purple arrows indicate applied loads, added to simulate real life forces during operation. The green arrows represent locations where components are fastened. Being that the FEA analysis was rudimentary and served only to supplement the calculations performed, the main forces considered were the reaction forces from the lift generated by the propellers.

The component of greatest concern were the 3D printed wing pieces. It was

vital that the factor of safety of these components was adequate as these were key structural components that not only supported the propellers, but gears and shafts to transmit power from the engine to the propellers. For the FEA analysis of the wings, they were treated as being fastened to the chassis via the four screw holes in the middle of the wing. A downward force was applied to either end of the wing, approximating the reaction force from the lift generated by the propellers. The FEA analysis confirmed that the 3D printed wing pieces can withstand a force of 17N with a factor of safety of 23. These results were confirmed both by the structural analysis calculations pertaining to the wing pieces, and by destructive testing performed on prototype specimens. The results of the FEA analysis are shown in Figure 3.29.

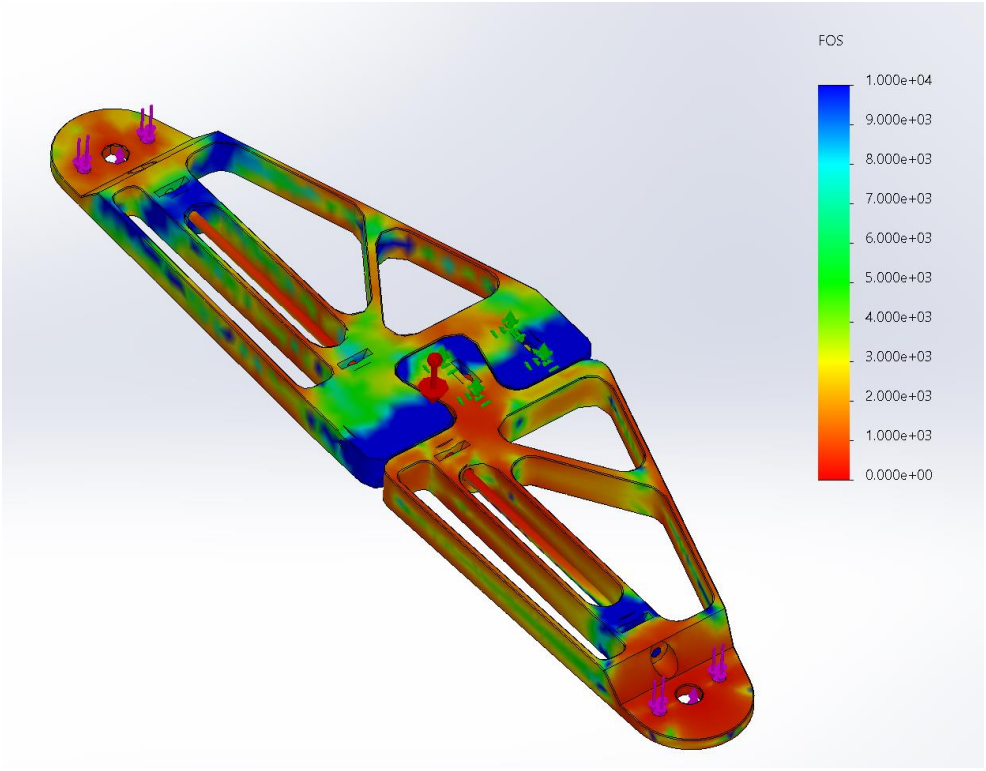

Figure 3.29 Finite Element Analysis of PLA bottom front wing

Secondary to the wing pieces, FEA was also conducted on the gears which were 3D printed for the transmission gearbox. The primary forces considered

were shear stress on the teeth of the gear. As a worst-case-scenario analysis, the shear stress experienced by the gear was concentrated on a single tooth of the gear. The goal of this analysis was to confirm that the teeth of the 3D printed gears can withstand the shear stress they are expected to undergo. As shown in Figure 3.30, it was demonstrated by the FEA that a single tooth of the 3D printed gear can withstand a shear stress of 313.1 Pa with a minimum factor of safety of 1.9.

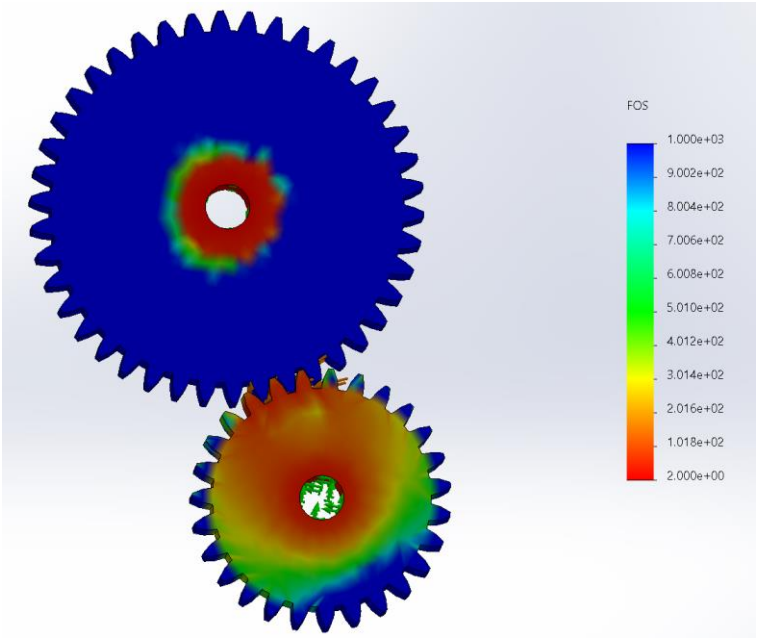

Figure 3.30 Finite Element Analysis of Transmission Gears

Thirdly, FEA was performed on the Evac frame. The top ring of the Evac frame was considered for the FEA as it was the critical location for the entire evac frame assembly. The FEA analysis confirmed that the 3D printed pieces for the evac frame can withstand a total force of 20N with a factor of safety of 59.

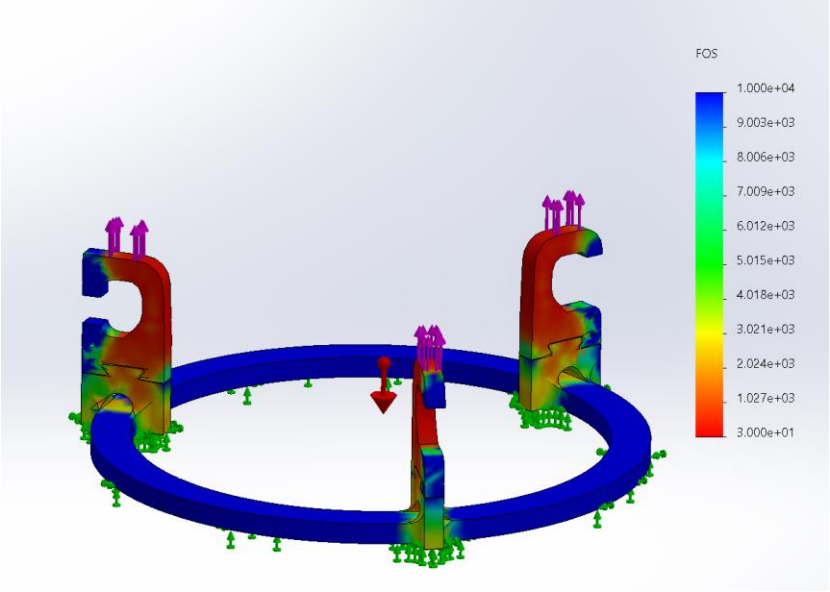

Figure 3.31 Finite Element Analysis of Top Piece of Lifting Frame

Finally FEA was conducted on the steel chassis of the VTOL body. The FEA analysis confirmed that the steel chassis can withstand a torque of 8Nm with a factor of safety of 3.2.

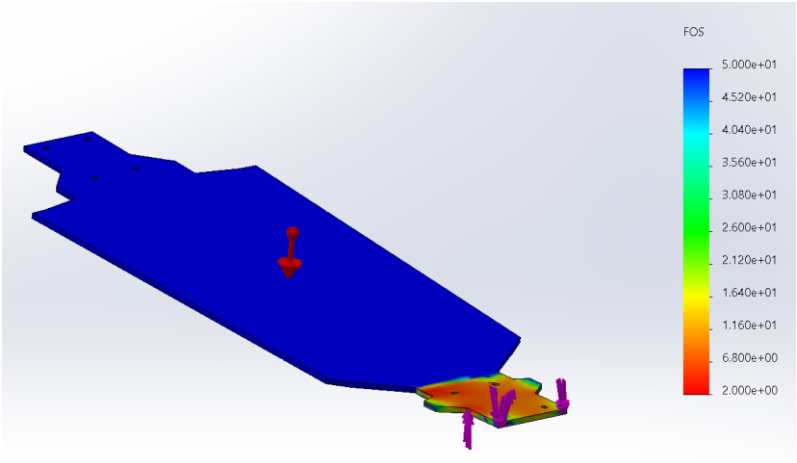

Figure 3.32 Finite Element Analysis of Drone metal frame.

From the figures above, it has been shown that the results from the FEA are congruent with the structural and dynamic analysis calculations that were performed. The FEA confirmed what was demonstrated with the calculations; that all components analysed meets or exceeds the demanded

factor of safety for each component.

3.3 Construction and Assembly of Scaled Model

3.3.1 The VTOL device

Step one: Disassembly

- Car mounted onto workstand
- Plastic cover/hood removed from original RC truck
- Front and rear differential and wheel assemblies were removed from the chassis. Each assembly was mounted with 4 screws threaded from the bottom of the chassis, and a support arm above the chassis. Front differential assembly was also mounted on two struts which acted as pivot points for the steering mechanism.

Step two: Repurposing of parts

- Front and rear universal shafts were preserved.
- Universal shaft couplers were salvaged from the front and rear differential assemblies
- The front and rear support arms, as well as the struts for the steering mechanisms were preserved and designed around for the VTOL body.

Step three: transmission gearbox

- The carrying handle was removed.
- The fuel tank was loosened.
- The screws mounting the plastic brace and servo motors to the chassis were loosened such that the plastic brace could be removed to create clearance to remove the transmission gearbox.
- The OEM transmission gearbox was removed and disassembled.
- All components of the OEM transmission gearbox aside from the gears and casing were repurposed to assemble the replacement transmission gearbox.

- The functionality of the centrifugal clutch was mechanically locked out.
- The replacement transmission gearbox was installed onto the chassis.
- The screws holding the plastic brace and servo motors to the chassis were reinstalled.
- The fuel tank was reinstalled in reversed orientation to create clearance for the new transmission gearbox.

Step four: Assembly of the VTOL Body

- The two halves of the 3D printed front bottom “wing” pieces were fitted together via the dovetail cutout.
- Six pillow block bearings were press fitted into the wing. *Due to issues with 3D printer calibration and tolerances the cavities for the pillow block bearings had to be enlarged with a rotary tool, and the bearings had to be heated with a heat gun before being pressed in.*

Figure 3.33 Heating up the pillow block bearings

- The long threaded rod was inserted through the wing piece and flange on the pillow block bearing.
- The original shafts and bevel gears were removed from the bevel gearbox.
- The casing for the bevel gearbox was positioned and the axle shafts and drive shaft were slid through the pillow block bearings into the casing. *Due to the swivelling capability of the pillow block bearings, it was difficult to align the axle shafts, as the swivelling added three extra degrees of freedom to the movement of the shaft while it was being slid into place.*
- The bevel gears from the bevel gearbox were installed onto the axle shafts and drive shaft within the bevel gearbox casing. Set screws were used to mount the bevel gears onto the shafts.
- The set screws on the pillow block bearings were tightened onto the axle and drive shafts.

Figure 3.34 Partially complete "wing" assembly

- The two halves of the 3D printed front top "wing" pieces were fitted together via the dovetail cut-out.

- The front top wing was pressed onto the bearings for the front bottom assembly.
- Another long threaded rod was inserted through the top front wing pieces and flanges on the pillow block bearings.
- Four nuts were tightened onto the threaded rods and secured with thread locker. *It was important that the pressure applied by the nuts onto the 3d printed parts was equal across all 4 nuts, as any deviation could result in the printed parts bowing and interfering with the alignment of the axle shafts.*

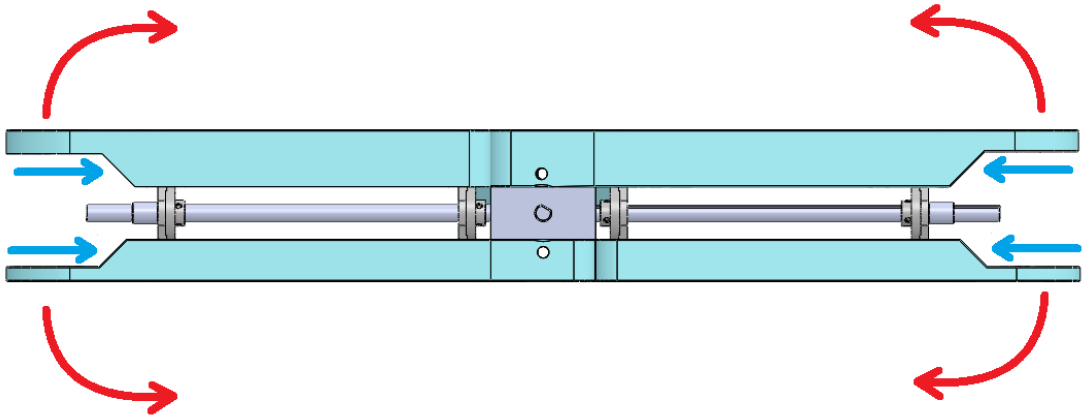

Figure 3.35 The bowing motion of the wing assembly

- A pillow block bearing was pressed into the top right wing of the assembly.
- A large bevel gear was slid onto the free end of the right side axle shaft.
- A pillow block bearing was positioned on the top left wing of the assembly. The propeller shaft was slid through this pillow block, a second large bevel gear, and the pillow block bearing that was pressed into the top right wing.
- The set screws on the pillow block bearings were tightened onto the propeller shaft.
- Two short threaded rods were inserted through the top and bottom pillow block bearings and secured into place with thread locker and

nuts.

- The large bevel gears were aligned and tightened onto their respective shafts via set screws.

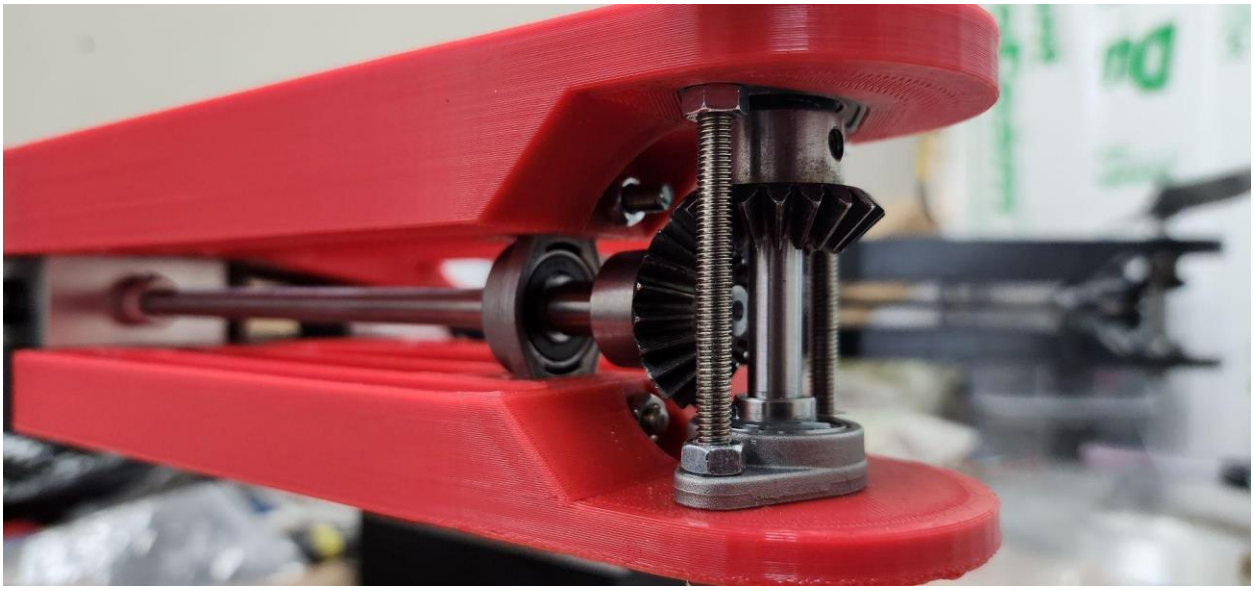

Figure 3.36 Closeup of how the 3d printed wing piece is supported by threaded rods

- The previous 6 steps were repeated for the left side of the front wing assembly.
- The previous 18 steps were repeated for the rear wing assembly.
- The front wing assembly was fastened to the chassis using the mounting points of the original differential assembly.
- The rear wing assembly was fastened to the chassis using the mounting points of the original differential assembly.
- The propellers were fastened onto all four propeller shafts.

Step eleven: Assembly of the landing gear

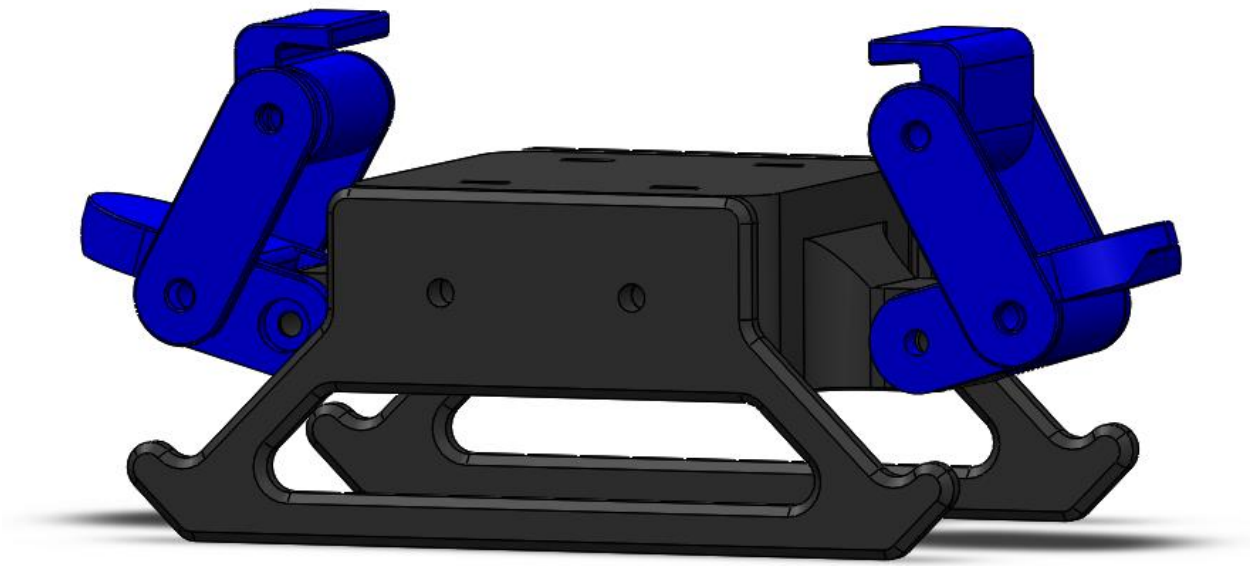

Figure 3.37 The landing gear for the drone. Reuses the same draw latch design as the workstand.

- The 3D printed parts were fastened together using various 10-32 screws and nuts.
- The landing gear used a draw latch mechanism to secure itself onto the chassis
- The draw latch mechanism allowed for modularity as the landing gear could easily be detached by undoing the latches.

The final design of the VTOL can be seen on Figure 3.38

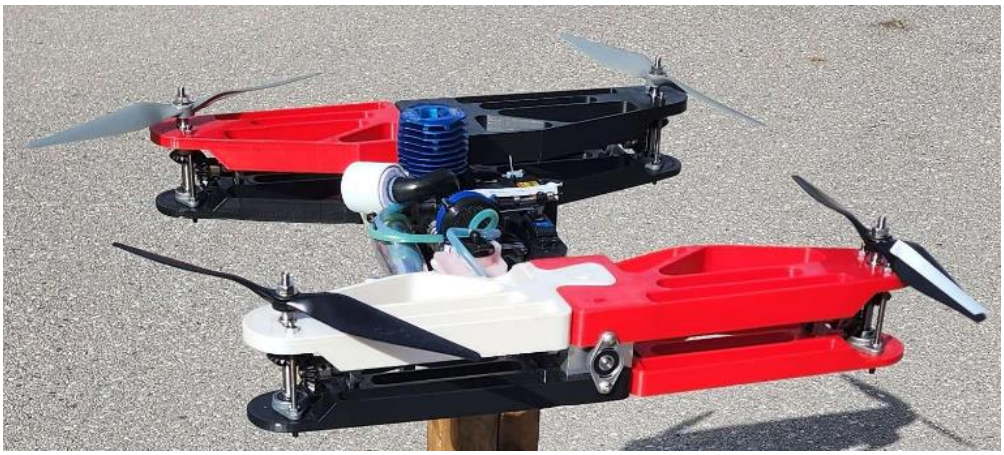

Figure 3.38 Final Design of the VTOL

3.3.2 The Evac Frame

Step one: assembly of top plate

Figure 3.39 The hooks on the top plate

- Slide top hooks through mating locations
- Fish, fishing wire through holes and create large knots to prevent

fishing wire from passing back through.

Step two: Assembly of spacer

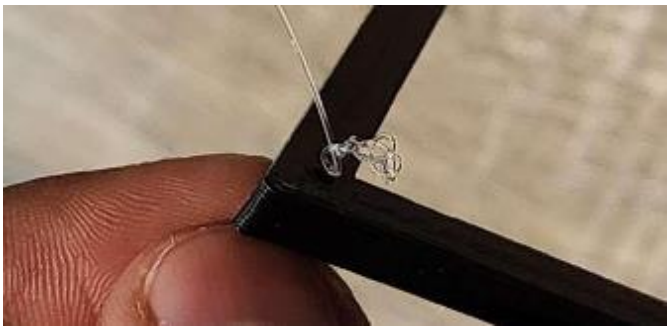

Figure 3.40 The wire passing through the spacer

- Fish, fishing wires through the spacers holes and create a knot under the spacer to ensure fishing wire from passing through.

Step three: Assembly of bottom plate

Figure 3.41 The underside of the bottom plate

- Pass and knot fishing wire through the spool to ensure they are secured

around the spool.

- Pass the fishing wires through the groove and onto the outside of the pulley, then connect to the rest of the frame with the use of knots.

3.4 System Analysis

The design of mechanical devices requires that the behaviour of the device is both safe and predictable, both during testing and actual operation. This is doubly important with mechanical devices that operate in close proximity to humans, so it is imperative to understand how a mechanical system behaves throughout its operation range. This involves analyzing the various components and subsystems of the device such as the engine, fuel system, cooling system, power transmission, control system and lubrication system, to identify areas for improvement and ensure that they are functioning effectively and efficiently.

3.4.1 Engine Analysis

Different engines have varying optimal operating conditions, thus, attributes such as air-to-fuel ratio, throttle response, engine load, and ambient temperature and other operating conditions must be benchmarked. System analysis may be used to identify the optimal fuel mixtures and pressure for an engine to maximise its power output while minimising fuel consumption and cooling of the system. It can also help identify potential sources of inefficiency or failure, such as leaks in the fuel system or inadequate lubrication of engine parts, and suggest solutions to these problems.

Measurement of the throttle opening of the engine is a vital part of understanding the behaviour of the system. The size of the throttle opening determines the amount of air-to-fuel mixture that is led in, which then determines the power output of the engine. The power output of the engine

can then be used to determine the engine behaviour under varying loads. The carburetor opening is dependent on the angle of the throttle trigger, so it is commonplace to gather data to determine a ratio between the size of the throttle opening in relation to the angle of the throttle trigger. A methodology for gathering this data is discussed in section 4.1.2.

Fuel system study needs to be done, with fluid dynamics, to ensure there is enough backpressure feeding fuel back into the engine so that the engine does not run lean or too rich; as in the former this it will lead to reduced engine power output, increased operation temperature, and faster wear of parts.

3.4.2 Mechanics Study

Another consideration is mechanics study; moments of inertia of various components need to be determined to determine how nimble the system is and how it will react under different loads and speeds. This information can help in optimising the design of the drone to ensure it meets its intended use case while maintaining optimal performance. Both rudimentary calculations and basic physical testing was used to determine the moments of inertia of individual components for the system. A description of the procedure for this testing is described in section 4.2.6. It is important to note that a proper mechanics study involves extensive application of metrology, which is out of the scope of this project.

3.4.3 Powertrain Analysis

In addition to the mechanics study and powertrain analysis, it is also important to measure vibrations near critical components such as where the wings attach to the drone body. Vibrations can cause stress and fatigue in components, leading to premature failure or reduced performance. Therefore, vibration analysis is necessary to ensure that the drone is operating within safe and acceptable limits.

Moreover, analysing the alignment of all the shafts in the system is also crucial. Misalignment of shafts can cause stress on the components, reduce efficiency and can cause premature wear and tear. Therefore, alignment analysis can identify potential misalignments and suggest corrective measures to reduce stresses and improve efficiency.

3.4.4 Thermodynamic Analysis

The thermodynamics of the system should also be analysed to ensure that all parts are operating within their optimal temperature range. If the engine operates outside of its operation range, it will lead to a case coined “heat soak” where engine power is reduced due to the change in gaps between moving parts [30]. Entering and surpassing this region will increase the probability of engine failure. Conversely, if an engine is operated too far below its operating temperature it will not be lubricated properly which will also lead to a reduced power output and risks premature failure. Finally, critical components such as the clutch and gearbox temperatures should also be considered. If the load on the clutch is too high it will lead to the failure of the clutch and sudden power loss. A procedure for gathering data on the thermal behaviour and characteristics of the system is discussed in section 4.2.4.

Overall, during system analysis of engines or engines in drones, a holistic approach is necessary, taking into consideration various factors such as mechanics, vibrations, alignment, inertias, and environmental conditions. By analysing these factors, it is possible to optimise engine design, improve performance, and reduce potential issues such as stress, premature wear and tear, and reduced efficiency.

CHAPTER 4: Benchmarking and Results

4.1 Design of evaluation procedure

4.1.1 The Workstand

To streamline the process of assembly and testing, a workstand was constructed to both suspend the VTOL device, and secure it in that suspended position. It was important that the stand suspend the VTOL device enough that work could be done to the underside of the VTOL device unhindered. It was also vital that the work stand could hold down the VTOL device when it was eventually tested and benchmarked.

Various mechanisms were considered for securing the VTOL device including tie straps, wingnuts, and even electromagnets. Ultimately, it was decided that a custom-designed draw latch mechanism would be best suited not only due to how well it can secure the VTOL device to the workstand, but also how quickly the VTOL device could be attached to and detached from the stand using the draw latches.

Figure 4.1 Draw latch mechanism.

The workstand was constructed using a custom-modelled 3D printed block with 3D printed draw latches on both sides. The draw latches were assembled using 10-32 screws of various lengths. The 3D printed latches would hook directly onto the chassis to secure it to the workstand. The base of the workstand was constructed out of scrap 2x4 wooden planks, which were cut to length and assembled using deck screws.

Figure 4.2 The CAD model of workstand.

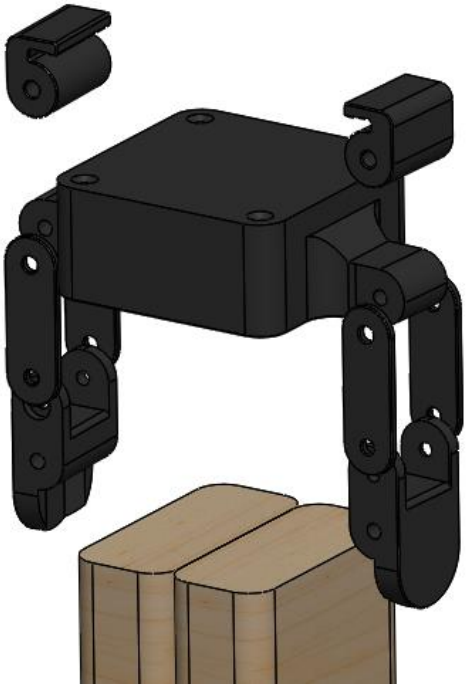

Figure 4.3 Exploded view of the workstand.

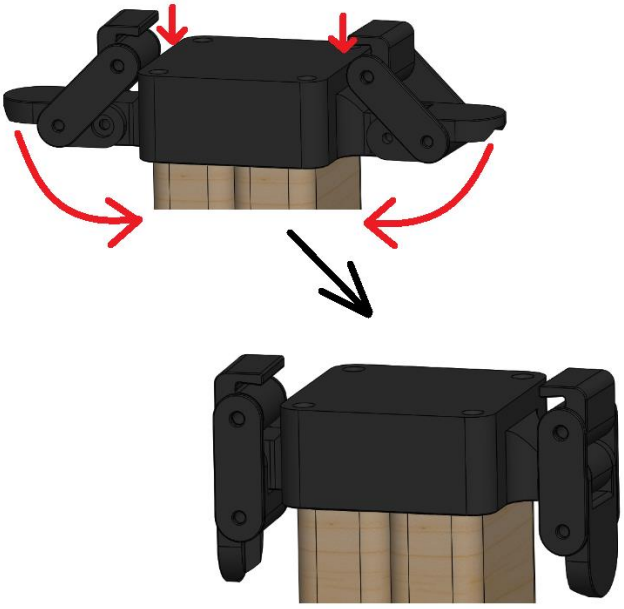

Figure 4.4 The functionality of the draw latch mechanism.

4.2 Benchmarking Procedures

4.2.1 Throttle Opening Calibration

The size of the throttle opening gap for the selected engine was determined by a crank-slider mechanism controlled by a servo motor. The servo motor was controlled wirelessly by the RC car's controller. To collect the relevant data, two apparatuses had to be constructed: a jig to measure the angle of the throttle trigger, and a jig to measure the travel distance of the throttle opening crank-slider. The data collected is shown below in Table 4.1.

The trigger angle jig was constructed using 3D printing, with careful consideration to ensure that the jig can be attached to the controller without modification of the controller itself. As shown in Figure 4.5, it was necessary to extend the length of the trigger to increase the arclength that the trigger travels, in order to obtain more precise measurements on the angle of the trigger. It was determined that the trigger ultimately had a throw of 30 degrees, hence the jig was made to be able to mechanically lock out the trigger in 5 degree increments, as shown in Figure 4.6.

Figure 4.5 The extended trigger on the trigger angle jig

Figure 4.6 Angle increments on the trigger angle jig

The throttle gap distance jig was simply a piece that mounted onto the existing components of the engine system next to the crank-slider for the throttle opening. A ruler was printed to scale and pasted onto the jig to measure the distance that the throttle opening crank-slider travelled per angle of tilt of the trigger.

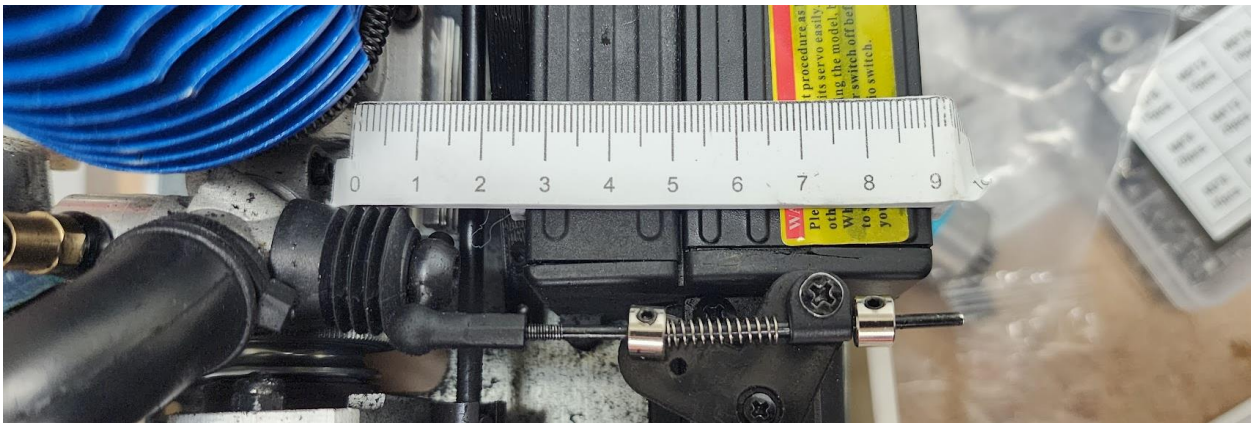

Figure 4.7 The throttle gap measurement tool

Apparatus

- Trigger angle jig
- Throttle gap distance jig

Testing Procedure

The following steps were followed to determine the relationship between throttle opening gap distance and trigger angle

1. The trigger angle jig was mounted onto the controller
2. The throttle gap distance jig was mounted next to the throttle gap crank-slider.
3. The trigger was mechanically locked out to 5 degrees, and tilted to the lockout.
4. The distance travelled by the throttle gap crank-slider was recorded.
5. Steps 3 and 4 were repeated with the trigger locked out to the 5, 10, 15, 20, 25, and 30 degree positions.

4.2.2 Payload Capacity

Payload capacity may be the most important metric measuring the success of the device. The objective of this benchmarking procedure is to measure the thrust generated by the device to determine the maximum payload capacity.

Apparatus

- VTOL
- Benchmarking stand
- Glow plug igniter
- Drill starter
- RC controller
- Laser tachometer

Testing Procedure

The following steps were followed to measure the thrust generated by device

6. The device was mounted on the working stand in an orientation allowing for easy measurement of propeller RPM
7. A safety check was conducted to ensure the device was in a stable position and properly secured to the stand
8. The RC controller for the engine was turned on
9. The servo motor controlling the engine throttle on the device is then turned on
10. The engine was ignited using the glow plug and turned over using the drill starter
11. The engine was left to idle until engine RPM settled
12. The propeller RPM was measured using the laser tachometer
13. The engine was slowly throttled in short increments until maximum throttle or maximum engine load was achieved
14. The RPM at each throttle increment was recorded
15. Once RPM at max throttle was recorded, the throttle of the RC car was released and brake was applied until engine turns off
16. Once engine was allowed to cool, the servo motor on the device was turned off
17. The RC controller was turned off, concluding the experiment

4.2.3 Endurance Testing

The success of the nitro engine VTOL device may be determined by its endurance capacity, which is a crucial metric for its performance. The objective of this benchmarking procedure is to measure the maximum theoretical flight time of the device by measuring the fuel consumption at different throttle levels.

Apparatus

- VTOL
- Benchmarking stand
- Glow plug igniter
- Drill starter
- Laser tachometer
- RC controller
- Calibrated fuel container
- 12.6mL container

Testing Procedure

The following steps were followed to measure the endurance capacity of the device:

1. The device was mounted on the working stand in a position that allows for easy access to the throttle control and fuel tank.
2. A safety check was conducted to ensure that the device was in a stable position and properly secured to the stand.
3. The RC controller for the engine was turned on, and the servo motor controlling the engine throttle on the device was then turned on.
4. The engine was ignited using the glow plug and turned over using the drill starter.
5. The engine was left to idle until the engine RPM settled.
6. The calibrated fuel container with a volume of 12.6 ml was used to fill the fuel tank of the device until it was full, and the starting fuel level was recorded by counting the number of times the container was used.
7. The engine was throttled up to 10% and left to run for 2 minutes while the fuel consumption was recorded.
8. The calibrated fuel container was used to fill the fuel tank again until it was full, and the fuel level was recorded by counting the number of times the container was used.
9. The engine throttle was then increased to 20%, and the device was

allowed to run until the fuel level dropped to the starting level.

10. Steps 8 and 9 were repeated for 30%, 40%, and 50% throttle levels.
11. The data obtained from the fuel consumption measurements were recorded in a data sheet.
12. The engine was then turned off
13. The servo motor on the device was turned off
14. The RC controller was turned off
15. The data was analysed to determine the endurance capacity of the nitro engine VTOL device.

4.2.4 Thermal Testing

The objective of this design evaluation procedure is to measure the temperature at different critical locations of the device during and after operation. This is important as it provides essential data on the thermal integrity of the device during operation. This data will lead to conclusions and future recommendations for the thermal safety profile of the device. The critical locations include the inside of the air cooling fin where the glow plug is, the crank case, the centrifugal clutch attached to the engine, the engine gearbox, the propeller gearbox, and the bevel gearbox.

Apparatus

- VTOL
- Benchmarking stand
- Glow plug igniter
- Drill starter
- RC controller
- Infrared Thermometer

Testing Procedure

1. The ambient temperature and pressure data were recorded initially

2. The device was mounted on the working stand in an orientation allowing for easy measurement of critical components
3. A safety check was conducted to ensure the device was in a stable position and properly secured to the stand
4. Temperature of critical components were recorded prior to the ignition of the engine as a baseline
5. The RC controller for the engine was turned on
6. The servo motor controlling the engine throttle on the device is then turned on
7. The engine was ignited using the glow plug and turned over using the drill starter
8. The engine was left to idle until engine RPM settled
9. Temperature measurements of critical components were taken to record data during idle
10. The engine was slowly throttled in short increments until maximum throttle or maximum engine load was achieved
11. Once maximum throttle was reached, throttle was released for safety
12. Temperature measurements of critical components were quickly taken to record temperatures at maximum load
13. Once maximum measurements were taken, the engine was allowed to cool until reaching stable temperatures, the time it takes for each critical component to cool was recorded.
14. Once device temperature has settled, the servo motor on the device was turned off
15. The RC controller was turned off, concluding the experiment

4.2.5 Fastener Torque

The objective of this design evaluation procedure is to ensure that all fasteners are torqued to the correct value before operation and to verify that their torque remains within an acceptable range after operation. To conduct

this evaluation, a torque wrench with a digital readout was used to torque all fasteners to 5Nm, and *Dap Tank Bond* vibration-absorbing threadlocker was applied to prevent vibration and ensure that the fasteners do not come loose during operation. After operation, the torque wrench was used again to verify that all nuts remained within the acceptable torque range.

Apparatus

- VTOL
- Benchmarking stand
- Glow plug igniter
- Drill starter
- RC controller
- Digital torque wrench
- *Dap Tank Bond* vibration-absorbing threadlocker

Testing Procedure

The following steps were followed to ensure that all fasteners were torqued correctly and to verify their torque values after operation:

1. All fasteners which needed to be torqued were identified.
2. The device was mounted on the working stand.
3. A safety check was conducted to ensure the device was in a stable position and properly secured to the stand.
4. The threadlocker was applied to each fastener.
5. The torque wrench was set to 5 Nm and applied to each fastener to ensure it is torqued properly.
6. The RC controller for the engine was turned on.
7. The servo motor controlling the engine throttle on the device is then turned on.
8. The engine was ignited using the glow plug and turned over using the drill starter.

9. The engine was left to idle until engine RPM settled.
10. Temperature measurements of critical components were taken to record data during idle.
11. The engine was slowly throttled until operating speed was reached, where the throttle was held for five minutes.
12. The engine was then turned off using the RC controller.
13. The servo motor on the device was turned off.
14. The RC controller was turned off.
15. Torque value measurements of each fastener were taken and recorded after operation using the torque wrench.

4.2.6 Moment of Inertia of the Propeller

The moment of inertia of the propeller was conducted as part of the basic mechanics study conducted on the VTOL device. Due to the complexity of performing a mechanics study, only the propeller was considered for the mechanics study. The propeller was chosen to be considered due to its moment of inertia having a significant effect on the forces the propeller will experience when spun at operating speeds. The procedure for finding the moment of inertia of the propeller was predicated on the principles governing a pendulum, where if the mass, length, and swinging period of the pendulum are known, the moment of inertia of the pendulum's mass can be calculated. A custom jig was created from which the propeller could be hung using a fishing line and treated as a pendulum mass.

Figure 4.8 The pendulum jig

Apparatus

- Moment of inertia testing jig
- Propeller
- Fishing Line
- Camera with slow-motion recording capabilities
- Video editing software

Testing Procedure

The following steps were followed to determine the moment of inertia of the propeller.

1. The mass of the propeller was recorded.
2. The propeller was tied to the pendulum jig using fishing line.
3. The length of the fishing line was recorded.
4. The propeller was released from a known height and allowed to swing

back and forth for several revolutions.

5. A camera with slow motion recording capabilities was used to record the swinging motion of the propeller.
6. Video editing software was used to analyse the footage of the propeller swinging to determine its swinging period.
7. The moment of inertia was calculated from the data gathered.

4.3 Evaluation of Results

4.3.1 Results from Throttle Opening Calibration

The data for the relationship between the throttle opening distance and trigger angle was collected across 3 trials to provide a larger set of data to generate averaged values. It was determined that the relationship between the angle of the trigger and the increase in distance of the throttle opening gap was linear, where an increase of 5 degrees in the angle of the trigger, results in a deflection of 2.33mm of the throttle opening crank-slider.

Table 4.1 The data for throttle opening distance vs trigger angle

Trigger angle (degrees)	Throttle opening crank-slider distance travelled (mm)				
	Trial 1	Trial 2	Trial 3	Average	STD Error
0	0	0	0	0	0
5	1	3	3	2.33	0.67
10	3	5	5	4.33	0.67
15	6	6	7	6.33	0.33
20	8	7	8.5	7.83	0.44

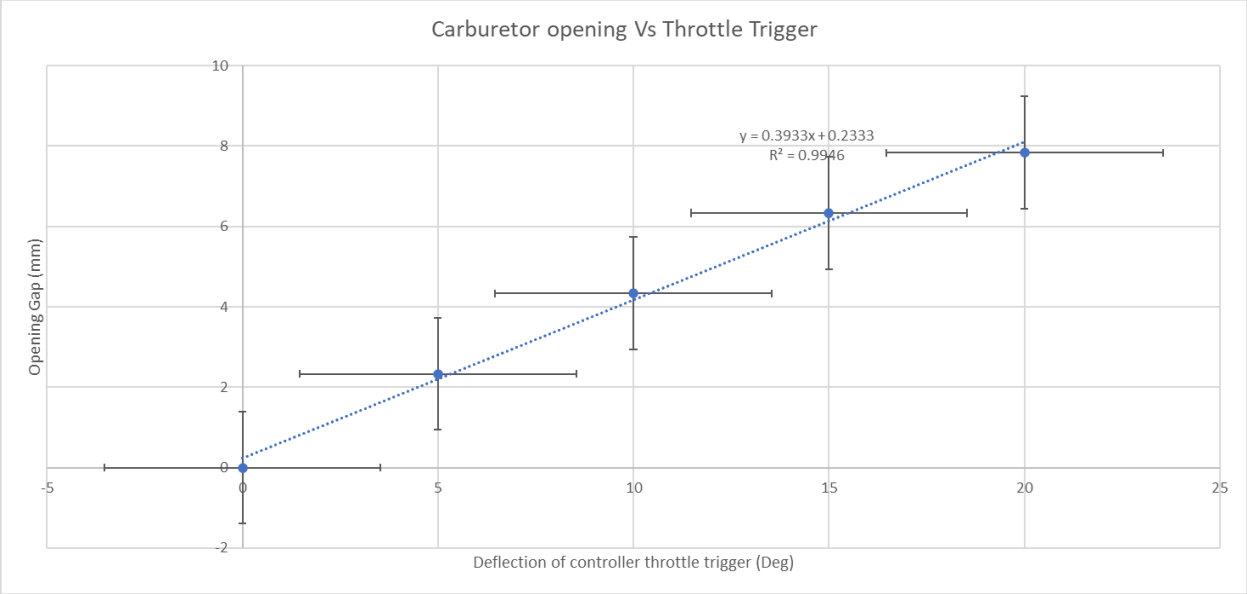

Figure 4.9 A graph of the trigger angle vs throttle opening gap.

$$\%Throttle\ Opening = \frac{(0.39338 \cdot Deg\ Opening + 0.2333) \cdot 100}{Full\ Range\ of\ throttle\ opening} \quad (4.1)$$

4.3.2 Results from Payload Testing

The results of the payload testing were inconclusive due to the centrifugal clutch failing during the testing process. The centrifugal clutch serves as a safety mechanism to ensure that the engine could be started without stalling by disengaging the engine from the rest of the mechanics until the engine has reached operating speed. The centrifugal clutch failed because the OEM nylon pawls could not handle the loads being placed upon them.

Prior to the centrifugal clutch failing, it was recorded that the propellers achieved 5000 RPM with a throttle opening gap of 40%. From the manufacturer's specifications, each propeller could generate 2lb of lift at 5000 RPM [25]. Extrapolating from this, it is estimated that the current design for the VTOL device can achieve a lifting force of 20lb.

Table 4.2 The manufacturer's specifications for lift generation.

Propeller Speed (RPM)	Theoretical Lift Generated (lb)
4000	1.287
5000	2.018
6000	2.917
7000	3.989
8000	5.237
9000	6.669
10000	8.291

4.3.3 Results from Endurance Testing

The fuel consumption data collected was analysed to determine the endurance capacity of the nitro engine VTOL device by plotting the fuel consumption against the throttle level. The data was then interpolated to estimate the fuel consumption at 60%, 70%, 80%, and 90% throttle levels.

The endurance capacity of the nitro engine VTOL device was compared to the design specifications to identify any deviations or areas for improvement. The endurance capacity was evaluated to assess the performance of the device and identify any areas for improvement. Additionally, the data obtained from the procedure were used to optimise the fuel consumption of the device and improve its endurance capacity.

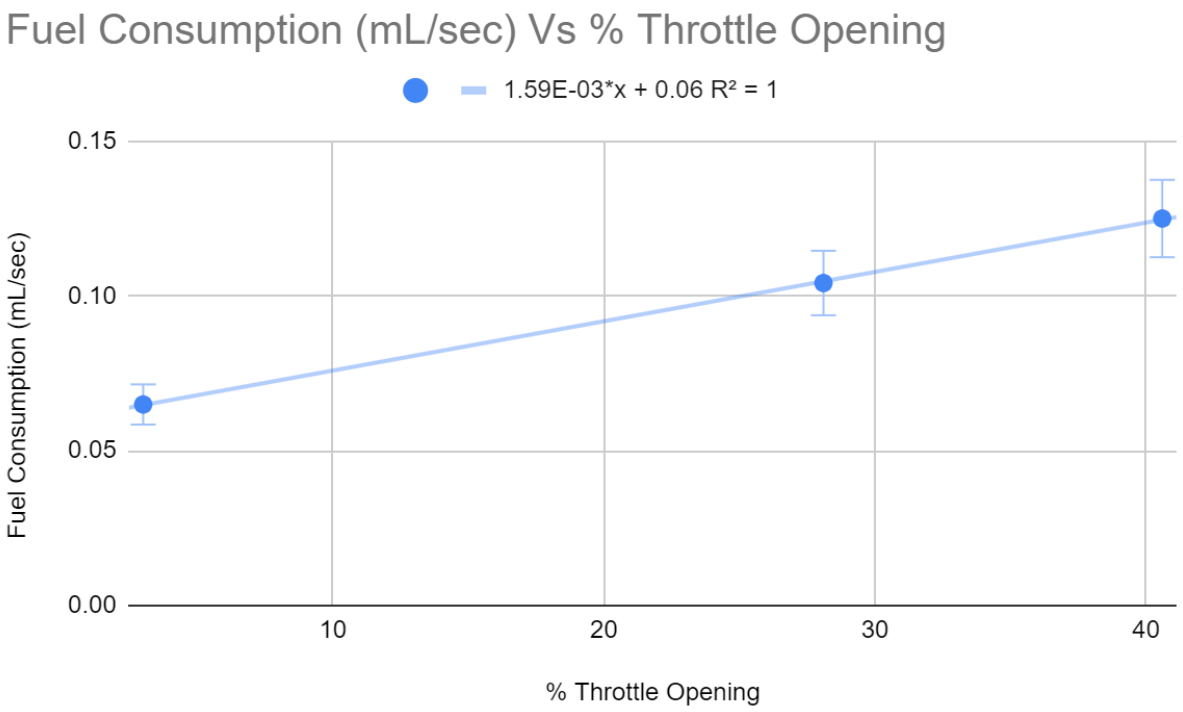

Figure 4.10 The fuel consumption vs throttle opening percentage.

Table 4.3 The data for fuel consumption vs time elapsed

Throttle Opening (%)	Fuel Consumption (mL)	Time Elapsed (s)	Consumption Rate (mL/s)
3	30	462	0.065
28.1	12.5	120	0.104
40.6	15	120	0.125

$$operation\ time\ (min) = \frac{Fuel\ Tank\ capacity(mL)}{60 \cdot (0.00159 \cdot (\%throttle\ opening) + 0.06)} \quad (4.2)$$

4.3.4 Results from Thermal Testing

The results of the radiator and crankcase temperature measurements were conclusive, as both components achieved a steady state temperature during break-in and operation at an ambient temperature of 32°F. After calibrating the air/fuel mixture, the engine was run at 50% throttle and reached a steady-state temperature of 220°F at an ambient temperature of 48.2°F with wind conditions of 5 km/h. Stable operation was achieved by the crankcase at a temperature of 165°F. Both the radiator and crankcase did not exceed their operating temperature of 200°F. The graph showing these results is shown in Figure 4.8.

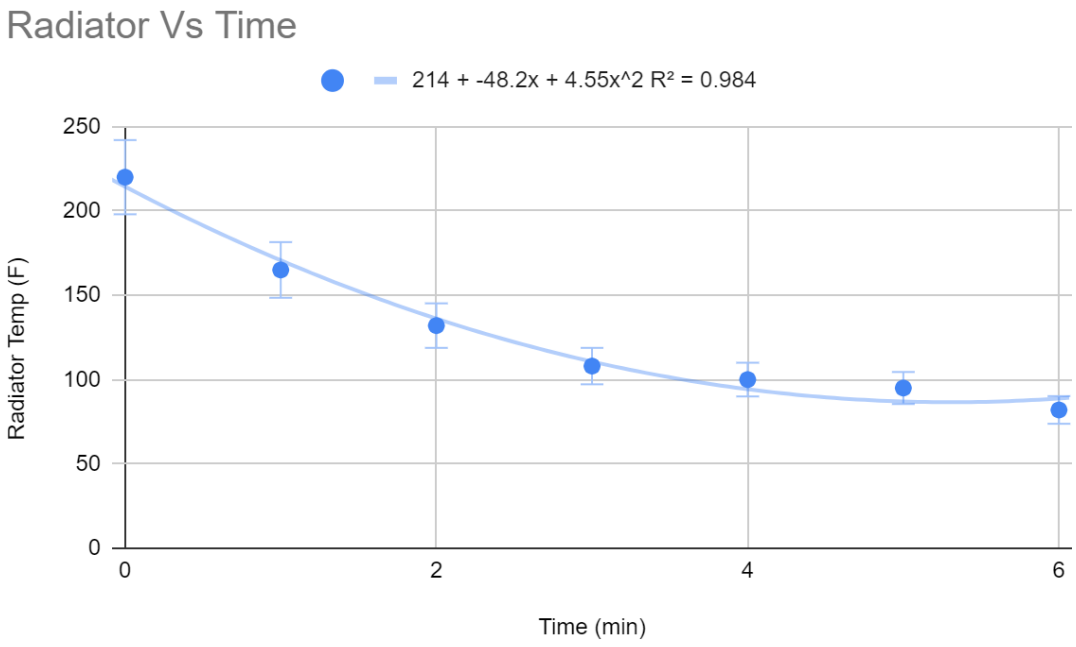

Figure 4.11 The radiator temperature vs time.

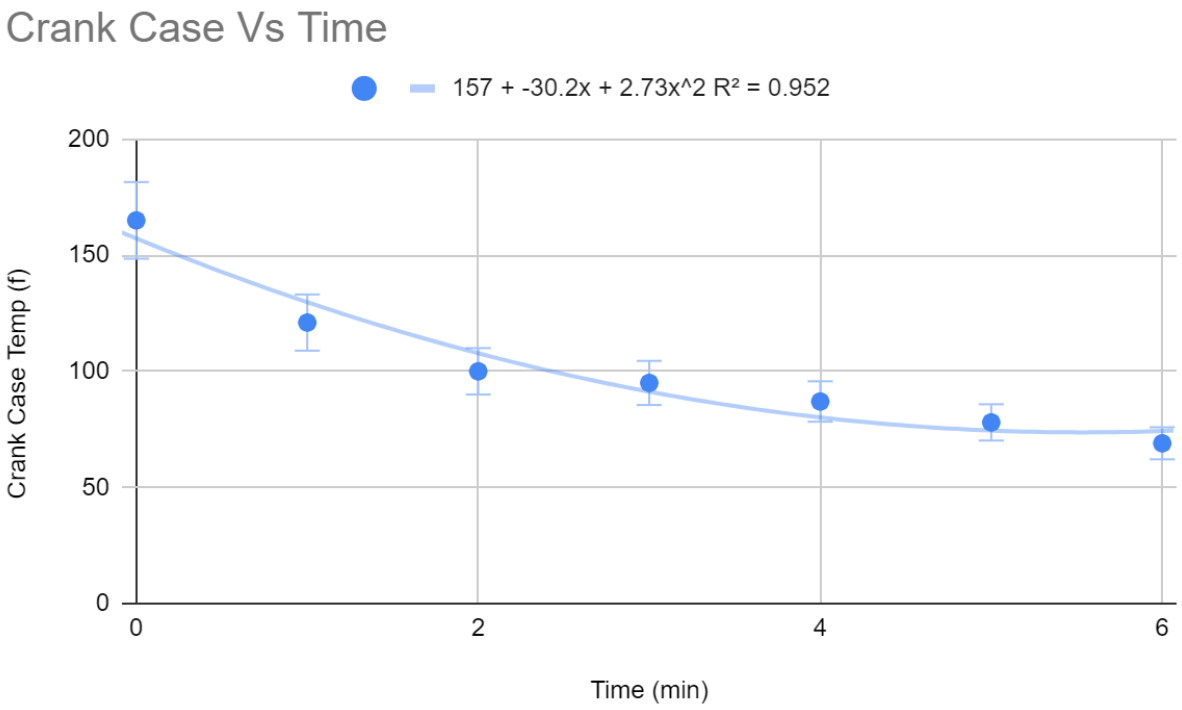

Figure 4.12 The crankcase temperature vs time.

Temperature data obtained from the centrifugal clutch was inconclusive due to the clutch failing during operation. It was determined that the OEM clutch, which employed nylon pawls, could not properly sustain the load demanded, causing the clutch to continuously slip and generate excessive heat from friction. At failure, the clutch had reached a temperature of 520°F. The graph showing these results is shown in Figure 4.9.

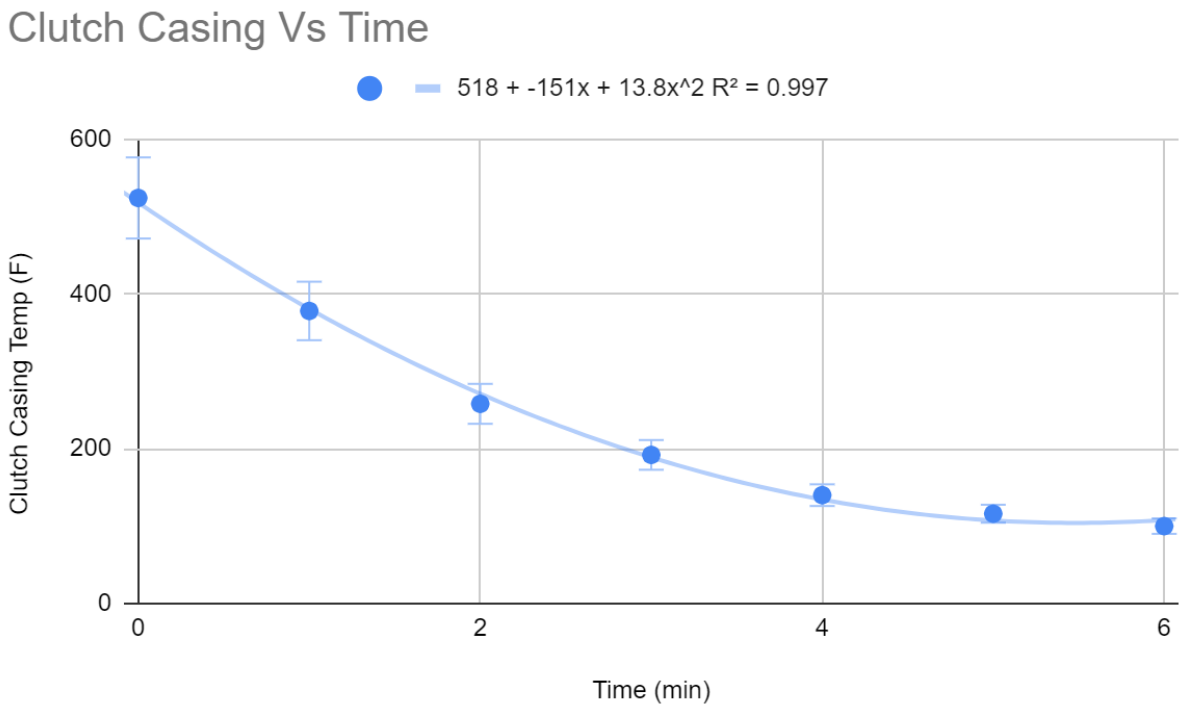

Figure 4.13 The clutch gearbox temperature vs time.

The engine gearbox, bevel gearbox, and propeller gearbox were well within their operating temperature limits. The engine gearbox posed the only concern for operating temperature, due to its proximity to the centrifugal clutch and radiator fins; components with a relatively high operating temperature. Nevertheless, all three gearboxes did not exceed their respective operating temperature ranges. The steady-state temperatures for the gearboxes were 73°F, 66°F, and 65°F, respectively. The graph showing these results is shown in Figure 4.10.

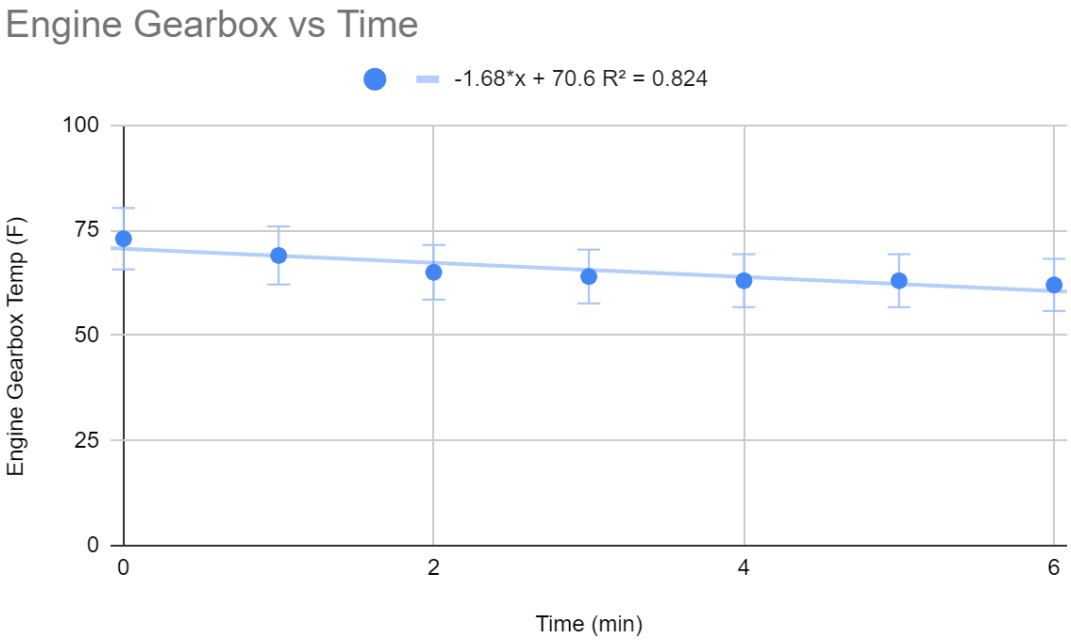

Figure 4.14 The engine gearbox temperature vs time.

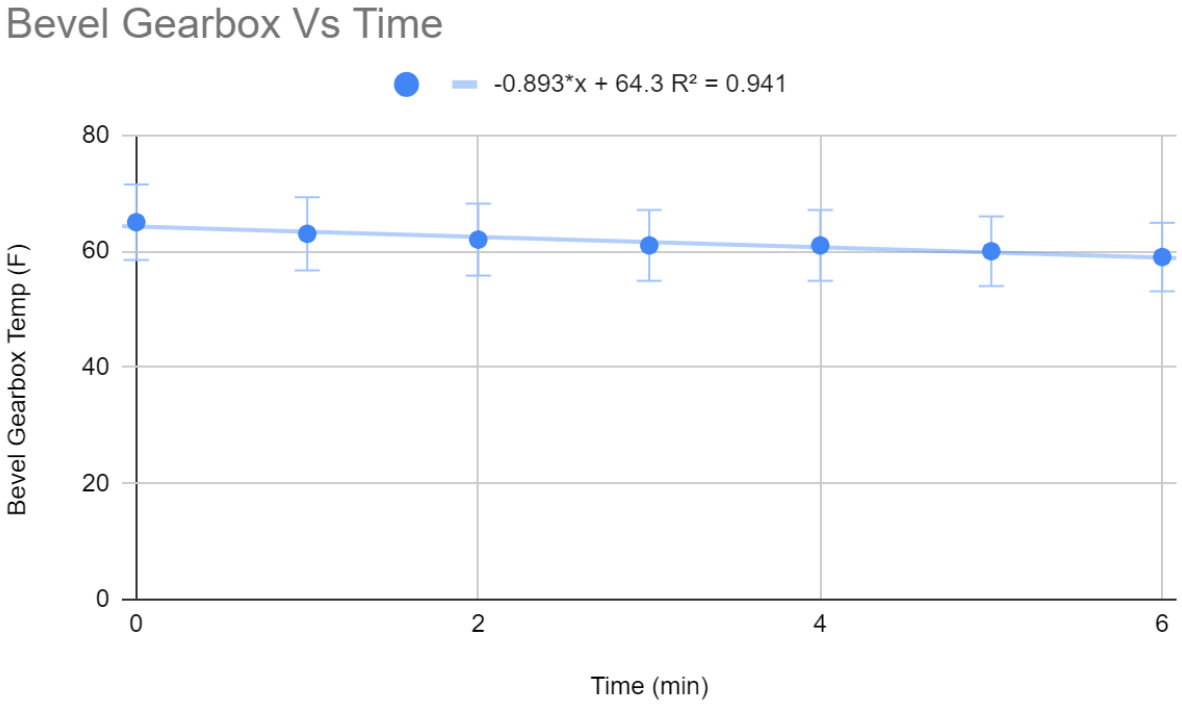

Figure 4.15 The bevel gearbox temperature vs time.

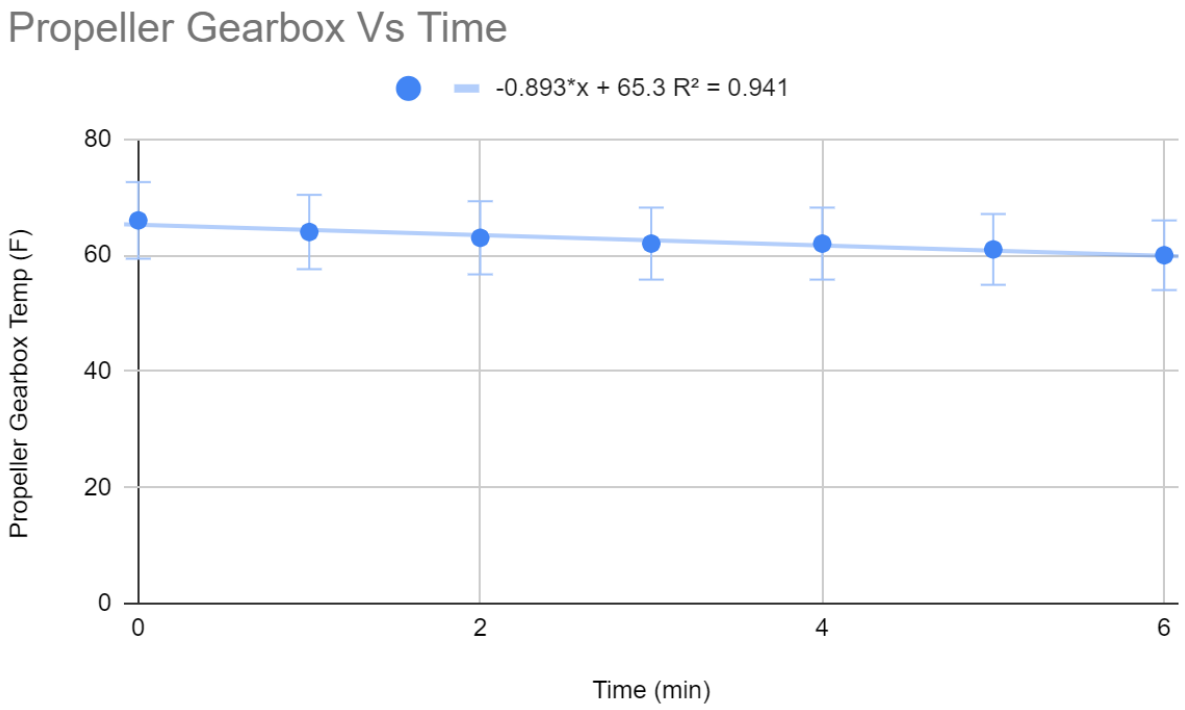

Figure 4.16 The propeller gearbox temperature vs time.

4.3.5 Results from Fastener Torque Testing

Due to the vibrations involved with the VTOL device, it was vital to ensure that the fasteners used to construct the VTOL device would not vibrate loose during operation. Shown in Table 4.3 is the data collected pertaining to the measured torques of various fasteners on the VTOL frame subsequent to operating. The torque test was used to prove the efficacy of the *Dap Tank Bond* threadlocker, which was advertised to absorb vibration. Being that the measured torque values were within 10% of the desired 5Nm, it could be stated that the threadlocker served its purpose.

Table 4.4 The measured torque of various fasteners after operating.

	Trial 1	Trial 2	Trial 3	Trial 4
Prop 1	4.991	4.628	4.635	4.613
Prop 2	4.903	4.883	4.974	4.624
Prop 3	4.945	4.656	4.697	4.992
Prop 4	4.795	4.933	4.741	4.912
Short Rod 1	4.903	4.535	4.552	4.626
Short Rod 2	4.608	4.822	4.935	4.699
Long Rod 1	4.720	4.655	4.797	4.747
Long Rod 2	4.577	4.640	4.505	4.834

4.3.6 Results from Moment of Inertia Testing

The data for the swinging period of the propeller was collected across eight separate trials, with an average value of 3.722 seconds. From this, it was determined that the moment of inertia of a single propeller was $0.0208 kg \cdot m^2$. Table 4.4 shows the data collected from the moment of inertia testing.

Table 4.5 The propeller swinging period data.

Trial #	Propeller Swinging Period (s)
1	3.767
2	3.833
3	3.567
4	3.676
5	4.033
6	3.6
7	3.7
8	3.6

4.3.7 Results from Vibration Testing

In this study, an inertial measurement unit (IMU) was used to measure the angles of rotation around the x, y, and z axes of a nitro engine drone. The IMU was placed on the body of the drone, including the engine, the front wing furthest from the engine, the back wing closer to the engine, and the gearbox located beside it. As the equipment to measure vibrations such as strain gauges was lacking, the IMU was affixed somewhat loosely, which enabled quantification and qualification of vibrations by observing changes in the reported angles. The results showed that the vibrations increased with throttle increase. Moreover, the big peaks on the graph indicated that the gearbox was not rotating smoothly at all times. This explains why the gearbox seemed to get stuck at some points relative to how smooth it was on other parts of the rotation. It is important to note that these measurements were made with the engine idling, and the vibrations are expected to increase with increased throttle.

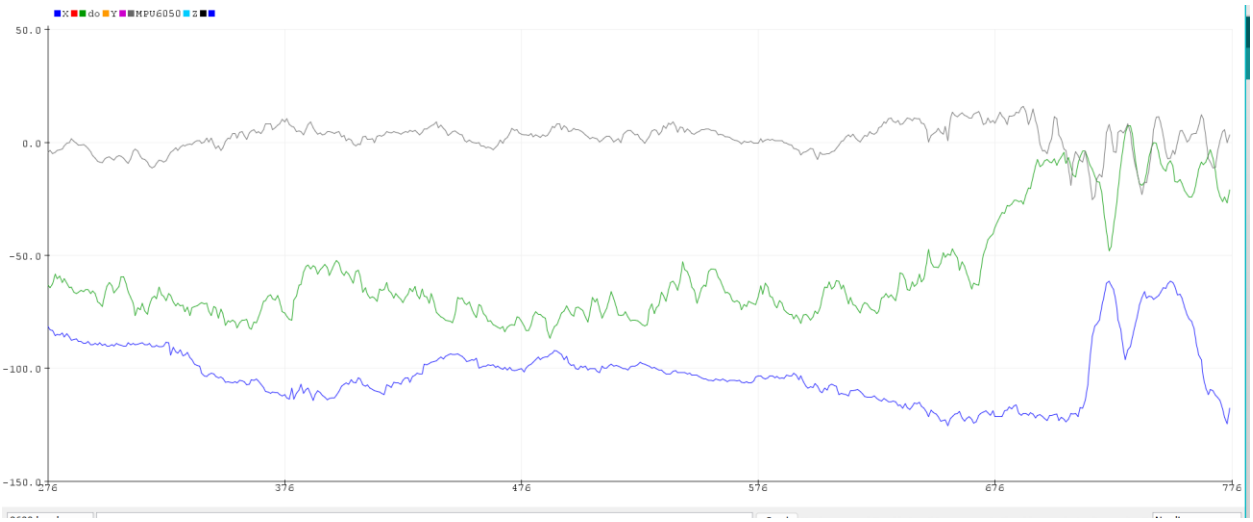

Figure 4.17 Engine

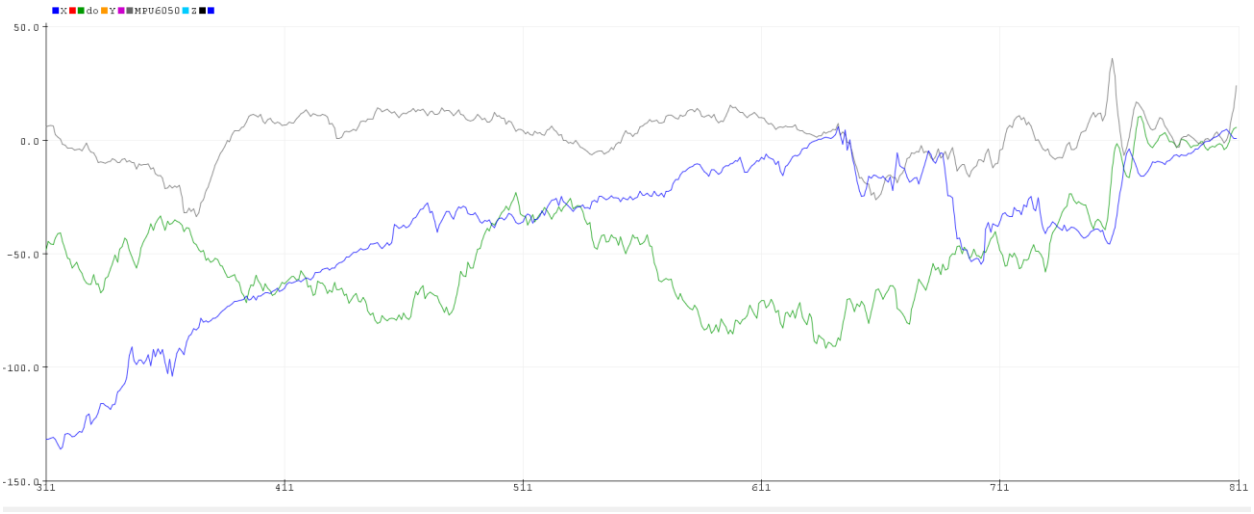

Figure 4.17 Gearbox

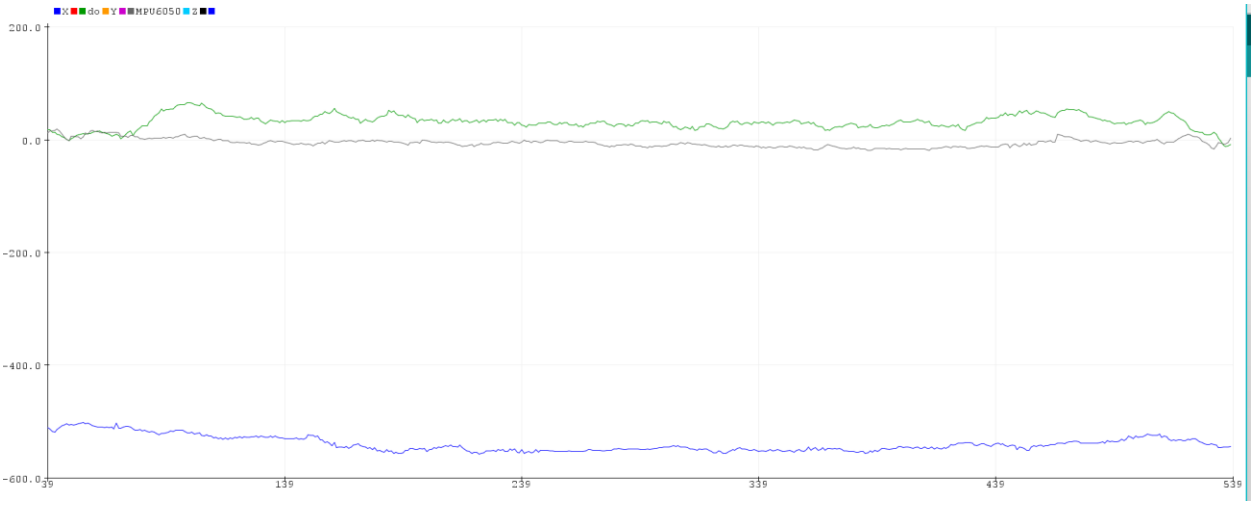

Figure 4.18Front wing

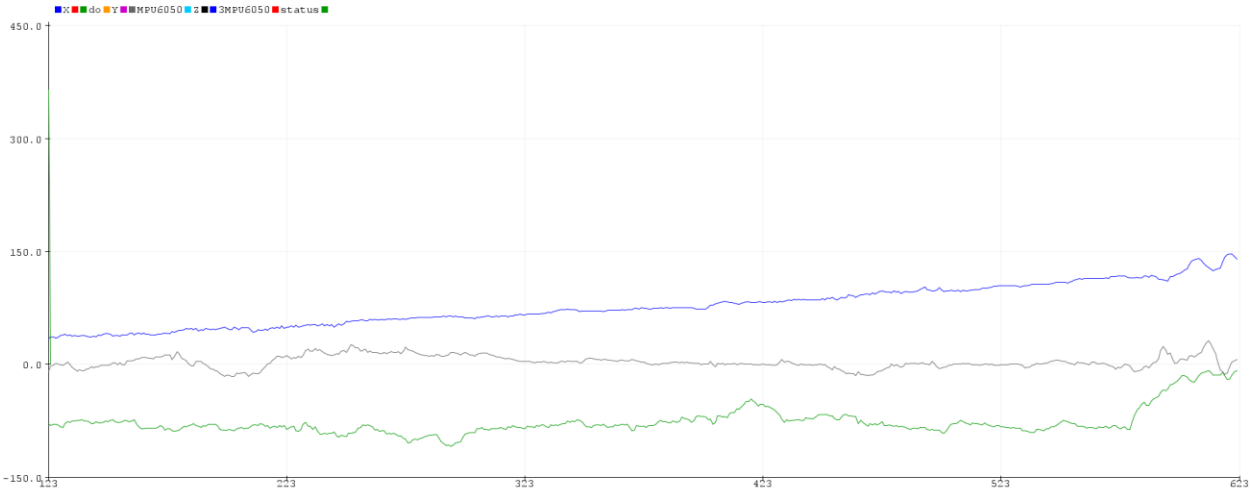

Figure 4.19 Back wing

CHAPTER 5: Discussions and Conclusions

5.1 Discussion and Comparison to existing designs

The system analysis and benchmarking tests completed and showcased in chapter 4 provide a comprehensive evaluation, based on the originally established design criteria. Each test performed, provides insight into the efficiency and performance of the subsystems comprising the VTOL device. Analysing and interpreting the results from the benchmarking evaluations, lead to generally positive implications for the use of ICEs for a VTO.

When comparing the results to performance metrics, the scaled model achieves the required level of performance for material strength, physical footprint as well as safety. To achieve these metrics, thoughtful and thorough design procedure was undertaken, reflecting well on the calculations and considerations taken for each subsystem. Moreover, these results imply that the design of a versatile and accessible lifting solution is plausible. This suggestion comes from the fact that the scaled model was able to achieve all proportion and physical constraints without sacrificing FOS. The compact footprint of the model, allows the device to operate in limited access areas, unlike current existing solutions, such as aerial lifting platforms which are gargantuan relative to the model. Therefore, the versatility of the device is established.

In contrast, the scaled model did not meet the set criteria for payload capacity, as well as the operation and thermal endurance. Analysing the results within section 4.3, it is clear that these results are caused by several reasons. Firstly, examining the payload capacity, the VTOL was unable to meet the targeted thrust values. This is ultimately due to the fact when

conducting the evaluation, the OEM nylon clutch was unable to sustain the loads exerted by the powertrain. These excessive loads caused the clutch to continuously slip, resulting in sudden power loss. This slippage prevented the transmission of kinetic energy from the engine, and instead converted the engine's kinetic energy solely into thermal energy. This excessive thermal energy would then burn the clutch entirely, ultimately causing the failure of the thermal performance metrics as well. Investigating this mode of failure, it is apparent that an extensive metrology of system components should have been conducted prior to benchmarking. This study would serve to provide a risk analysis of each mechanical component. While in the system analysis procedure, a mechanics study of the entire system was curated and planned. However, due to substantial time and budget constraints, it became unfeasible. As such one promising area for future improvements would be the conducting of a performance analysis of each mechanical component. In addition to this, metal aftermarket performance clutches were investigated and procured for use within the powertrain. It is expected that if the OEM clutch was replaced, the device would potentially be able to generate enough thrust. This is determined as even with the low transmission efficiency, a propeller RPM of 5000 was achieved, close to the target RPM values.

Examining the endurance of the device next, the device was calculated to have an estimated operation time of 23 minutes based on a fuel consumption evaluation. These values fall slightly short of the desired goal of 30 minutes. When compared to multi propeller systems examined within the literature review, the operation time of the model is underwhelming. However, this is mainly due to the small fuel capacity of the system, as the measured fuel consumption of the device is more than satisfactory. This is reflected in the fact that if the fuel tank was increased to 750ml, the operation time would substantially increase, matching and exceeding the devices examined in literature [9].

One significant area for improvement would be the power transmission

efficiency. In the current design, the powertrain utilises three different gearboxes to transmit the power from the horizontal plane, into the vertical plane. This must be done as there is only one power source in the system, which must be transmitted into four different directions. This excessive amount of power transmission, results in a significant loss of power, and ideally should be avoided. As such, one recommendation is the use of multiple different power sources. Utilising a system with multiple separate engines would allow for a simpler powertrain design, ultimately reducing the losses experienced in the system. This approach is heavily seen within the literature, as virtually all VTOL solutions utilising ICEs for power, rely on multiple different power sources. These are usually either brushless DC motors or a separate engine all together. It is also important to note that the

An investigation into the vibration of the system to evaluate the stability was also conducted. Based on the evaluation, it was determined that the vibration experienced by the system would be negligible during operation. It is important to note however, that one cylinder engines are unbalanced, and a potential method for improving stability may be to utilise even numbered cylinder engines.

5.2 Conclusions and Recommendations

The culmination of work completed in this project leads to the confirmation of several conclusions and recommendations. Overall, based on the research conducted, as well as the results observed in the evaluation of the scaled model, the development of a gas-powered propeller device has shown promise for personnel lifting operations in high-altitude scenarios. However, further research and development is required to make a definite recommendation on the technology. It is abundantly clear that the benefits of internal combustion engines such as high power density make this power source viable for use in aerial lifting operations, which require high payload and long operation times. In spite of this, there are numerous characteristics

of combustion power which remain as obstacles in the pursuit of this technology. In particular, the extremely slow response time of ICEs leads to difficulties in developing a device control system, hindering the implementation of this technology in existing solutions.

While benchmarking of the scaled model showcased generally positive results, inconclusive payload and endurance testing prevent decisive conclusions at this time. As such, it is the author's recommendation to pursue further improvements of the scaled model, to properly evaluate the feasibility of this concept. Notable areas of improvement of the device include the investigation of clutches, bearings with fewer degrees of freedom, improving gearbox alignment, lubrication, and the remaking of gearbox casings. Moreover, the conducting of a full system analysis, the investigation of multiple different power systems (including electric motors), and the development of a proper engine control system are imperative to improving the performance and efficiency of the device.

Appendix

A.1 References

[1] M. Fischer, M. Werber, and P. V. Schwartz, “Batteries: Higher energy density than gasoline?,” *Energy Policy*, vol. 37, no. 7, pp. 2639–2641, Apr. 2009.

[2] M. F. Cabanas, S. B. Duque, J. D. González, F. P. González, and M. G. Fernández, “Preliminary results of a hybrid thermoelectric propulsion system for a multirotor UAS with active rectifying, electronic throttle control and Supercapacitors,” *Applied Sciences*, vol. 11, no. 17, p. 7899, 2021.

[3]“DLE111,”*DLE*.[Online].Available:https://www.dlengine.com/en/rcengine/dle111/. [Accessed: 06-Apr-2023].

[4] W. J. Fredericks, M. D. Moore, and R. C. Busan, “Benefits of hybrid-electric propulsion to achieve 4X cruise efficiency for a VTOL UAV,” *2013 International Powered Lift Conference*, 2013.

[5] “Diesel vehicles using biodiesel,” *Alternative Fuels Data Center: Diesel Vehicles Using Biodiesel*. [Online]. Available: https://afdc.energy.gov/vehicles/diesel.html. [Accessed: 06-Apr-2023].

[6] “Aerospace Unmanned Aerial Vehicle (UAV),” *Cosworth*, 21-May-2021. [Online].Available:https://www.cosworth.com/capabilities/electrification/motor/aerospace-uav/. [Accessed: 06-Apr-2023].

[7] “JetQuad: Quad Turbine Vtol Drone - FusionFlight.” [Online]. Available: https://fusionflight.com/JetQuad/. [Accessed: 06-Apr-2023].

[8] “Micro turbine engines for drones propulsion - iopscience.” [Online].

Available: https://iopscience.iop.org/article/10.1088/1757-899X/148/1/012063. [Accessed: 06-Apr-2023].

[9] C. E. Lin et al., "Engine controller for hybrid powered dual quad-rotor system," IECON 2015 - 41st Annual Conference of the IEEE Industrial Electronics Society, Yokohama, Japan, 2015, pp. 001513-001517, doi: 10.1109/IECON.2015.7392315.

[10] C. E. Lin and T. Supsukbaworn, “Development of dual power multirotor system,” *International Journal of Aerospace Engineering*, 30-Jul-2017. [Online]. Available: https://doi.org/10.1155/2017/9821401. [Accessed: 06-Apr-2023].

[11] J. Gebauer, P. Kočí and P. Šofer, "Multicopter potentialities," Proceedings of the 13th International Carpathian Control Conference (ICCC), High Tatras, Slovakia, 2012, pp. 194-197, doi: 10.1109/CarpathianCC.2012.6228638.

[12] X. Xia, D. Ma, L. Zhang, X. Liu, and K. Cong, “Blade shape optimization and analysis of a propeller for VTOL based on an inverse method,” *MDPI*, 06-Apr-2022. [Online]. Available: https://doi.org/10.3390/app12073694. [Accessed: 06-Apr-2023].

[13] J. Verbeke, D. Hulens, H. Ramon, T. Goedemé and J. De Schutter, "The design and construction of a high endurance hexacopter suited for narrow corridors," 2014 International Conference on Unmanned Aircraft Systems (ICUAS), Orlando, FL, USA, 2014, pp. 543-551, doi: 10.1109/ICUAS.2014.6842296.

[14] B. Theys, G. Dimitriadis, P. Hendrick and J. De Schutter, "Influence of propeller configuration on propulsion system efficiency of multi-rotor Unmanned Aerial Vehicles," 2016 International Conference on Unmanned Aircraft Systems (ICUAS), Arlington, VA, USA, 2016, pp. 195-

201, doi: 10.1109/ICUAS.2016.7502520.

[15] F. Jianjun, H. Jiyong, and D. Chenghao, “Study on safety management of Guy Wires in the construction of UHV (EHV) transmission lines,” Journal of Physics: Conference Series, vol. 2005, no. 1, p. 012244, 2021.

[16] “Xiang Racing S30 SH-28 HSP RC Model Engines 4.57cc blue 28 nitro engine 4.57cc RC 1:8 Car Buggy truck truggy by XIANGTAT, Combustion Engines & parts - Amazon Canada,” , *Combustion Engines & Parts - Amazon Canada*. [Online]. Available: https://www.amazon.ca/Xiang-Racing-Engines-4-57cc-Engine/dp/B00YBBLVV6. [Accessed: 06-Apr-2023].

[17] “HSP Nokier savagery 94762 1/8 scale 4WD Off Road Nitro ... - aliexpress.com.” [Online]. Available: https://www.aliexpress.com/item/32670182144.html. [Accessed: 06-Apr-2023].

[18] “13x6.5E Product Page,” *APC Propellers*. [Online]. Available: https://www.apcprop.com/product/13x6-5e/. [Accessed: 06-Apr-2023].

[19] “62005 HSP 1/8 scale center gearbox complete (62008 / 62907),” RC High Performance Hobbies, 12-Dec-2022. [Online]. Available: https://www.rchighperformancehobbies.com.au/product/62005-hsp-1-8-scale-center-gearbox-complete-62008-62907/. [Accessed: 06-Apr-2023].

[20] “PGFUN 1:1 right angle bevel gearbox 1 module 20 teeth 90° Angle Drive Steering Gear Device Simple Mechanical DIY module with 8mm shaft,” Amazon.ca: Industrial & Scientific. [Online]. Available: https://www.amazon.ca/dp/B09V5PRH8S/ref=twister_B0BWJMXCHP?_encoding=UTF8&th=1. [Accessed: 06-Apr-2023].

[21] S. Hermann, “Comparing Pla, Petg & Asa - feat. Prusament,” *CNC Kitchen*, 03-Feb-2020. [Online]. Available: https://www.cnckitchen.com/blog/comparing-pla-petg-amp-asa-feat-prusament. [Accessed: 06-Apr-2023].

[22] S. Hermann, “The difference of PLA and PLA+ tested! (feat. Polymaker),” *CNC Kitchen*, 16-Aug-2020. [Online]. Available: https://www.cnckitchen.com/blog/the-difference-of-pla-and-pla-tested-feat-polymaker. [Accessed: 06-Apr-2023].

[23] R. G. Budynas, J. K. Nisbett, J. E. Shigley, and K. Tangchaichit, Shigley's Mechanical Engineering Design. Singapore: McGraw-Hill Education, 2021.

[24] “Uxcell F8-19m thrust ball bearings 8mm x 19mm x 7.2mm chrome steel single direction,” Amazon.ca: Industrial & Scientific. [Online]. Available: https://www.amazon.ca/uxcell%C2%AE-Miniature-Bearings-8x19x7-2mm-Washers/dp/B07Q1MH892?th=1. [Accessed: 06-Apr-2023].

[25] “Uxcell 4pcs KFL08 8mm zinc alloy self aligning pillow block flange bearing,” *Amazon.ca: Industrial & Scientific*. [Online]. Available: https://www.amazon.ca/dp/B073L2SQMZ/ref=twister_B07HD9Y4KZ?_encoding=UTF8&th=1. [Accessed: 06-Apr-2023].

[26] “Lubrication of Gears,” *KHK*. [Online]. Available: https://khkgears.net/new/gear_knowledge/gear_technical_reference/lubrication-of-gears.html. [Accessed: 06-Apr-2023].

[27] “Performance data” *APC Propellers*. [Online]. Available: https://www.apcprop.com/files/PER3_13x65E.dat. [Accessed: 06-Apr-2023].

[28] L. Burgess, “Which is better: Gear Drive or belt and Pulley Drive System?,” Design Engineering, 01-Mar-2022. [Online]. Available:

https://www.design-engineering.com/which-is-better-gear-drive-or-belt-and-pulley-drive-system-1004038188/. [Accessed: 06-Apr-2023].

[29] “Understanding Motor and Propeller Rotation,” *GetFPV*. [Online]. Available: https://www.getfpv.com/learn/fpv-essentials/motor-propeller-rotation/. [Accessed: 06-Apr-2023].

[30] C. Bloom, “Understanding Heatsoak,” *CJB Fire Consultants*. [Online]. Available: https://www.team-bhp.com/forum/attachments/technical-stuff/237721d1259733884-coolant-spilling-out-reservoir-after-i-switch-off-engine-heatsoak.pdf. [Accessed: 06-Apr-2023].

A.2 Calculations

Bearing Calculations:

To calculate the equivalent force of the axial and radial loads, in addition to Eq 3.9a and 3.9b, the following tables from Shigley's Mechanical Engineering Design textbook were used.

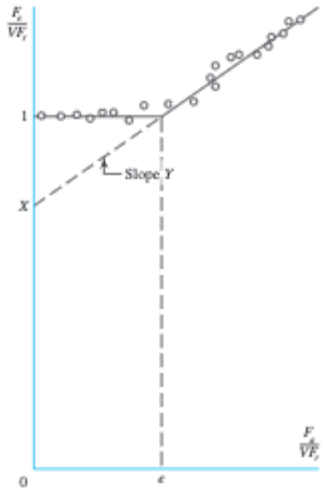

Figure A.1 Relationship of the dimensionless group $\frac{F_e}{V\,F_r}$, *and* $\frac{F_a}{VF_r}$ *and the straight line segments representing the data* [21]

Table A.1 Equivalent Radial load Factors for ball bearings [21]

		$F_a/(VF_r) \le e$		$F_a/(VF_r) > e$	
F_a/C_0	e	X_1	Y_1	X_2	Y_2
0.014*	0.19	1.00	0	0.56	2.30
0.021	0.21	1.00	0	0.56	2.15
0.028	0.22	1.00	0	0.56	1.99
0.042	0.24	1.00	0	0.56	1.85
0.056	0.26	1.00	0	0.56	1.71
0.070	0.27	1.00	0	0.56	1.63
0.084	0.28	1.00	0	0.56	1.55
0.110	0.30	1.00	0	0.56	1.45
0.17	0.34	1.00	0	0.56	1.31
0.28	0.38	1.00	0	0.56	1.15
0.42	0.42	1.00	0	0.56	1.04
0.56	0.44	1.00	0	0.56	1.00

*Use 0.014 if $F_a/C_0 < 0.014$.

Propeller inertia calculation:

A pendulum was made for the propeller with reference points behind the proller, the propeller was swing and its period was measure on 10 different trial runs. The video recorded was recorded using slow motion iphone feauthre and the data was analyzed using physics software called tracker to determine the period of the pendulum. Then the period was averaged out and used in the equation of a pendulum to calculate for moment of interia.

LUBE

Type of gears	Spur gears and helical gears		Bevel gears	Worm gear pair	
Gear orientation	Horizontal shaft	Vertical shaft	(Horizontal shaft)	Worm - above	Worm -below
Oil level Level O	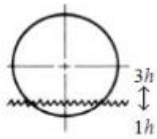	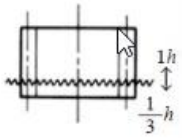	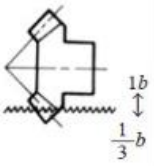	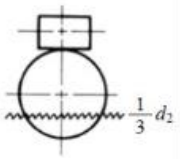	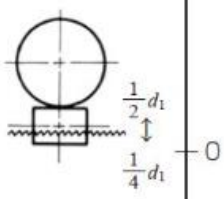

h = Tooth depth, b = Facewidth, d2 = Reference diameter of worm wheel, d1 = Reference diameter of worm

Figure A.2

No.	Properties	Description
1	Correct and proper viscosity	Lubricant should maintain proper viscosity to form a stable oil film at the specified temperature and speed of operation.
2	Antiscoring property	Lubricant should have the property to prevent the scoring failure of tooth surface while under high-pressure of load.
3	Oxidization and heat stability	A good lubricant should not oxidize easily and must perform in moist and high-temperature environment for long duration.
4	Water antiaffinity property	Moisture tends to condense due to temperature change when the gears are stopped. The lubricant should have the property of isolating moisture and water from lubricant
5	Antifoam property	If the lubricant foams under agitation, it will not provide a good oil film. Antifoam property is a vital requirement.
6	Anticorrosion property	Lubrication should be neutral and stable to prevent corrosion from rust that may mix into the oil.

Figure A.3

JIS Gear Oils			IDEMITSU	COSMO OIL	JAPAN ENERGY	SHOWA SHELL	ENEOS	MOBIL
For Industrial Usage	1	ISO VG 32	Daphne Super Multi Oil 32	NEW Mighty Super 32 Cosmo Allpus 32	JOMO Lathus 32	Shell Tellus Oil C 32	Super Mulpus DX32	Mobil DTE Oil Light
		ISO VG 68	Daphne Super Multi Oil 68	NEW Mighty Super 68 Cosmo Allpus 68	JOMO Lathus 68	Shell Tellus Oil C 68	Super Mulpus DX68	Mobil DTE Oil Heavy Medium
		ISO VG 100	Daphne Super Multi Oil 100	NEW Mighty Super 100 Cosmo Allpus 100	JOMO Lathus 100	Shell Tellus Oil C 100	Super Mulpus DX100	Mobil DTE Oil Heavy
		ISO VG 150	Daphne Super Multi Oil 150	NEW Mighty Super 150	JOMO Lathus 150	Shell Tellus Oil C 150	Super Mulpus DX150	Mobil Vacuoline 528
	2	ISO VG 100	Daphne Super Multi Oil 100	Cosmo Gear SE100 Cosmo ECO Gear EPS100	JOMO Reductus 100	Shell Omala Oil 100	Bonnoc AX M100 Bonnoc AX AX100	Mobil gear 600 XP 100
		ISO VG 150	Daphne Super Multi Oil 150	Cosmo Gear SE150 Cosmo ECO Gear EPS150	JOMO Reductus 150	Shell Omala Oil 150	Bonnoc AX M150 Bonnoc AX AX150	Mobil gear 600 XP 150
		ISO VG 220	Daphne Super Multi Oil 220	Cosmo Gear SE220 Cosmo ECO Gear EPS220	JOMO Reductus 220	Shell Omala Oil 220	Bonnoc AX M220 Bonnoc AX AX220	Mobil gear 600 XP 220
		ISO VG 320	Daphne Super Gear Oil 320	Cosmo GearSE320 Cosmo ECO Gear EPS320	JOMO Reductus 320	Shell Omala Oil 320	Bonnoc AX M320 Bonnoc AX AX320	Mobil gear 600 XP 320
		ISO VG 460	Daphne Super Gear Oil 460	Cosmo Gear SE460 Cosmo ECO Gear EPS460	JOMO Reductus 460	Shell Omala Oil 460	Bonnoc AX M460 Bonnoc AX AX460	Mobil gear 600 XP 460
		ISO VG 680	Daphne Super Gear Oil 680	Cosmo Gear SE680	JOMO Reductus 680	Shell Omala Oil 680	Bonnoc AX M680 Bonnoc AX AX680	Mobil gear 600 XP 680

Figure A.4

```
module = 1.5;
teeth = 20;
rpm = 8000;
torque = 0.9;
d = 18 / (1000 * 2);
v = 0.28;
E = 200 * 10^9;
alpha = 20 * pi/180; % convert to radians
r = module * teeth / 2;
F = torque / r;
W = F / cos(alpha);
sigma_c = (2 * torque) / (pi * d^2);
Pmax = (2 * sigma_c) / (sqrt(3) * (1 - v^2/E + 1 - v^2/E));
a = sqrt(W/Pmax) / (pi * (1 - v^2/E + 1 - v^2/E));
h0 = (0.5/pi) * ((rpm/r) * log(d/a) + log(d/a) - 1);
```

Pulley/Shaft/Bearing Itteration One and Two

```
idle = 33000/15;

%

radps=idle*2*pi/60;

Power = 3.6 *(745.7) ;
```

```
%Torque of the engine shaft

torque = (Power)/(radps);

%Cnetre-to-centre distance of pulleys

C=224/1000;

%Diamtere of smaller pulley

D2=16/1000 ;Shaft

%Diamtere of bigger pulley

D1=42/1000 ;

force = torque/(D1/2);

%Wrap angle of bigger pulley

theta1= (pi)-(2*asin(((D1/2)-(D2/2))/(C)));

%Coeffieciant of friction between belt and pulley

u=0.9;

%Slack and Tension Ratio (tension side and slack side)

syms T1 T2

eqn1 = T2/T1 == exp(u*theta1);

eqn2 = Power == (T2-T1)*(D1/2)*(radps);

sol= solve([eqn1,eqn2],[T1,T2]);

T1=double(sol.T1);

T2=double(sol.T2);

%Total Tension on Pulley

T_total=T1+T2;

syms Rb Rc

moment_b =Rc*((29.88)/1000)-614.14*((14.94)/1000) ==0;
```

```
moment_c=-Rb*((29.88)/1000)+614.14*((14.94)/1000) ==0;

solreact=solve([moment_b,moment_c],[Rb,Rc]);

%Reaction forces acting on shaft

Reaction_b=double(solreact.Rb);

Reaction_c=double(solreact.Rc);

%Maximum Monet on the shaft

Max_moment=Reaction_b*(14.94/1000);

%Inital guess of diamatere of the shaft

d=9/1000;

%Second moment of Inertia

I=pi*((d/2)^4)/4;

%Calcualtion for Taum

Tau_m=(16*torque)/(pi*(d^3));

%Calcualtion for Sigma_a

Sigma_a=(Max_moment*(d/2))/(I);

%Calcualtion for Mean Stress

Sigma_m_prime=(sqrt(3)) * Tau_m ;

%Calcualtion for Sigma_a_prime

Sigma_a_prime=Sigma_a;

%Calucalting Sy

Sy=4.60*10^8;

%Calucalting Sut

Sut=5.5*10^8;

%Calculating Se'
```

```
Se_prime=(0.5)*Sut;

%Calcualting Ka

Ka=3.04*(Sut^(-0.217));

%Calcualting Kb

de=0.370*d;

Kb=1.24*(de^(-0.107));

%Calucalting Se

Se=Ka*Kb*Se_prime;

%Goodman Factor of Safety

n=((Sigma_a_prime/Se)+(Sigma_m_prime/Sut))^-1;

%Calculating SIgma max

Sigma_max=sqrt((Sigma_a_prime+Sigma_m_prime)^2 + (3*(Tau_m)^2));

ny=Sy/Sigma_max;

%itteration 2 moving up shaft size, therefore we need shoulders

%calculating bending kf

sqr_a=1.24-((2.25*10^-3)*Sut) + ((1.6*10^-6)*(Sut)^2)-((4.11*10^-10)*Sut^3);

%calculating torsion kfs

sqr_as=0.958-((1.83*10^-3)*Sut)      +      ((1.43*10^-6)*(Sut)^2)-((4.11*10^-
10)*Sut^3);

%r/d=0.3 small d=8mm

r=8*0.3/1000;

kt=1.35;

kts=1.3;

Kf=1 +((kt-1)/(1+(sqr_a/sqrt(r))));
```

```
Kfs=1 +((kts-1)/(1+(sqr_as/sqrt(r))));

%Bearing Calculations

V=1;

F_a=6*4.448;

F_r=6*4.448;  %this force is not there in reality, but it is included here to
account for vibrations and to increase the factor of saftey

C_0=1.91*1000;

c_10=4.65*1000;

ratio=F_a/C_0

%insert picture of table

%for Fa/Co e=0.19

e=0.19;

F_a/(V*F_r)

%Fa/V*Fr is greater than e therefore interpolating for Y2 and X2

Y2=2.3;

X2=0.56;

F_e=X2*V*F_r + Y2*F_a

L_10=((10^6)/60*8000)*(c_10/F_e)^3

%L_10=3.0148E13 therefore sufficent life span
```

SHAFT ITTERATION 3

```
idle = 33000/15;

%
```

```
radps=idle*2*pi/60;

Power = 3.6 *(745.7) ;

%Torque of the engine shaft

torque = (Power)/(radps);

%Cnetre-to-centre distance of pulleys

%C=224/1000;

%Diamtere of smaller pulley

%D2=16/1000 ;

%Diamtere of bigger pulley

%D1=42/1000 ;

%force = torque/(D1/2);

%Wrap angle of bigger pulley

%theta1= (pi)-(2*asin(((D1/2)-(D2/2))/(C)));

%Coeffieciant of friction between belt and pulley

%u=0.9;

%Slack and Tension Ratio (tension side and slack side)

%syms T1 T2

%eqn1 = T2/T1 == exp(u*theta1);

%eqn2 = Power == (T2-T1)*(D1/2)*(radps);

%sol= solve([eqn1,eqn2],[T1,T2]);

%T1=double(sol.T1);

%T2=double(sol.T2);

%Total Tension on Pulley

%T_total=T1+T2;
```

```
%syms Rb Rc

%moment_b =Rc*((29.88)/1000)-614.14*((14.94)/1000) ==0;

%moment_c=-Rb*((29.88)/1000)+614.14*((14.94)/1000) ==0;

%solreact=solve([moment_b,moment_c],[Rb,Rc]);

%Reaction forces acting on shaft

%Reaction_b=double(solreact.Rb);

%Reaction_c=double(solreact.Rc);

%Maximum Monet on the shaft

%Max_moment=Reaction_b*(14.94/1000);

%Inital guess of diamatere of the shaft

d=8/1000;

%Second moment of Inertia

I=pi*((d/2)^4)/4;

%Calcualtion for Taum

Tau_m=(16*torque)/(pi*(d^3));

%Calcualtion for Sigma_a

%Sigma_a=(Max_moment*(d/2))/(I);

Sigma_a=0;

%Calcualtion for Mean Stress

Sigma_m_prime=(sqrt(3)) * Tau_m ;

%Calcualtion for Sigma_a_prime

Sigma_a_prime=Sigma_a;

%Calucalting Sy

Sy=4.60*10^8;
```

```
%Calucalting Sut

Sut=5.5*10^8;

%Calculating Se'

Se_prime=(0.5)*Sut;

%Calcualting Ka

Ka=3.04*(Sut^(-0.217));

%Calcualting Kb

de=0.370*d;

Kb=1.24*(de^(-0.107));

%Calucalting Se

Se=Ka*Kb*Se_prime;

%Goodman Factor of Safety

n=((Sigma_a_prime/Se)+(Sigma_m_prime/Sut))^-1;

%Calculating SIgma max

Sigma_max=sqrt((Sigma_a_prime+Sigma_m_prime)^2 + (3*(Tau_m)^2));

ny=Sy/Sigma_max;
```

FRAME

```
theta_rot=10*3.14/180  %rads

r_frame=150/1000; % the distance of each wire from the center of the frame

lenght=1 %lenght of frame wire

arc=r_frame*theta_rot %arc lenght the frame rotates by in mm
```

```
distance = lenght*sin(theta_rot)   % projection of how much the frame would displaed on the ground

F_thrust=20 *4.448; %thrust force in N

T_x=F_thrust*sin(theta_rot)  %the force compinent of the wire tension in the x-cord

T_x_per=T_x/3;  %the tension in each wire

M_resist=T_x*r_frame;

m_rated=17.8; %the weight the fishing wire is rated for in kg

r_wire=0.45/1000; %the radius of the wire in m

Fr_wire=m_rated*9.81;

sigma_rated=Fr_wire/(3.14*r_wire^2);

sigma_load=T_x_per/(3.14*r_wire^2);

n=sigma_rated/sigma_load
```

FASTNERS

```
Sy=4.60*10^8;

F=6*4.448;

d=(0.25)*25.4;

thread_per_inch=20;

p=(1/16)*25.4;

d_c=(0.25)*25.4;

f_c=1;

f=0.15;

n=1;
```

```
d_m=d- p/2;

d_r=d-p;

l=n*p;

T_r=(F*d_m/2)*((l+ (3.14*f*d_m))/((3.14*d_m )- (f*l)))+ ((F*f_c*d_c)/(2));

tau=(16*T_r)/(3.14*d_r^3);

sigma=(-4*F)/(3.14*d_r^2);

sigma_B=(-2*0.38*F)/(3.14*d_m*p);

sigma_b=(6*0.38*F)/(3.14*d_r*p);

tau_2=(-4*0.38*T_r)/(p*3.14*d_r^2);

sigma_prime=(1/sqrt(2))*((sigma_b-sigma)^2  +  (sigma)^2  +  (sigma_b)^2  +
(6*tau^2) + (6*tau_2^2))^1/2;

n=Sy/sigma_prime;
```

A.3 Engineering Drawings & Technical Schematics (*Drawings not visually to scale)*

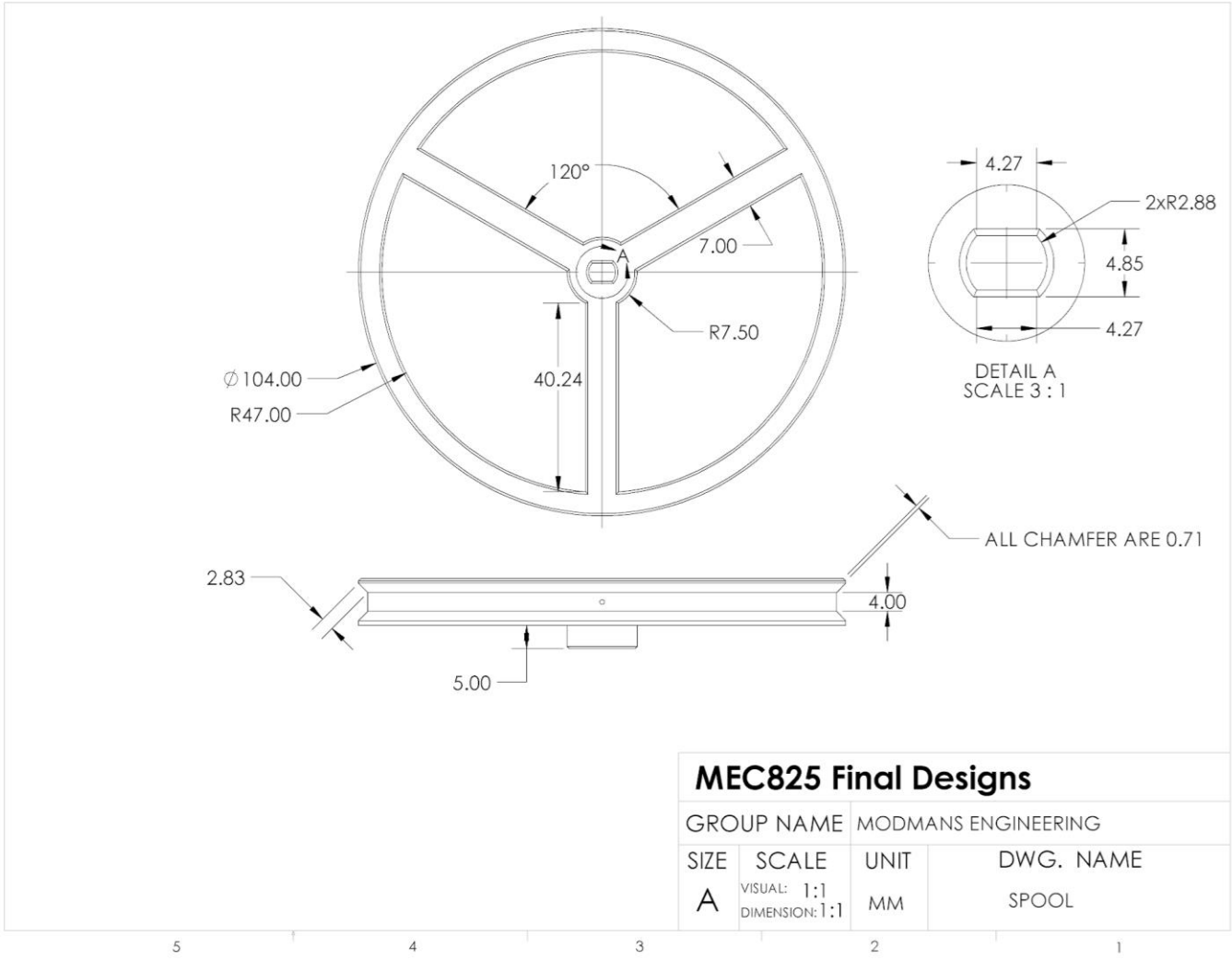

Figure A.5

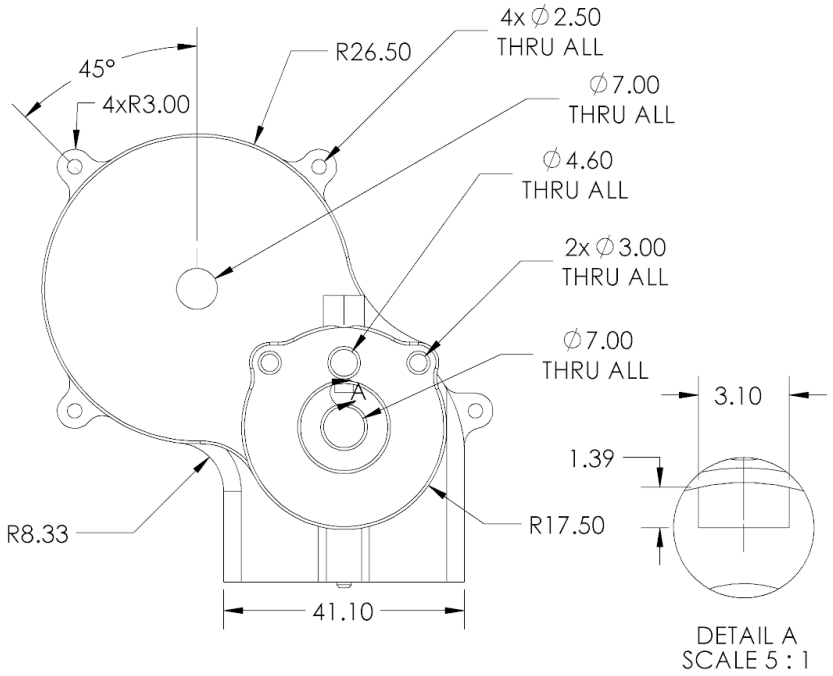

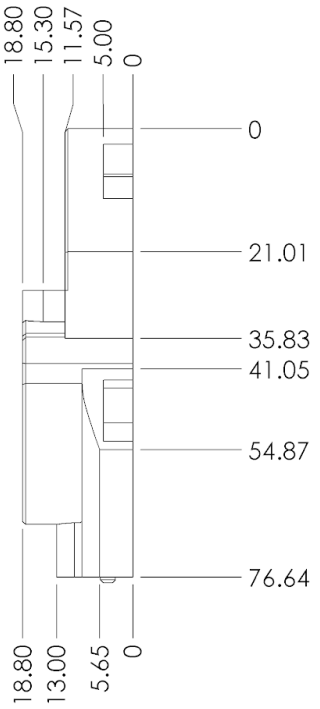

MEC825 Final Designs

GROUP NAME	MODMANS ENGINEERING		
SIZE	SCALE	UNIT	DWG. NAME
A	VISUAL: 1:1 DIMENSION: 1:1	MM	FRONT GEAR BOX COVER

5 4 3 2 1

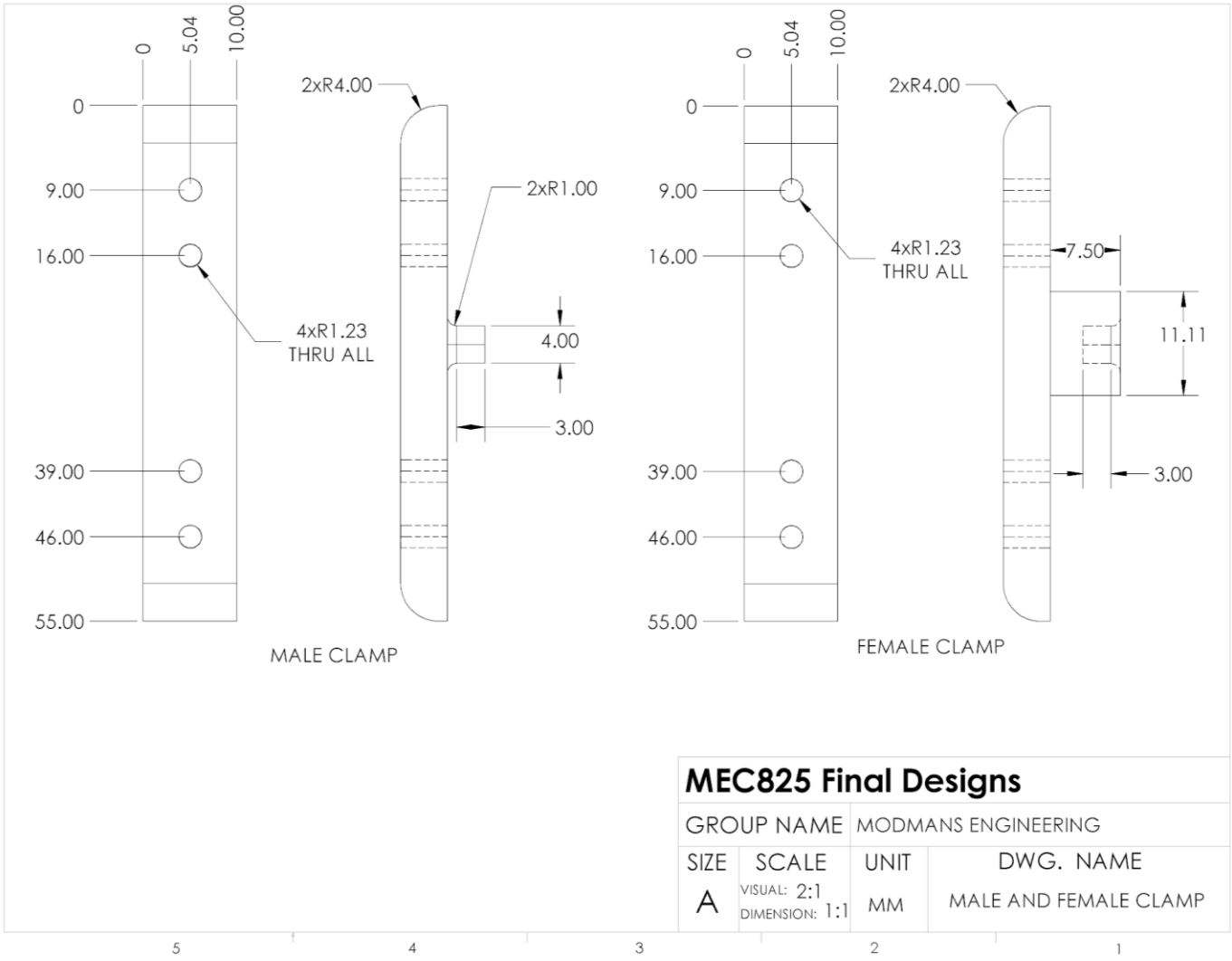
0
5.04
10.00
0
9.00
16.00
39.00
46.00
55.00
2xR4.00
2xR1.00
4xR1.23
THRU ALL
4.00
3.00
MALE CLAMP
7.50
11.11
FEMALE CLAMP
MEC825 Final Designs
GROUP NAME
MODMANS ENGINEERING
SIZE
A
SCALE
VISUAL: 2:1
DIMENSION: 1:1
UNIT
MM
DWG. NAME
MALE AND FEMALE CLAMP
5
4
3
2
1

Figure A.7

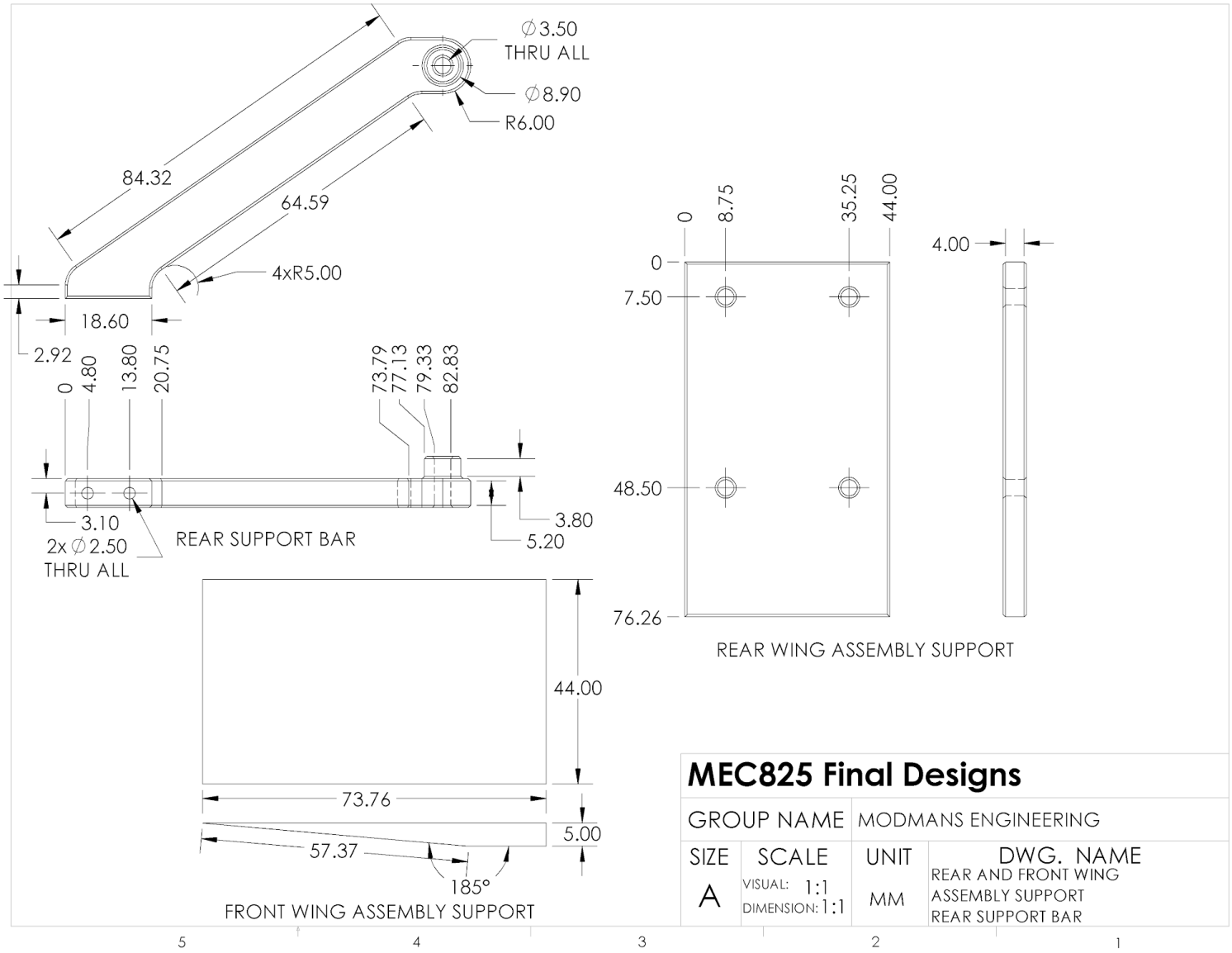
∅3.50
THRU ALL
∅8.90
R6.00
84.32
64.59
4xR5.00
18.60
2.92
0
4.80
13.80
20.75
73.79
77.13
79.33
82.83
3.10
2x ∅2.50
THRU ALL
REAR SUPPORT BAR
3.80
5.20
0
8.75
35.25
44.00
4.00
0
7.50
48.50
76.26
REAR WING ASSEMBLY SUPPORT
44.00
73.76
5.00
57.37
185°
FRONT WING ASSEMBLY SUPPORT
MEC825 Final Designs
GROUP NAME
MODMANS ENGINEERING
SIZE
A
SCALE
VISUAL: 1:1
DIMENSION: 1:1
UNIT
MM
DWG. NAME
REAR AND FRONT WING
ASSEMBLY SUPPORT
REAR SUPPORT BAR
5
4
3
2
1

Figure A.8

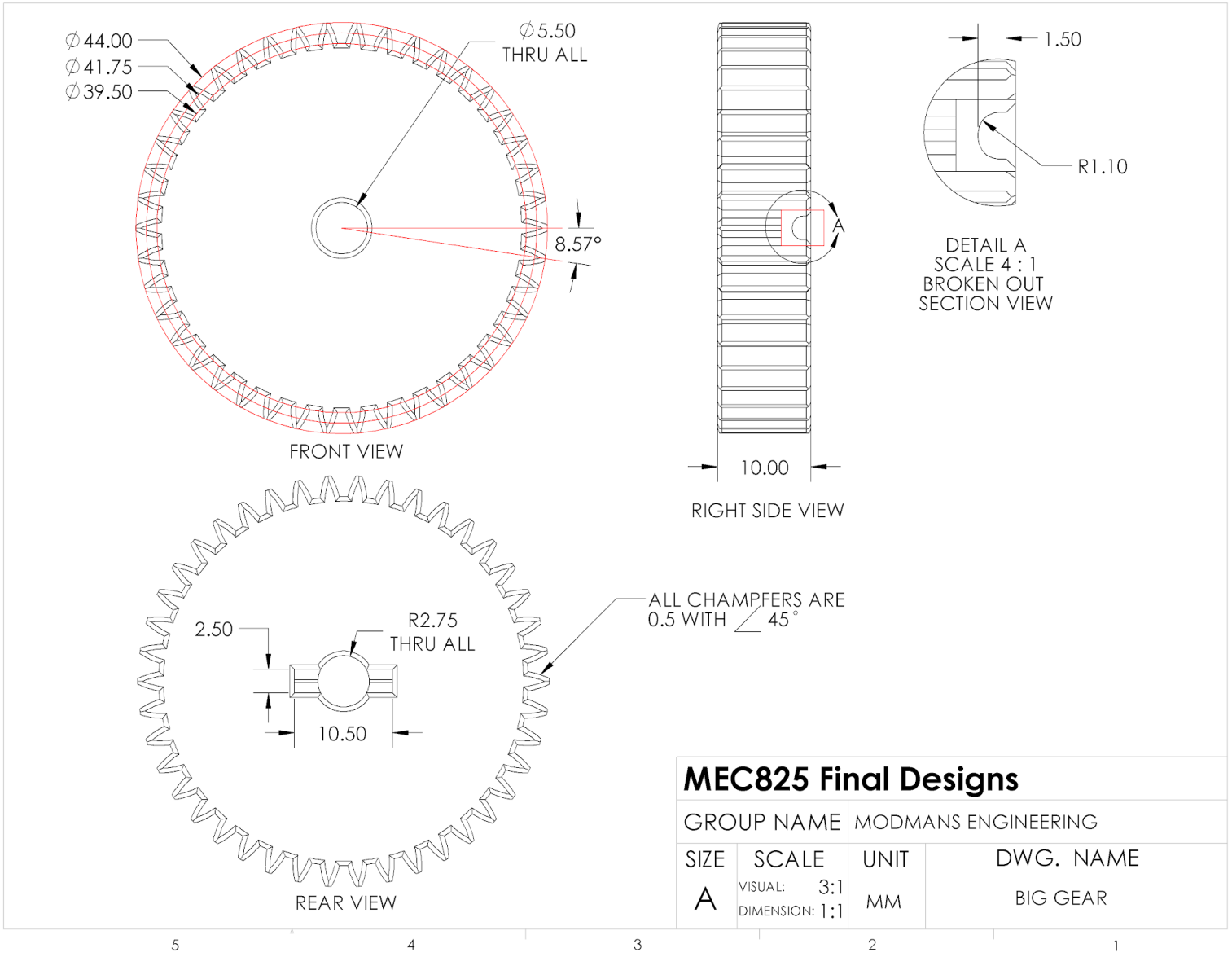
∅44.00
∅41.75
∅39.50
∅5.50
THRU ALL
8.57°
FRONT VIEW
10.00
RIGHT SIDE VIEW
A
1.50
R1.10
DETAIL A
SCALE 4 : 1
BROKEN OUT
SECTION VIEW
2.50
R2.75
THRU ALL
10.50
ALL CHAMPFERS ARE
0.5 WITH 45°
REAR VIEW
MEC825 Final Designs
GROUP NAME
MODMANS ENGINEERING
SIZE
A
SCALE
VISUAL: 3:1
DIMENSION: 1:1
UNIT
MM
DWG. NAME
BIG GEAR
5
4
3
2
1

Figure A.9

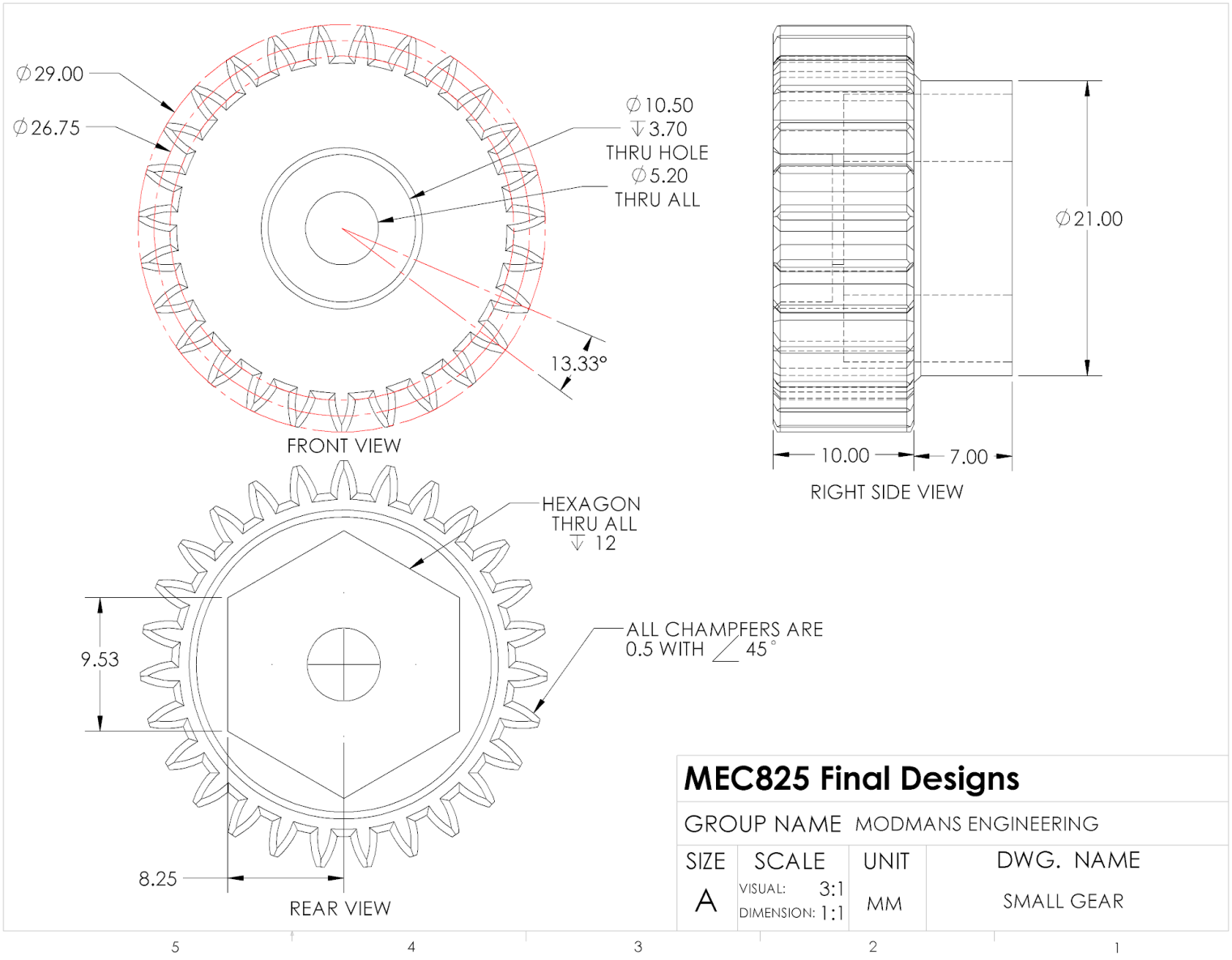
∅29.00
∅26.75
∅10.50
↧3.70
THRU HOLE
∅5.20
THRU ALL
13.33°
FRONT VIEW
∅21.00
10.00
7.00
RIGHT SIDE VIEW
HEXAGON
THRU ALL
↧ 12
9.53
ALL CHAMPFERS ARE
0.5 WITH ∠ 45°
8.25
REAR VIEW
MEC825 Final Designs
GROUP NAME MODMANS ENGINEERING
SIZE
A
SCALE
VISUAL: 3:1
DIMENSION: 1:1
UNIT
MM
DWG. NAME
SMALL GEAR
5
4
3
2
1

Figure A.10

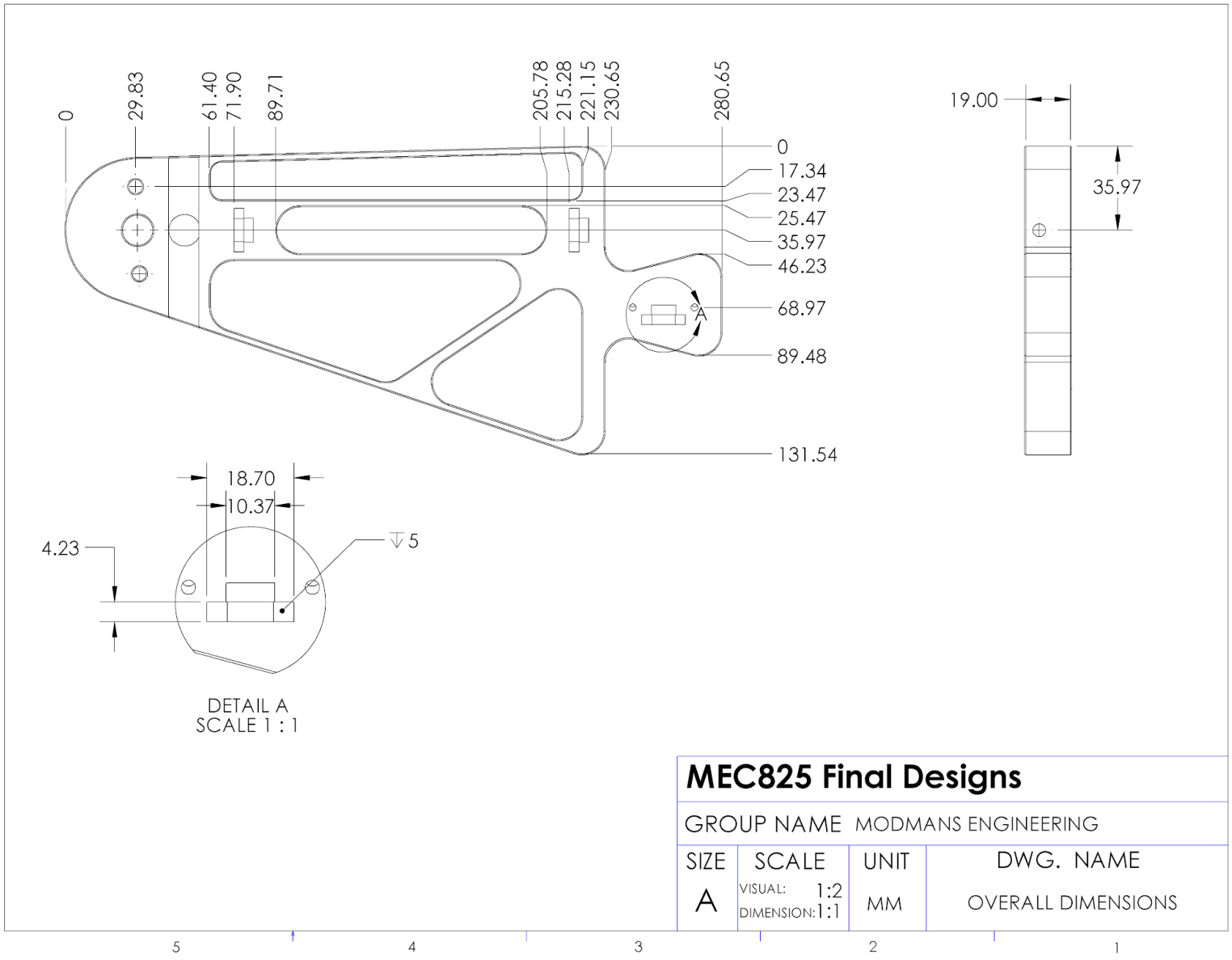

Figure A.11 Wing Front Bottom Left Overall Dimensions

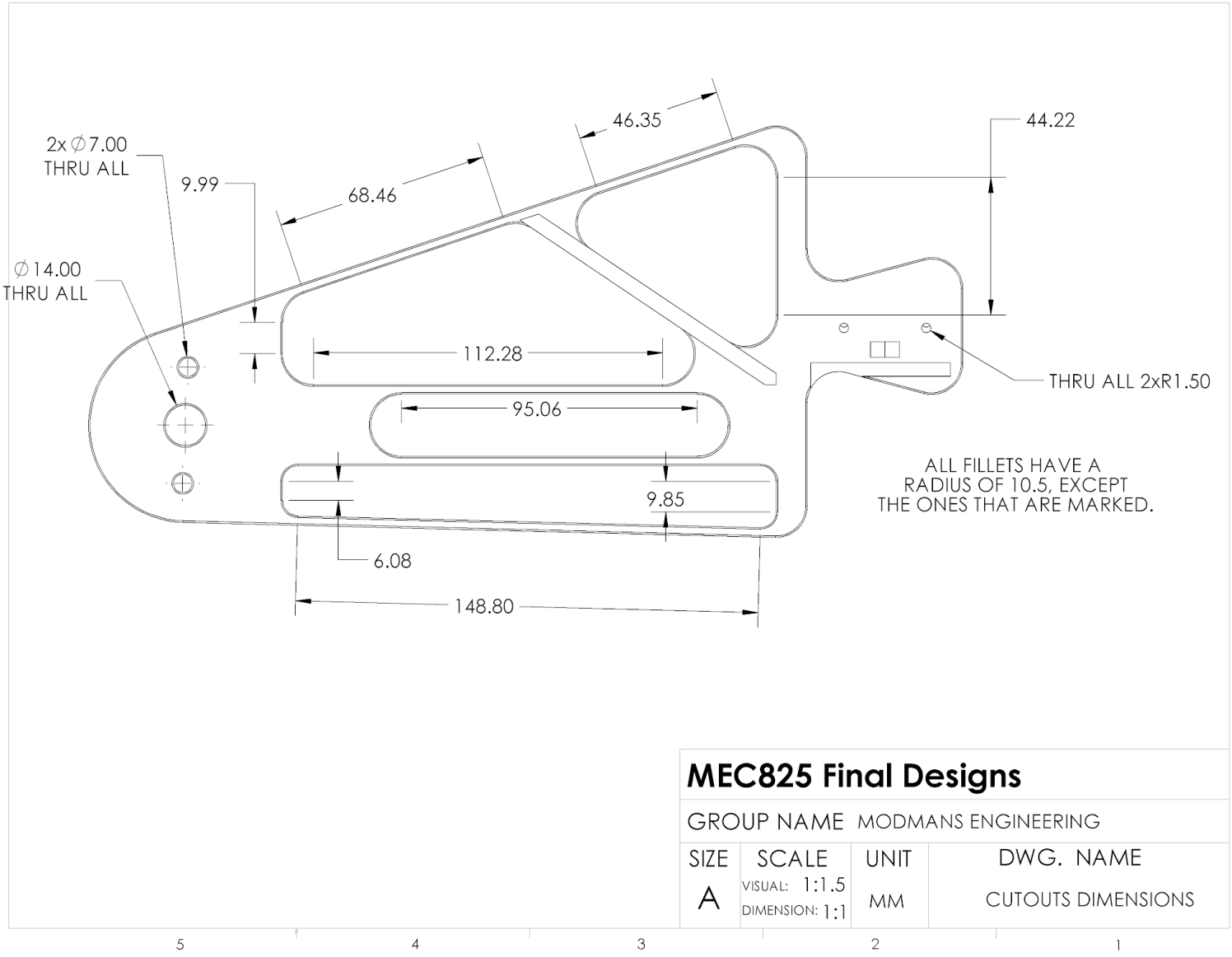

Figure A.12 Wing Front Bottom Left Cutout Dimensions

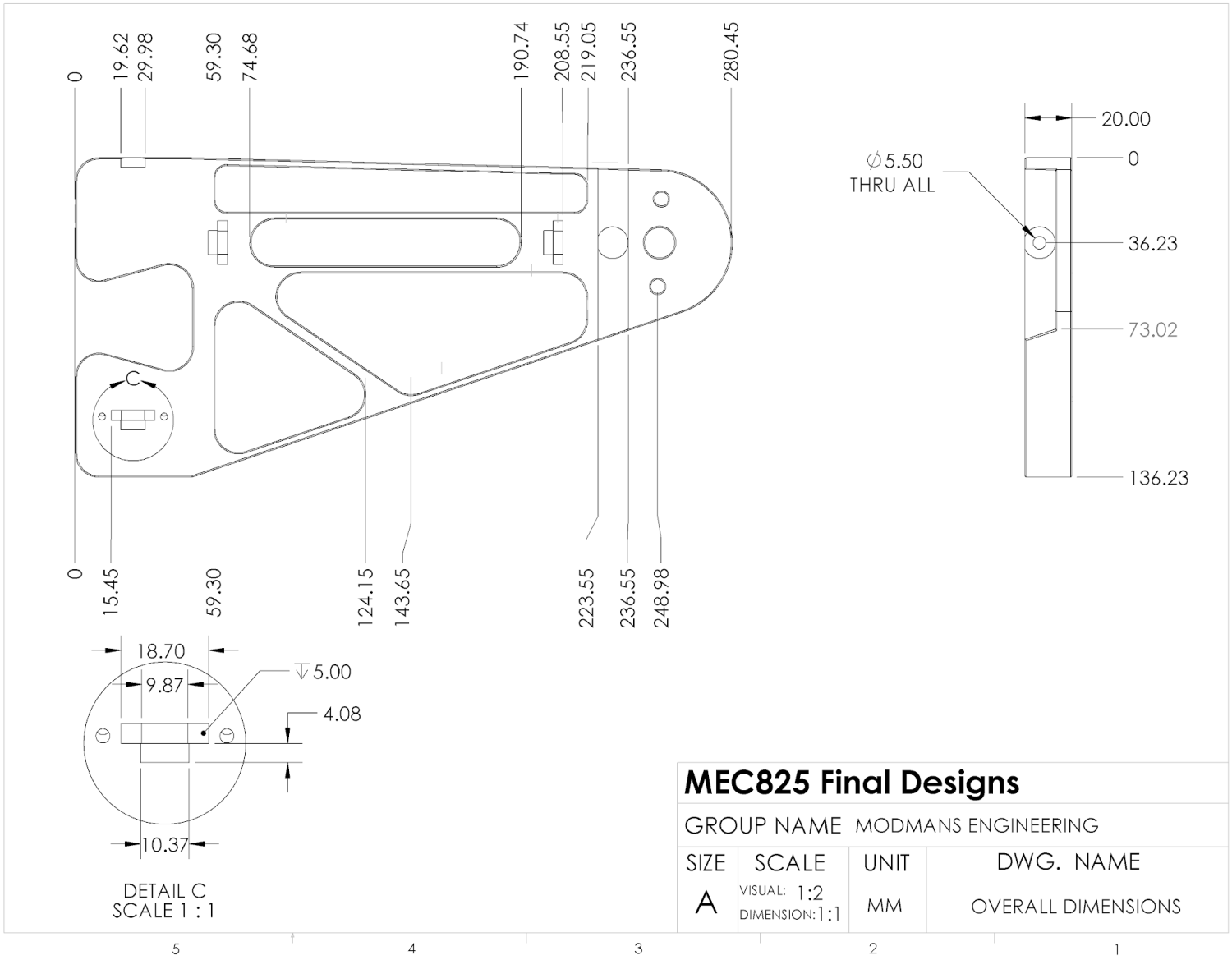

Figure A.13 Wing Front Bottom Right Overall Dimensions

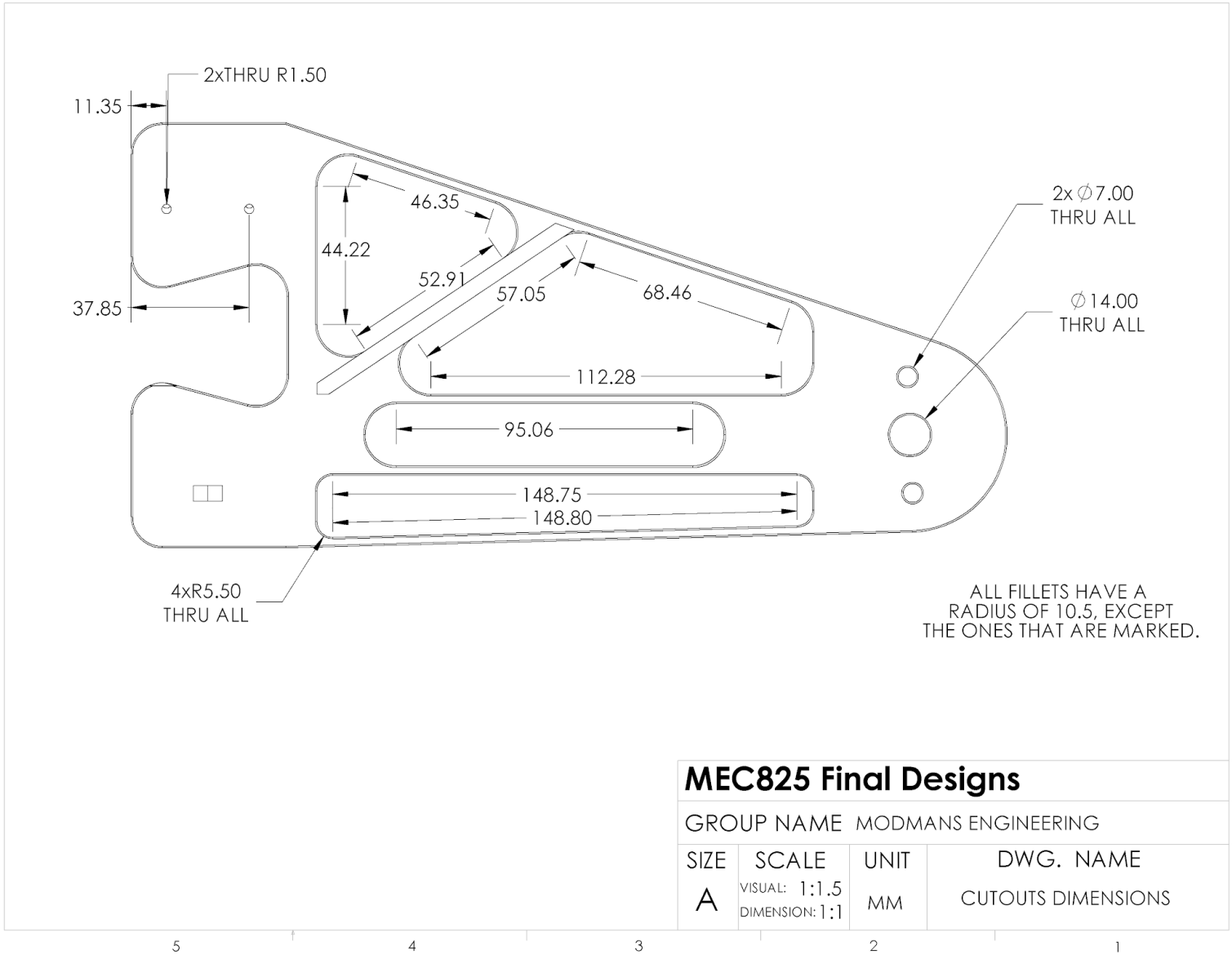

Figure A.14 Wing Front Bottom Right Cutouts Dimensions

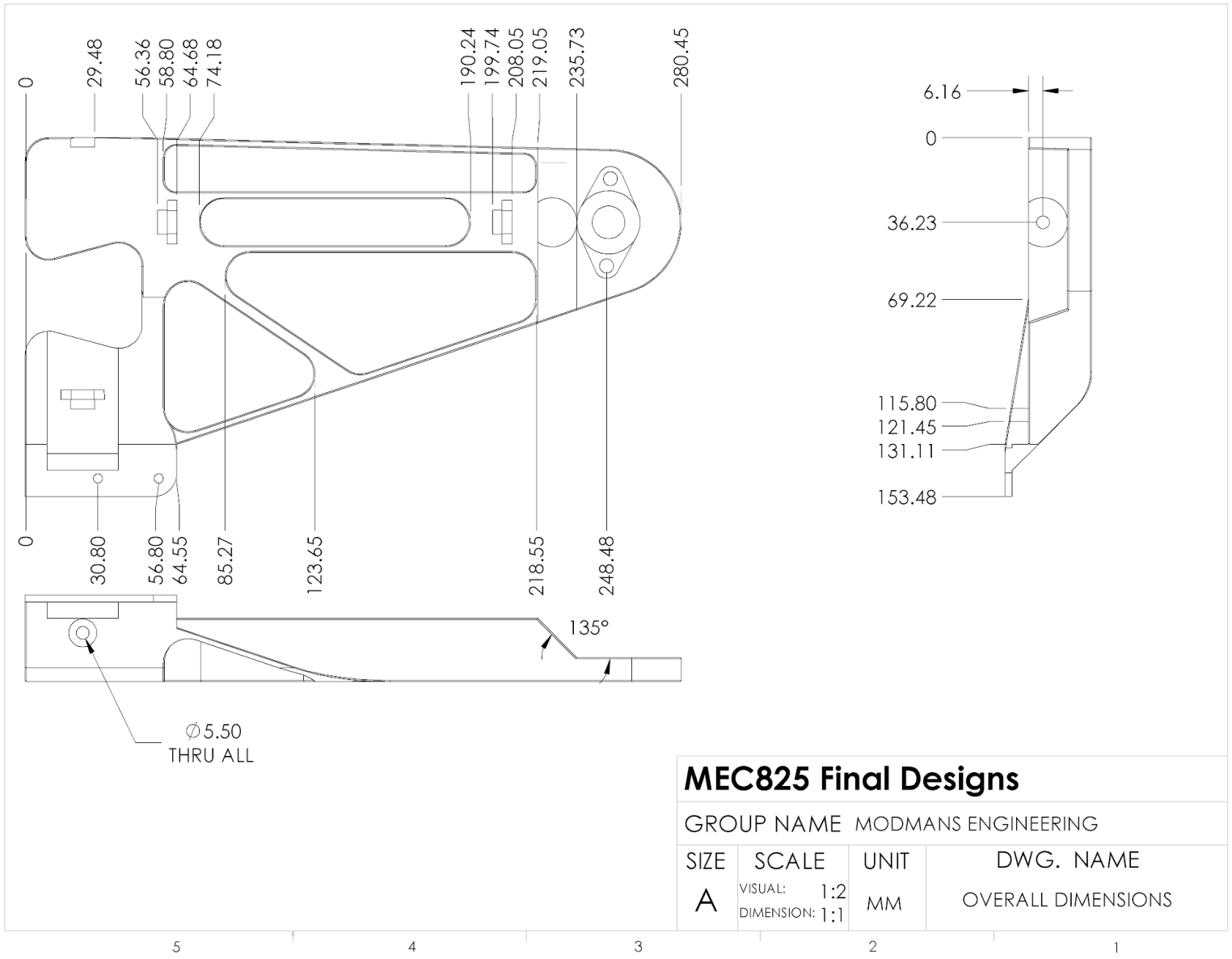

Figure A.15 Wing Front Top Left Overall Dimensions

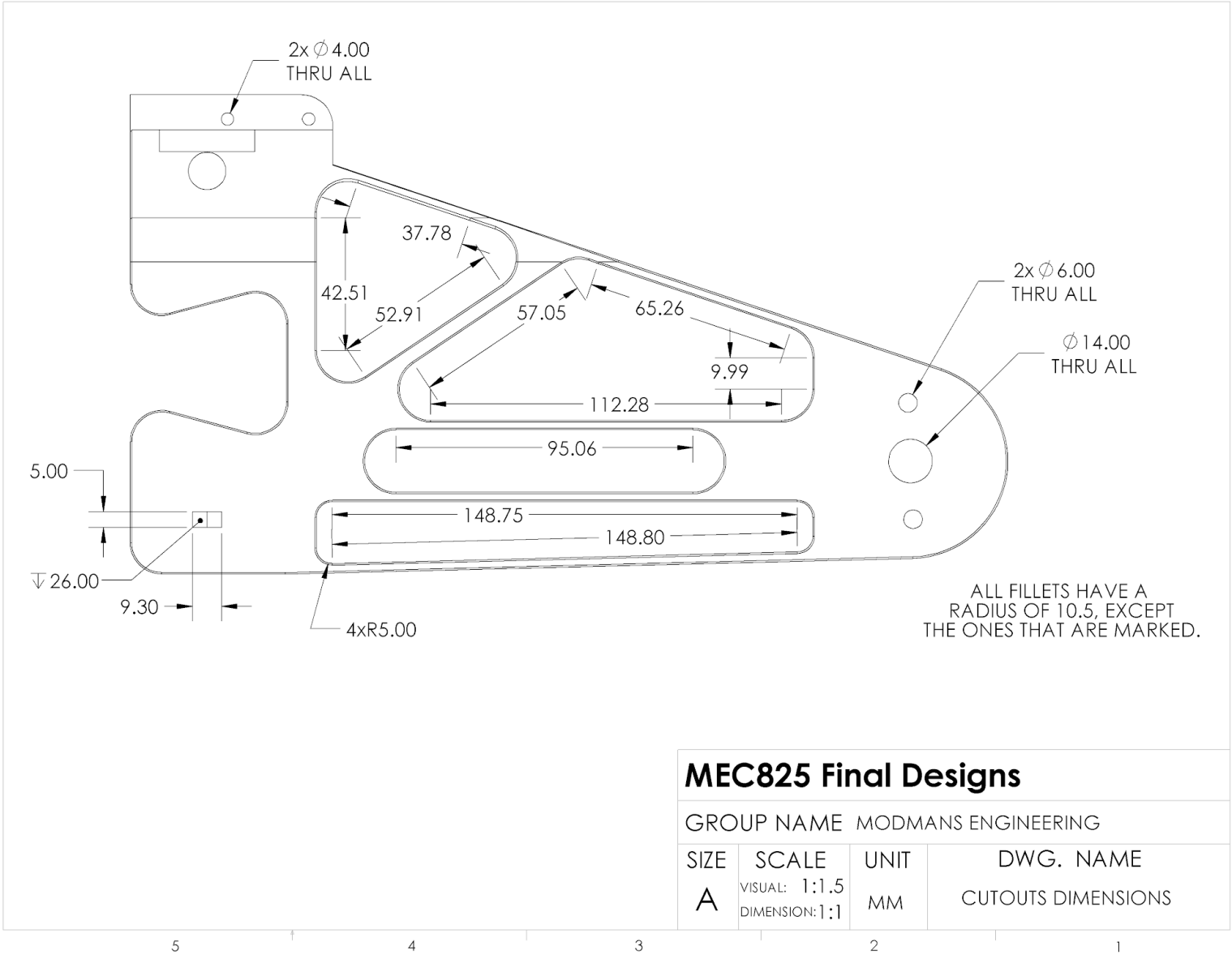

Figure A.16 Wing Front Top Left Cutout Dimensions

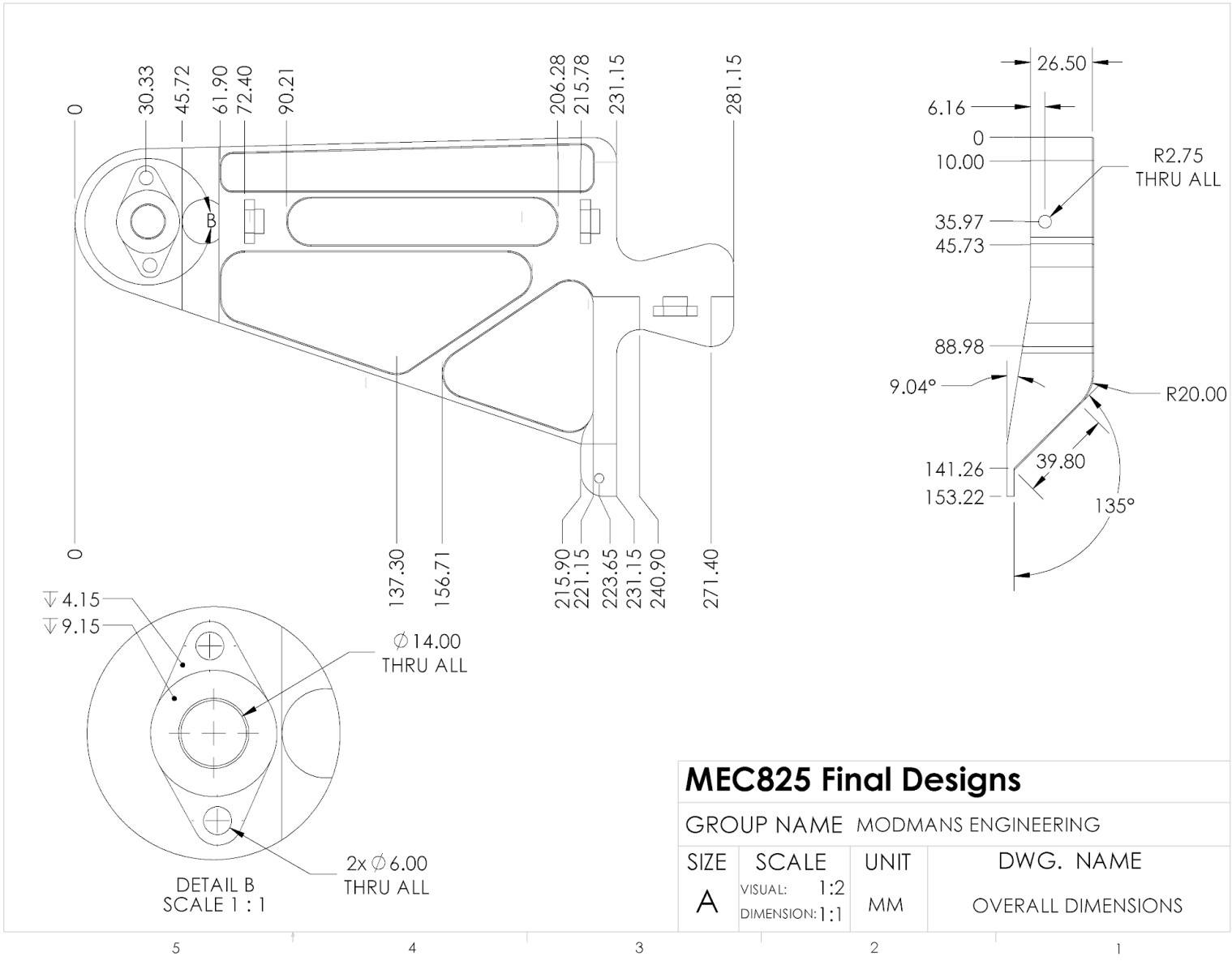

Figure A.17 Wing Front Top Right Overall Dimensions

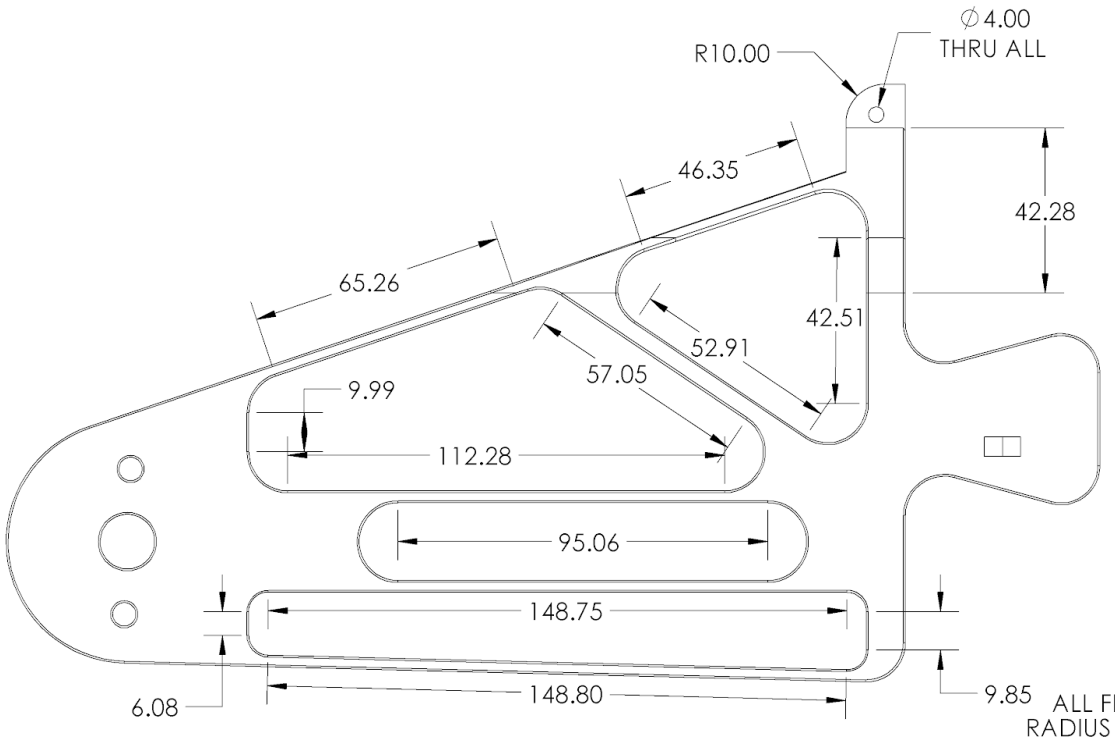

MEC825 Final Designs

GROUP NAME MODMANS ENGINEERING

SIZE	SCALE	UNIT	DWG. NAME
A	VISUAL: 1:1.5 DIMENSION: 1:1	MM	CUTOUTS DIMENSIONS

5 4 3 2 1

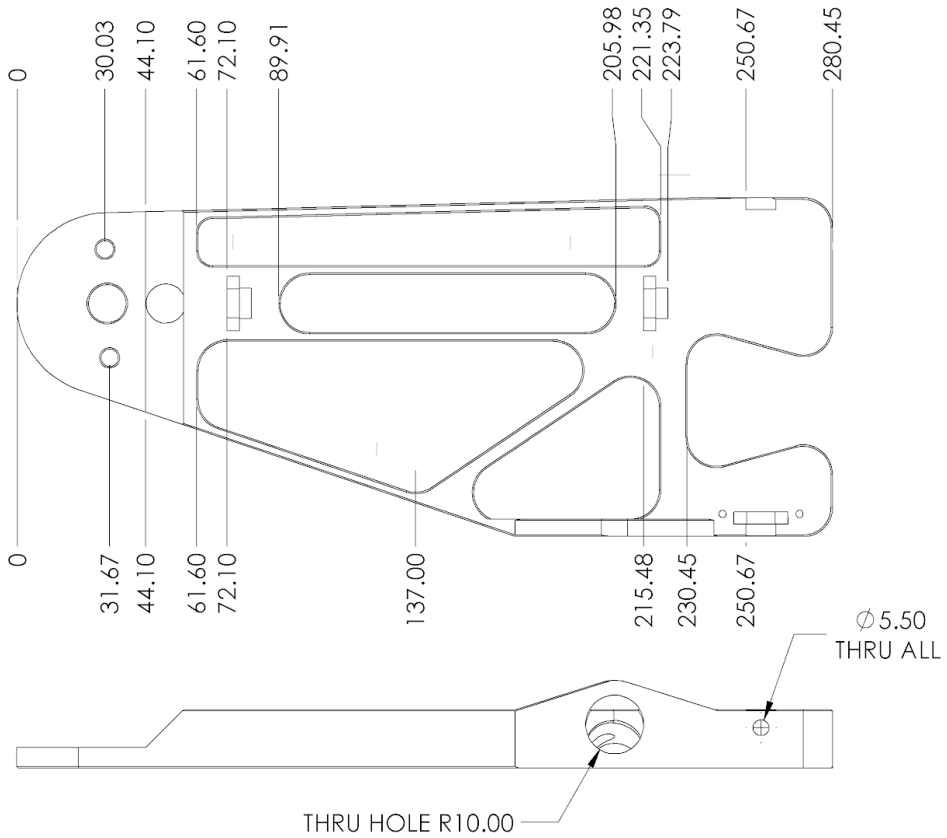

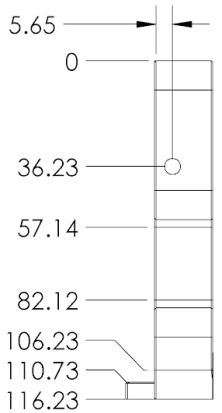

MEC825 Final Designs

GROUP NAME MODMANS ENGINEERING

SIZE	SCALE	UNIT	DWG. NAME
A	VISUAL: 1:2 DIMENSION: 1:1	MM	OVERALL DIMENSIONS

5 4 3 2 1

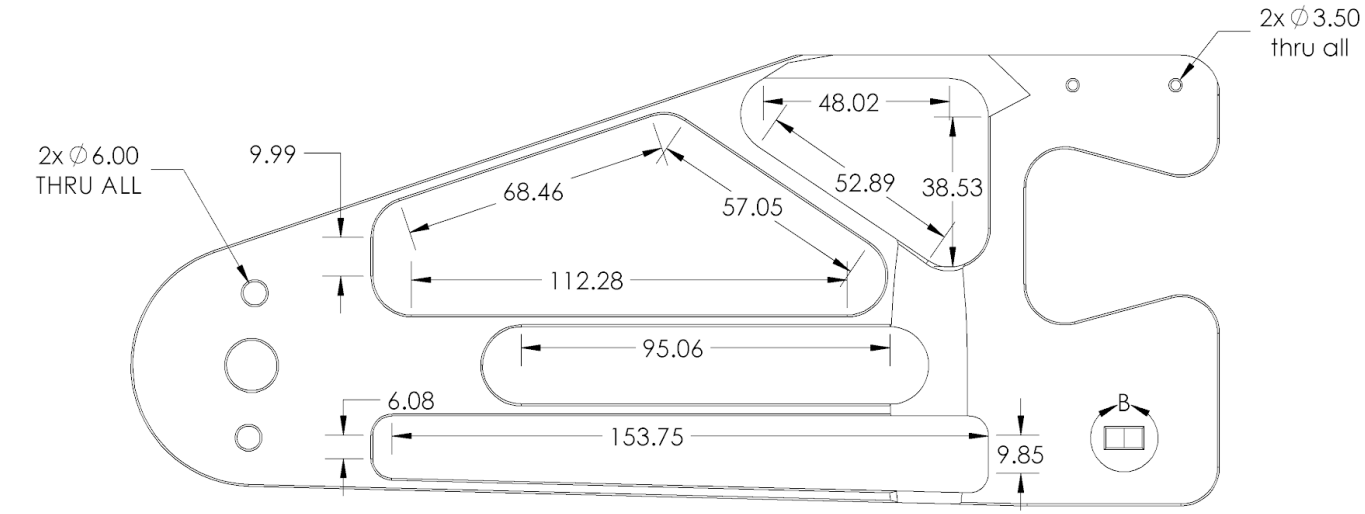

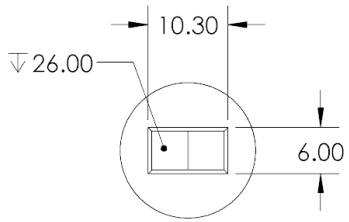

DETAIL B
SCALE 2 : 1.5

ALL FILLETS HAVE A
RADIUS OF 10.5, EXCEPT
THE ONES THAT ARE MARKED.

MEC825 Final Designs

GROUP NAME MODMANS ENGINEERING

SIZE	SCALE	UNIT	DWG. NAME
A	VISUAL: 1:1.5 DIMENSION: 1:1	MM	CUTOUTS DIMENSIONS

5 4 3 2 1

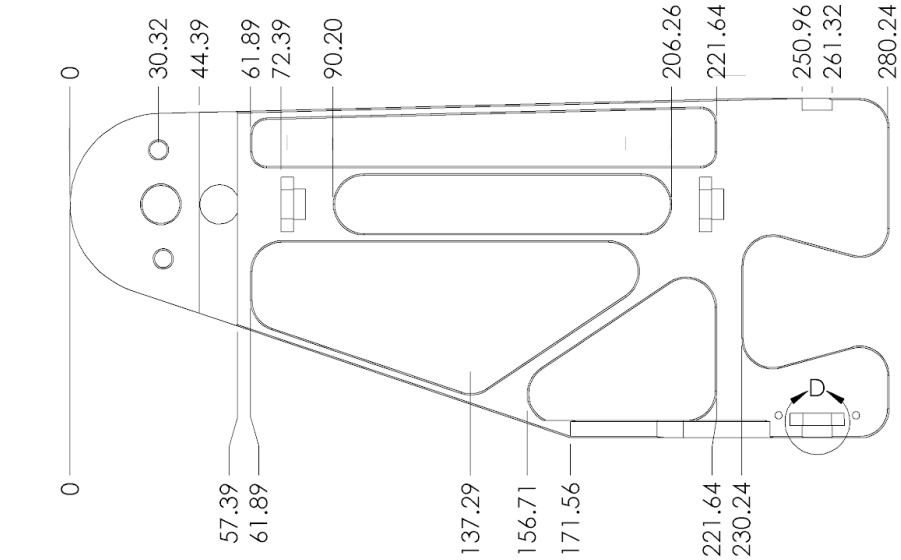

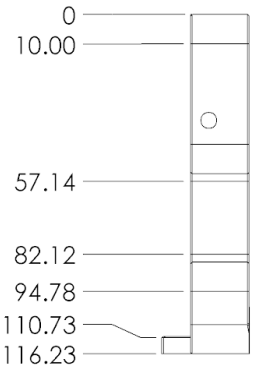

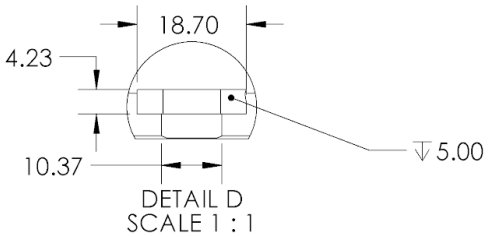

MEC825 Final Designs

GROUP NAME MODMANS ENGINEERING

SIZE	SCALE	UNIT	DWG. NAME
A	VISUAL: 1:2 DIMENSION: 1:1	MM	OVERALL DIMENSIONS

5 4 3 2 1

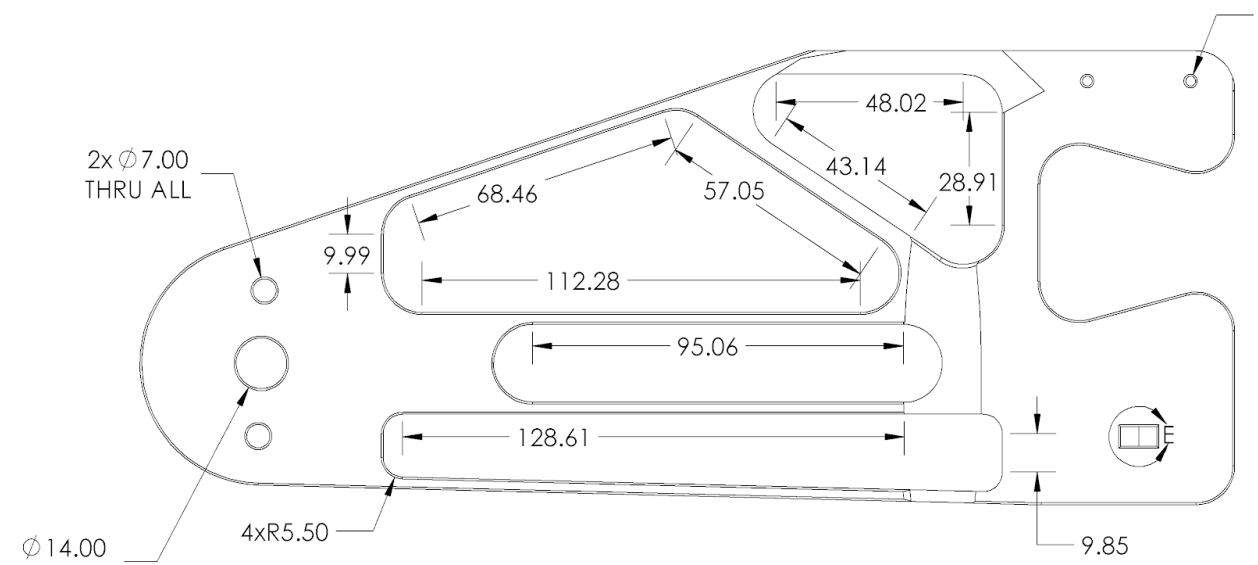

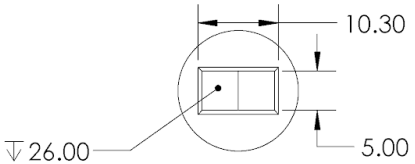

DETAIL E
SCALE 2 : 1.5

ALL FILLETS HAVE A
RADIUS OF 10.5, EXCEPT
THE ONES THAT ARE MARKED.

MEC825 Final Designs

GROUP NAME MODMANS ENGINEERING

SIZE	SCALE	UNIT	DWG. NAME
A	VISUAL: 1:1.5 DIMENSION: 1:1	MM	CUTOUTS DIMENSIONS

5 4 3 2 1

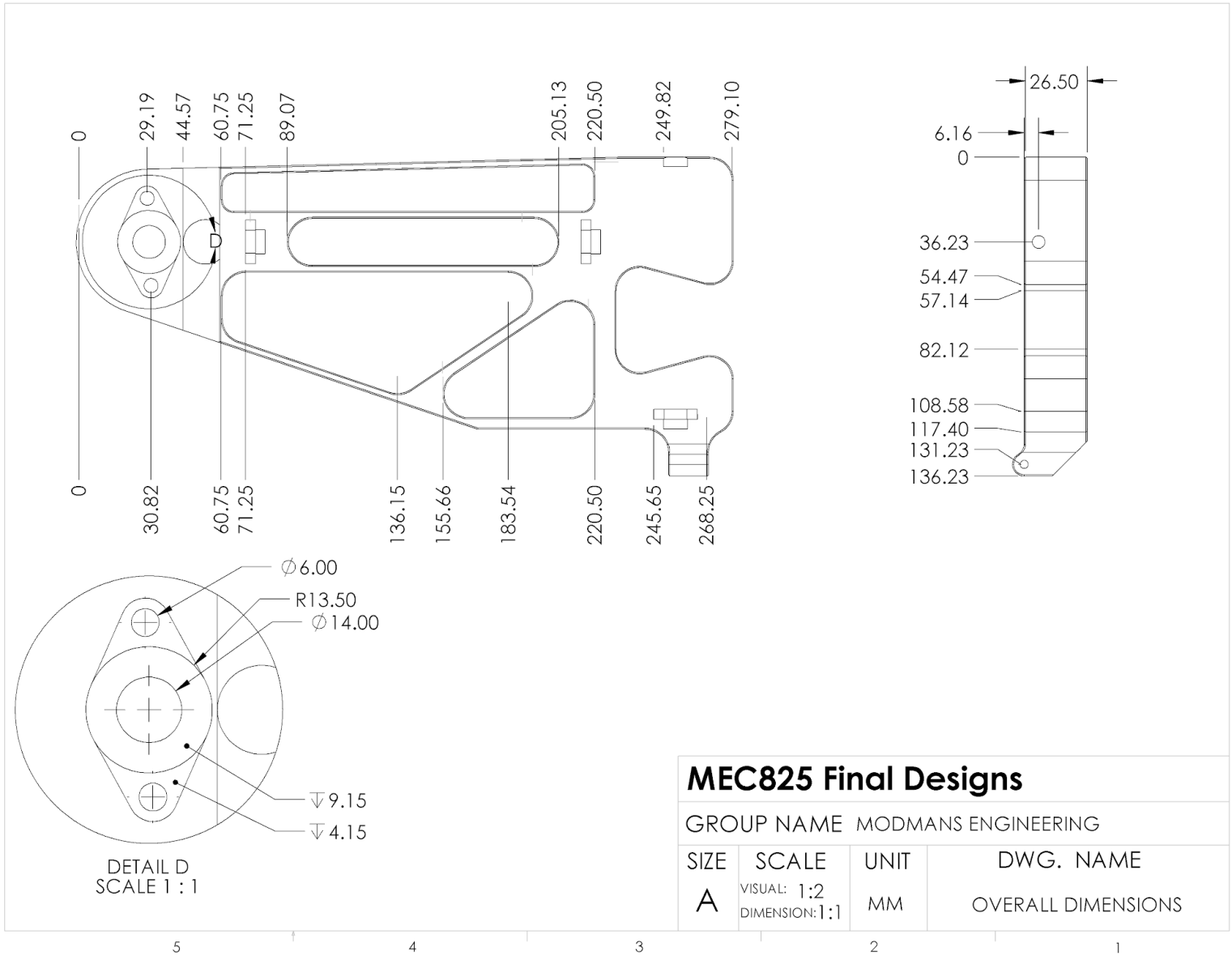

Figure A.23 Wing Rear Top Left Overall Dimensions

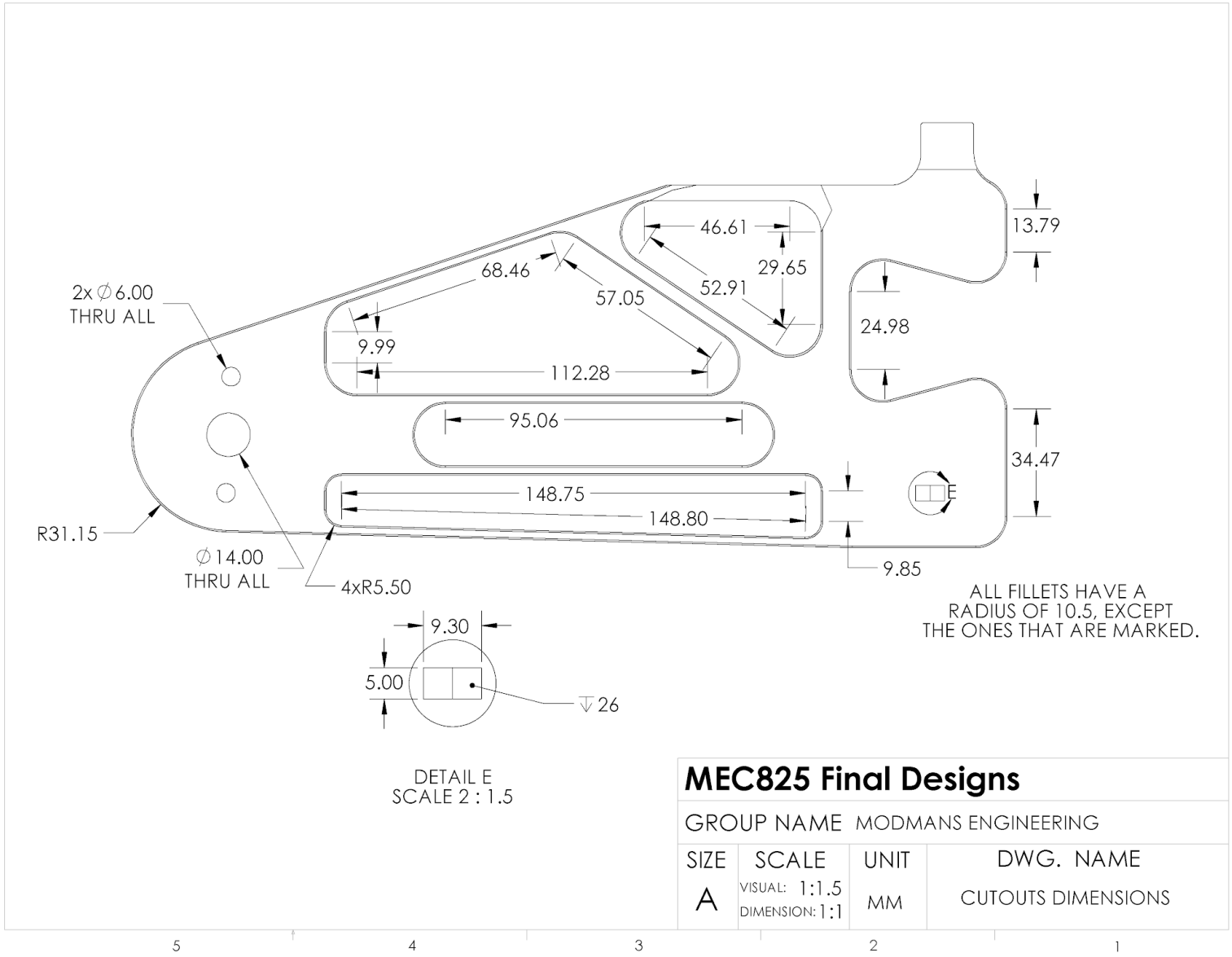

Figure A.24 Wing Rear Top Left Cutout Dimensions

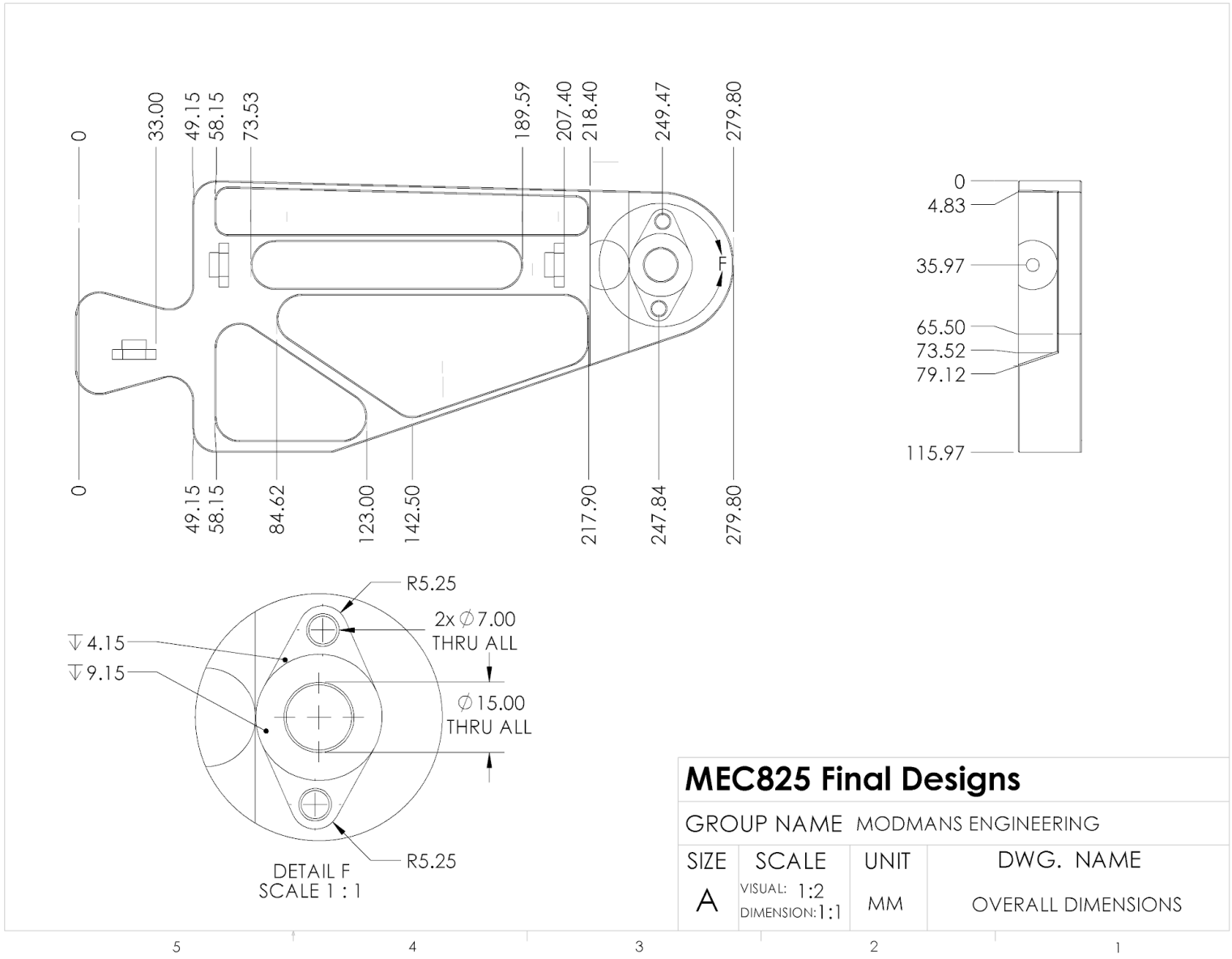

Figure A.25 Wing Rear Top Right Overall Dimensions

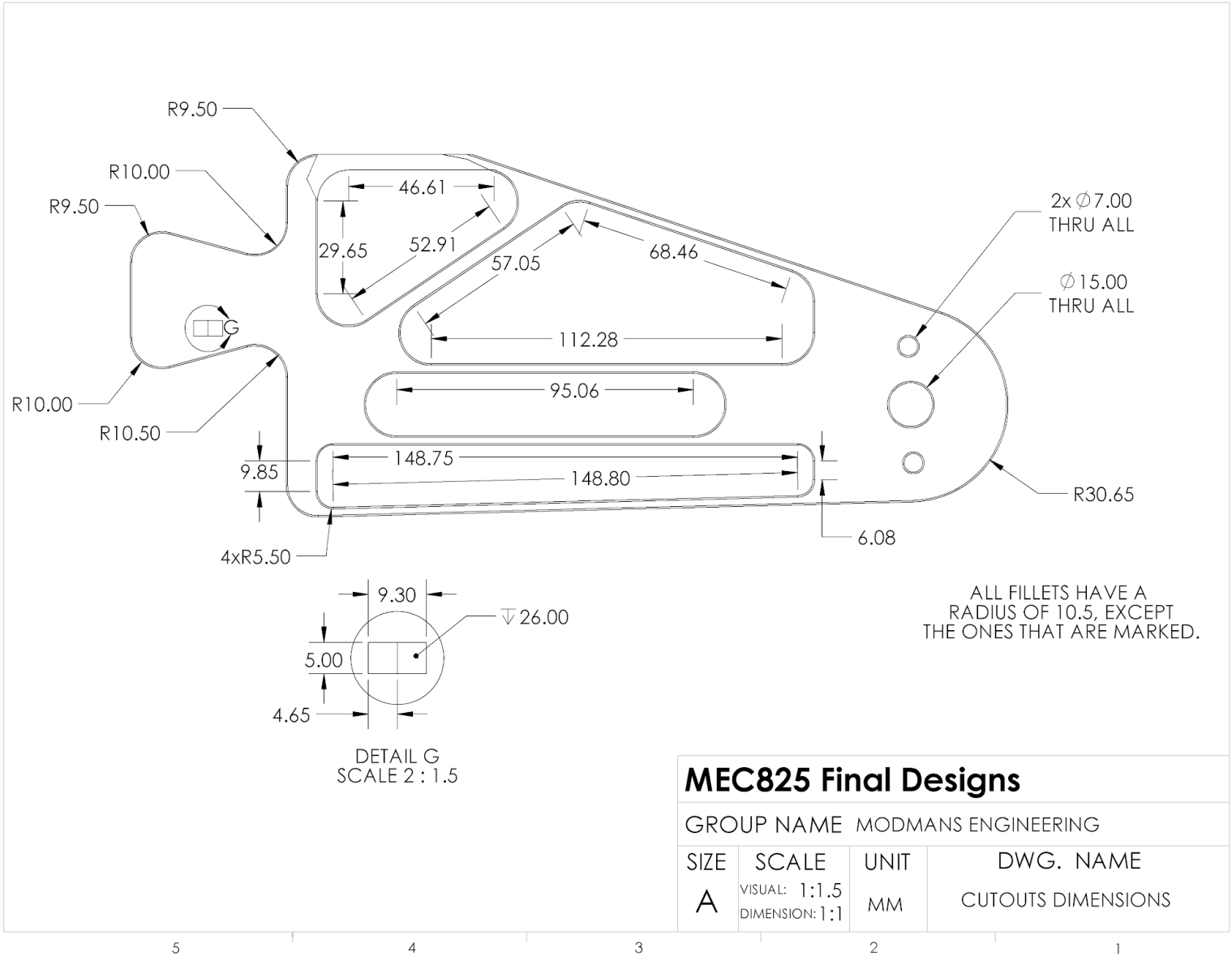

Figure A.26 Wing Rear Top Right Cutout Dimensions

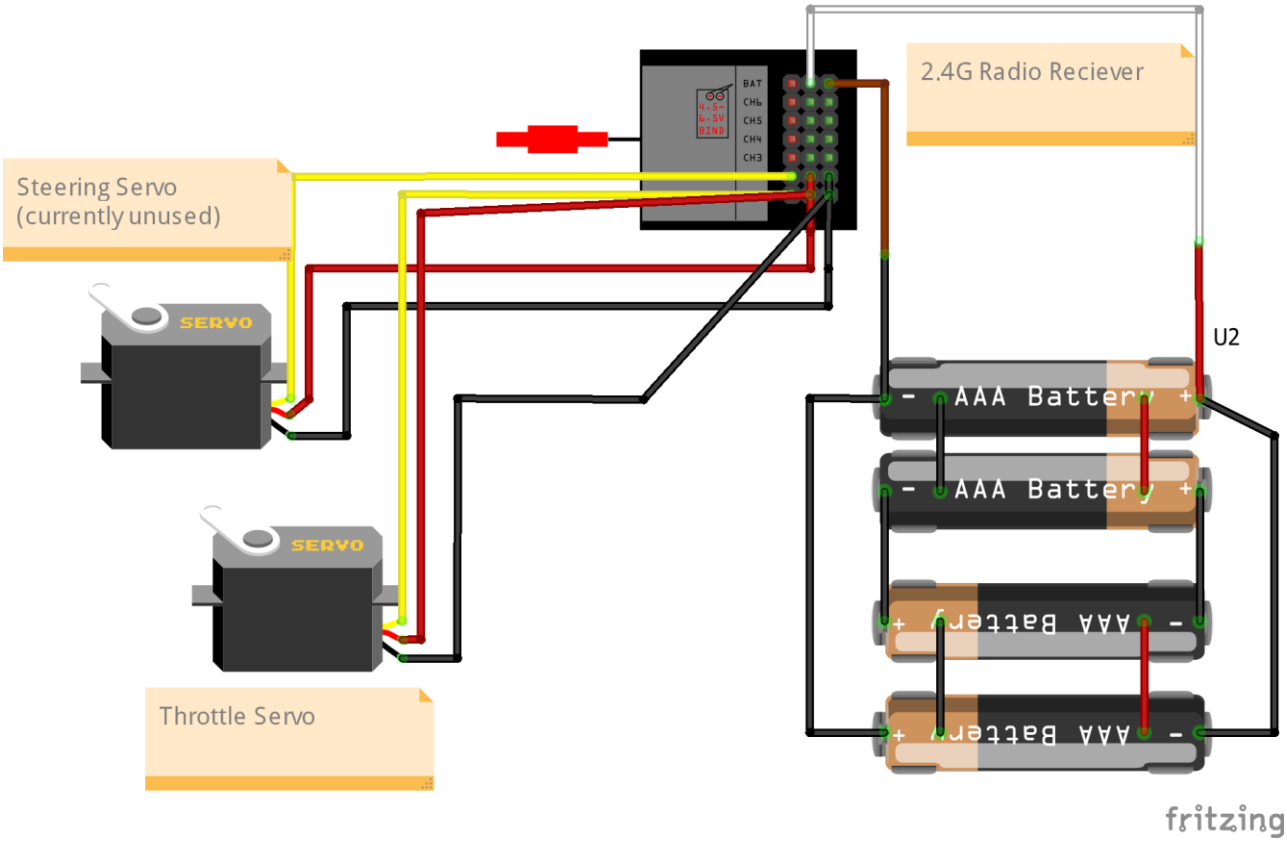

Figure A.27 Electric Diagram of the VTOL

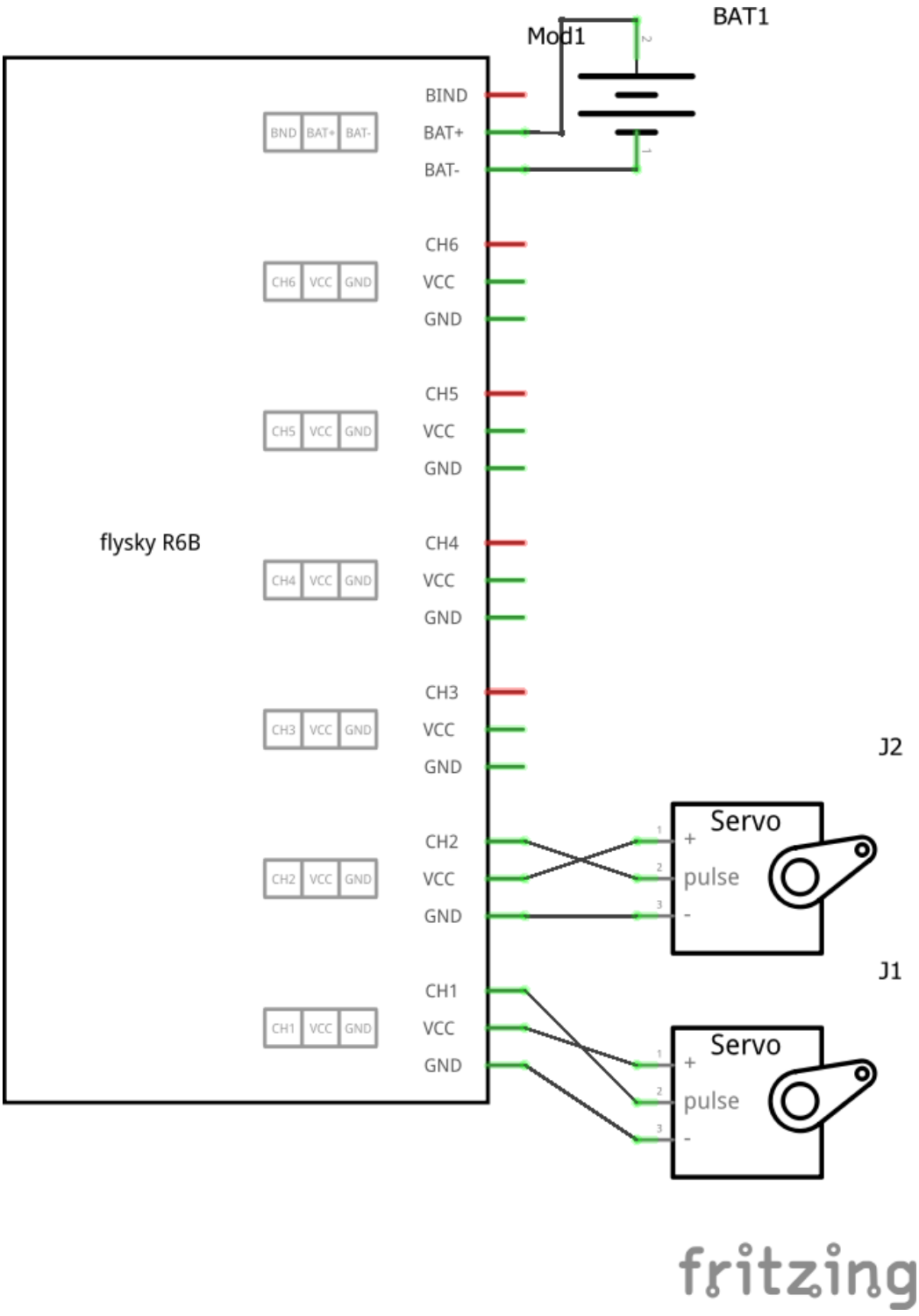

Figure A.28 Electric Schematic Diagram of the VTOL

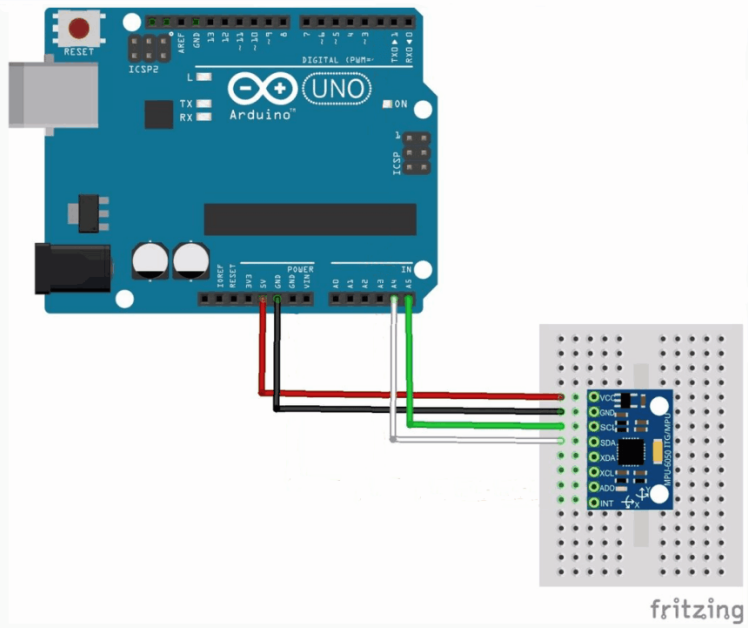

Figure A.29 Vibration testElectric Diagram

Code (For the Vibration test)

IMU CODE

```
#include "Wire.h"
#include <MPU6050_light.h>
MPU6050 mpu(Wire);
unsigned long timer = 0;
void setup() {
  Serial.begin(9600);
  Wire.begin();
  byte status = mpu.begin();
  Serial.print(F("MPU6050 status: "));
  Serial.println(status);
  while(status!=0){ }
  Serial.println(F("Calculating offsets, do not move MPU6050"));
  delay(1000);
  mpu.calcOffsets();
  Serial.println("Done!\n");
}
void loop() {
  mpu.update();
```

```
  if((millis()-timer)>10){
    Serial.print("X : ");
    Serial.print(mpu.getAngleX());
    Serial.print("\tY : ");
    Serial.print(mpu.getAngleY());
    Serial.print("\tZ : ");
    Serial.println(mpu.getAngleZ());
    timer = millis();
  }
}
```